

ATOMISTIC SIMULATION OF CEMENTITIOUS SYSTEMS: AN INSIGHT INTO ADSORPTION OF IONS AND SMALL MOLECULES ONTO PORTLANDITE AND C-S-H SURFACES

Présentée le 19 janvier 2022

Faculté des sciences et techniques de l'ingénieur
Laboratoire des matériaux de construction
Programme doctoral en science et génie des matériaux

pour l'obtention du grade de Docteur ès Sciences

par

Masood VALAVI

Acceptée sur proposition du jury

Dr J. C. Plummer, président du jury
Prof. P. Bowen, Dr S. C. Galmarini, directeurs de thèse
Prof. S. Parker, rapporteur
Dr A. Yazdan Yar, rapporteuse
Prof. P. Derlet, rapporteur

Acknowledgement

I'd like to express my gratitude to everyone who contributed to this thesis and made my PhD experience fun. There were primarily five people who contributed to the fascinating nature of this PhD. I'd like to begin by thanking Professor Paul Bowen (EPFL), who is one of the best PhD directors. He is a fantastic mentor who gives me a lot of flexibility and devotes a lot of time to my project. He is a knowledgeable project manager who walked me through the process. During my PhD, he ensured that I could meet the project's objectives. I'd also like to express my gratitude to Professor Karen Scrivener for welcoming me into the lab and supporting me during my PhD. I'd want to express my gratitude to Dr. Sandra Galmarini for her feedback on my project. She is a really competent individual who encourages me to examine the project in greater depth. I am grateful to Dr. Aslam Kunhi Mohamed for guiding me through the project and for every meeting we had. I'm also grateful to Dr. Azade Yazdan Yar, with whom I met several times to better understand some computational methods.

I'd want to express my gratitude to my office mates, Dr. Aslam Kunhi Mohamed, Dr. Azade Yazdan Yar, Ziga Casar, and John Maxwell, for creating a welcoming and pleasant environment in which to complete my PhD. I'm also grateful to Anna, Maya, and Gabie, my PTG colleagues.

I'd also like to express my gratitude to the LMC secretaries Anne-Sandra, Maude, Mirabella, and Marie-Alix for always being kind and helpful.

Life will be motionless without friends. During the four years of my thesis I had many amazing experiences and memories with friends. I'd want to express my gratitude to my friends, who, in my opinion, make the PhD experience more enjoyable. I'd want to express my gratitude to Farzad, Babak, Salar, Shayan, Yasmin, Fateme, Mohammad Reza, Ali

Finally, I would Like to thank my parents, My Brother and my sister for their continuous love and support. My thesis is dedicated to my parents who always supported me with their love.

Masood

Lausanne, 2021

Abstract

Portland Cement (PC) is the most widely used material on the planet. Human civilization has been using Portland cement for almost a century. We still don't fully grasp the hydration reaction mechanisms because of the system's complexity and the fact that it continues to react over time, making it difficult to investigate experimentally. Furthermore, it accounts for roughly 10% of global carbon dioxide emissions. Ions like calcium, hydroxyl, and sulfate, as well as compounds like gluconate, have a significant impact on the hydration of cement. How these ions effect the nucleation and growth of the main hydrates such as portlandite (CH) and Calcium- Silicate Hydrates (C-S-H) is still an area of active research. Unfortunately, little is known about how exactly these ions and compounds alter cement hydrate process mechanisms. As a result, a greater knowledge of the mechanisms underlying the influence of these ions and molecules on cement hydrates is required.

Force fields utilized in cement modeling, on the other hand, are specific to the application. As a result, it is critical to use a force field that can accurately represent structural, mechanical, and reaction enthalpies for the particular system of interest. In this thesis, a comprehensive Force Field (ERICA FF) was developed that includes many atom types found in cement (the force field has parameters for the species Ca, OH, sulfate, water, Si, Al, Na, K and Cl.). The force field was then tested to see if it could be used to predict structural, energetic, and mechanical aspects in cementitious systems. The created Force Field works effectively. The results are generally in good accord with experimental data, indicating that these force fields can be utilized to simulate cementitious systems with reasonable accuracy.

Application of the ERICA FF for ion adsorption (Ca^{2+} , OH^- , SO_4^{2-}) on the surface of portlandite and C-S-H by employing molecular dynamics and metadynamic simulations. With the goal to know how these ions affected the surface and thus the growth of the systems outlined. For the adsorption of Ca^{2+} and OH^- onto 00.1 CH surface we found outer sphere adsorption and for interaction of sulfate with 00.1 and 10.1 CH surface we found both inner sphere and outer sphere adsorption. We performed simulation on the adsorption of Ca^{2+} onto 00.1 Ca terminated C-S-H surface and we found that that Ca^{2+} ion has a strong propensity adsorb on the surface and even to go into the structural main layer of C-S-H.

Furthermore, the adsorption of a gluconate molecule on the surfaces portlandite and C-S-H was simulated. The results show regarding interaction of gluconate with 00.1 and 10.1 CH surface, gluconate will interact more with positive CH surfaces rather than neutral surface. We performed simulation on the adsorption of gluconate with 00.1 Ca terminated C-S-H surface and the result are well consistent with previous works showing a strong adsorption. This strong adsorption can to some degree explain gluconates retarding effects in cements and special aggregation behavior of C-S-H in the presence of gluconates. The ERICA FF had concerns with the CH system whereby dissolution made full interpretation of results difficult and needs some modifications. However, the ERICA FF performed very well for the most important hydrate .C-S-H and can be used by the community to get better insights into the properties of surfaces and interfaces for this ubiquitous but complex material.

Keyword: Cement, portlandite, C-S-H, Molecular Dynamics, and Metadynamics

Résumé

Le ciment Portland (CP) est le matériau le plus utilisé sur la planète. La civilisation humaine utilise le ciment Portland depuis près d'un siècle. Nous ne comprenons toujours pas les mécanismes de la réaction d'hydratation en raison de la complexité du système et du fait qu'il continue à réagir dans le temps, ce qui le rend difficile à l'étudier expérimentalement. En outre, il est à l'origine d'environ 10 % des émissions mondiales de dioxyde de carbone. Des ions comme le calcium, l'hydroxyle et le sulfate, ainsi que des composés comme le gluconate, ont un impact important sur l'hydratation du ciment. La façon dont ces ions affectent la nucléation et la croissance des principaux hydrates tels que la portlandite (CH) et les hydrates de calcium et de silicate (C-S-H) fait toujours l'objet de recherches actives. Malheureusement, on sait peu de choses sur la manière exacte dont ces ions et composés modifient les mécanismes du processus d'hydratation du ciment. Par conséquent, une meilleure connaissance des mécanismes qui sous-tendent l'influence de ces ions et molécules sur les hydrates de ciment est nécessaire.

Les champs de force utilisés dans la modélisation du ciment, d'autre part, sont spécifiques à l'application. Par conséquent, il est essentiel d'utiliser un champ de force capable de représenter avec précision les propriétés enthalpiques, structurales, mécaniques et réactionnelles pour le système d'intérêt particulier. Dans cette thèse, un champ de force complet (ERICA FF) a été développé qui inclut de nombreux types d'atomes trouvés dans le ciment (le champ de force a des paramètres pour les espèces Ca, OH, sulfate, eau, Si, Al, Na, K et Cl.). Le champ de force a ensuite été testé pour voir s'il pouvait être utilisé pour prédire les aspects structurels, énergétiques et mécaniques dans les systèmes cimentaires. Le champ de force créé dans cette thèse fonctionne efficacement. Les résultats sont généralement en bon accord avec les données expérimentales, ce qui indique que ces champs de force peuvent être utilisés pour simuler les systèmes cimentaires avec une précision raisonnable.

Application du FF ERICA pour l'adsorption d'ions (Ca^{2+} , OH^- , SO_4^{2-}) à la surface de la portlandite et du C-S-H en utilisant des simulations de dynamique moléculaire et de métadynamique. Dans le but de savoir comment ces ions ont affecté la surface et donc la croissance des systèmes décrits. Pour l'adsorption de Ca^{2+} et OH^- sur la surface 00.1 CH, nous avons trouvé une adsorption en sphère externe et pour l'interaction du sulfate avec les surfaces 00.1 et 10.1 CH, nous avons trouvé une adsorption en sphère interne et externe. Nous avons

effectué une simulation de l'adsorption de Ca^{2+} sur la surface de 00.1 Ca C-S-H et nous avons constaté que l'ion Ca^{2+} a une forte propension à s'adsorber sur la surface et même à pénétrer dans la couche principale structurale de C-S-H.

De plus, l'adsorption d'une molécule de gluconate sur les surfaces de portlandite et de C-S-H a été simulée. Les résultats montrent qu'en ce qui concerne l'interaction du gluconate avec les surfaces 00.1 et 10.1 CH, le gluconate interagit davantage avec les surfaces CH positives qu'avec les surfaces neutres. Nous avons effectué une simulation de l'adsorption du gluconate sur la surface 00.1 Ca terminée de C-S-H et les résultats sont cohérents avec les travaux précédents montrant une forte adsorption. Cette forte adsorption peut dans une certaine mesure expliquer les effets retardateurs des gluconates dans les ciments et le comportement particulier d'agrégation des C-S-H en présence de gluconates. L'ERICA FF a eu des problèmes avec le système CH, la dissolution rendant l'interprétation complète des résultats difficile et nécessitant quelques modifications. Cependant, le FF ERICA a très bien fonctionné pour l'hydrate le plus important, le C-S-H, et peut être utilisé par la communauté pour mieux comprendre les propriétés des surfaces et des interfaces de ce matériau omniprésent mais complexe.

Mots clés : Ciment, portlandite, C-S-H, dynamique moléculaire et métadynamique.

Contents

Acknowledgement.....	2
Abstract.....	3
Resume.....	5
Contents.....	7
Chapter 1 – Introduction.....	14
1.1 System.....	14
1.2 Atomistic modeling.....	15
1.3 The objectives of the thesis.....	16
1.4 Organization of thesis.....	16
1.5 References.....	17
Chapter 2-Methods.....	19
2.1 Potentials.....	19
2.1.1 Periodic boundary conditions.....	21
2.2 Energy minimization.....	22
2.2.1 Surface cell construction.....	23
2.3 Molecular dynamics.....	23
2.3.1 Ensembles.....	25
2.4 Metadynamics.....	26
2.4.1 Choice of collective variables.....	28
2.5 References.....	29

Chapter 3 - State of the Art.....	30
3.1 Potentials for Water.....	30
3.2 Potential for Sulfate.....	32
3.3 Force fields for Cementitious systems.....	33
3.3.1 ClayFF force field	34
3.3.2 Interface Force Field.....	35
3.3.3 Cement Force Field (CementFF).....	36
3.3.4 Reactive Force Field (ReaxFF).....	37
3.3.5 CSH force field (CSH-FF).....	38
3.4 Applications of force fields for molecule and ion adsorption on cementitious systems..	39
3.5 Summary and conclusion.....	45
3.5 References.....	45
Chapter 4 - Molecular dynamic simulations of cementitious systems using a newly developed force field suite ERICA FF.....	49
4.0 Abstract.....	49
4.1 Introduction.....	50
4.2. Methods.....	52
4.2.1 Ca, OH, water, sulfate force field core (ERICA FF1).....	53
4.2.2 Silicate-Aluminate extension (ERICA FF2).....	54
4.2.3 Hydrated ions extension (Na, K, Cl; ERICA FF3).....	55

4.2.4 Structural properties.....	56
4.2.5 Energetic validation.....	56
4.2.6 Hydration enthalpies.....	56
4.2.7 Surface energies.....	56
4.3 Result and Discussion.....	58
4.3.1 Structural Validation.....	58
4.3.2 Energetic validation.....	64
4.3.3 Validation of ERICA FF3 from Hydration enthalpies.....	65
4.3.4 Portlandite surface energies.....	69
4.3.5 Mechanical Properties	69
4.4. Conclusions.....	71
4.5. References.....	72
Chapter 5 - Adsorption of Calcium and Hydroxyl ions onto portlandite surfaces.....	79
5.1 Introduction.....	79
5.2 Simulation details.....	79
5.2.1 Simulation details for calculating the structure of water above CH surfaces.....	80
5.2.2 Details of MTD simulations for adsorption of Ca and OH ions onto 00.1 CH surface.....	80
5.2.3 Details of MD simulation for adsorption of Ca and OH ions onto 00.1 CH surface.....	81
5.3. Results.....	82
5.3.1 Structure of water above CH surfaces.....	83

5.3.1(a)Structure of water above 00.1 CH surface.....	84
5.3.1(b) Structure of water above 10.0 CH surface.....	85
5.3.1 (c) Structure of water above 10.1 CH surface.....	87
5.4 MTD simulation of adsorption of Ca and OH into 00.1 CH surface.....	89
5.4.1 Ca adsorption onto 00.1 CH surface.....	89
5.4.2 OH adsorption onto 00.1 CH surface.....	92
5.4.3 Dissolution problem in MTD.....	94
5.5 MD simulation of adsorption of Ca and OH into 00.1 CH surface.....	96
5.6 Summary and Conclusion regarding structure of water above CH surfaces and simulation of Ca and OH into 00.1 CH surface using MTD and MD methods.....	101
5.7 Preliminary MTD Simulation of adsorption of Ca adsorption onto 00.1 Ca terminated C-S-H surface.....	102
5.7.1 Simulation details for adsorption of Ca and OH onto 00.1 C-S-H surface.....	103
5.7.2 Analysis of results a for adsorption of Ca and OH onto 00.1 C-S-H surface.....	104
5.8 Summary and Conclusion.....	108
5.9 References.....	109
Chapter 6: Molecular simulations of adsorption of gluconate on portlandite and C-S-H surfaces.....	112
6.1 Adsorption of Gluconate on portlandite	112

6.2 Methods for adsorption of gluconate onto CH surfaces.....	114
6.2.1 Details of generation of gluconate molecule for simulation in vacuum and water.....	114
6.2.2 Details on simulations of gluconate, sodium water, and portlandite surfaces.....	114
6.3 Results and discussion.....	116
6.3.1 Adsorption of gluconate into 00.1 CH surface.....	116
6.3.2 Adsorption of gluconate into 10.1 CH surface.....	118
6.3.3 Investigation of gluconate adsorption site on 10.1 neutral CH surface at distance of 2Å	120
6.3.4 Summary and Conclusion.....	121
6.4 Simulation of gluconate adsorption onto a 00.1 Ca terminated C-S-H surface by MTD.....	122
6.4.1 Simulation of gluconate adsorption on a 00.1 Ca terminated C-S-H surface.....	123
6.4.2 Summary and conclusion.....	126
6.5 Summary and conclusion.....	127
6.6 References.....	128
Chapter 7 - Molecular simulations of adsorption of sulfate onto surfaces of portlandite and C-S-H.....	131
7.1 Introduction.....	131
7.2 Method.....	132
7.2.1 Details of simulation for study of Calcium-sulfate ion pair formation by MTD..	132

7.2.2 Details of molecular dynamic simulations of adsorption of sulfate into 00.1 and 10.1 CH surfaces.....	132
7.3 Results and discussion.....	133
7.3.1 Analysis of ion pair formation results for Calcium- Sulfate – MTD.....	133
7.3.2 Analysis of results for adsorption of sulfate into 00.1 and 10.1 CH surfaces – MD.....	136
7.3.3 Summary and Conclusions – CH.....	140
7.4 Preliminary attempts to investigate adsorption of sulfate onto C-S-H	140
7.5 References.....	141
Chapter 8: Conclusions.....	143
8.1 ERICA Force Field suite.....	143
8.2 Interaction ions and small molecules with CH surfaces.....	143
8.3 Interaction of ions and small molecules with Ca terminated 00.1 C-S-H surface.....	145
8.4 Outlook and Future Work.....	146
8.5 References.....	148
Annexes	148
Annex 1 - Supplementary Information for paper of chapter 4 submitted to the journal of Cement and Concrete Research.....	148
S1. Total energy calculations.....	148
S2. ERICA FF1 parameters.....	152

S3. ERICA FF2 parameters.....	155
S4. ERICA FF3 parameters.....	155
S5: Water correction term.....	157
S6. Error estimation for reaction enthalpies.....	158
S7. Details of simulations for structural validation.....	159
S8. Surface energy calculations and morphology predictions.....	160
S9. Elastic Constants.....	162
References.....	163
Annex 2. PLUMED code for adsorption of Ca²⁺ onto 00.1 Ca CH surface.....	165
Annex 3. LAMMPS input file for Gluconate Adsorption onto 00.1 Ca terminated C-S-H surface.....	166
Annex 4. LAMMPS input file for sulfate Adsorption onto 00.1 Ca terminated C-S-H surface.....	180
CV.....	188

Chapter 1: Introduction

In this very general introduction, the basic information of cement and why atomistic simulation can be of use in improving its sustainability is introduced. The outline of the thesis is given and more detailed discussions of the topics are given in the following chapters.

1.1 System

Cement is one of the most used materials in the world and when it is mixed with water it produces Hardened Cement Paste (HCP) via a hydration process, and the HCP is the glue that governs concrete's properties. There are many types of cements, of which the most important one is Portland Cement (PC). Concrete is a mixture of cement, sand, aggregates and water. In recent years Supplementary Cementitious Materials (SCM) are mixed with cement in an attempt to lower the carbon footprint and improve sustainability. SCMs are currently added to cement since the production of cement generally makes up to 10 percent of global CO₂ emissions from industry (1). It has been predicted that the demand for concrete will be doubled by 2050 (1) so there is huge and increased demand for more sustainable cements. Unfortunately, despite many years of research there remain many unknowns about the cement hydration process. One of the main reasons for that insufficient knowledge is linked to the difficulty of describing the atomistic structure of the main hydration product of cement paste, Calcium-Silicate -Hydrate (C-S-H) and its formation mechanism as it is nanocrystalline and poorly ordered i.e. difficult to characterize by standard diffraction techniques.

Portland cement is made by heat treating limestone-clay mixtures at temperatures close to 1400°C (2). This produces a mixture of mineral phases which are known as clinker and then ground with gypsum to produce the cement powder used in the construction industry. The main mineral phases in cement are alite, belite, aluminates, and ferrites (2). Therefore, the main atom types in Cement include oxygen, silicon, calcium, hydrogen, aluminum and iron. When these materials are mixed with water, a set of reactions will occur which cause nucleation and growth of different hydrated phases.

Alite, an impure tricalcium silicate (C₃S), is the main component of cement, about 50-70 percent, and when it is mixed with water it makes cement hydrates including portlandite (CH) and

Calcium- Silicate- Hydrate (C-S-H). Portlandite is the second most abundant phase in hydrated cement and it is known to influence nucleation and growth of C-S-H which the most abundant (3). The study of atomistic scale properties of portlandite and C-S-H is very important to help better understand their nucleation, growth, and the fundamentals behind hydration phenomena.

Portlandite is between 15-25 percent of the cement hydrates (4) and it plays an important role in buffering the pH and is also important in leaching and degradation mechanisms (5). The influence of portlandite on mechanical properties is dependent on the morphology (6). The morphology of portlandite in cementitious system depends on the composition of cement (7), the temperature and the solids to water ratio (8). The growth and change in the morphology of portlandite are poorly understood. This issue is coming from the low current knowledge and incomplete understanding of the solvent-solid interface. For example, how will the most important growth species interact with the surface and finally become incorporated to the crystal. This knowledge is important to determine the rate-determining step for the growth of facets. This effect determines the final morphology of crystals. At the surface, the solvent molecules will also interact with the solid which will influence the growth process (9) which also affect the final morphology of crystal. Also, other ions in the solution can greatly affect the morphology and properties of portlandite. Galluci and Scrivener (5) observed that sulfate may act as the nucleus for CH clusters or at least their neighborhood favors the crystallization of CH. They also observed that C_3S systems that contains calcium sulfate seems to have a smaller minimum particle size compared to the C_3S systems without sulfate. They also even observed that CH sometimes seems to grow directly from the surface of the gypsum.

Gollop and Taylor (10) found that when sulfate ions are incorporated into the cement-based materials, the crystal phases were changed dramatically due to many different chemical reactions. In addition to sulfate, organic molecules also can hugely impact the cement hydrates. Androniuk et al. (11) observed that the presence of organic molecules in the HCP pore water can also affect the long-term radionuclide mobility: organic molecules can form water-soluble complexes and compete with radio nuclide for sorption sites at the cement surface.

1.2 Atomistic modeling

Atomistic modeling nowadays is applied in many fields. This is due to increased computer power. In the atomistic simulation, we are looking at the arrangement of atoms in 3 dimensions,

and with the application of some algorithms we track the movement of the atom and study dynamic phenomena or some properties of the system. A unit cell is the smallest portion of a crystal lattice that shows the three-dimensional pattern of the entire crystal. A crystal can be thought of as the same unit cell repeated over and over in three dimensions (Super cell). The base of atomistic modeling is on repeating a unit cell in 1,2 or all directions, which later with the definition of periodic boundary condition changes to an infinitely large system representative of bulk materials. The ratio of atoms in the unit cell is based on the chemical formula of a substance for example in a unit cell of portlandite there is 1 Ca and 2 OH occupy the site of the unit cell. Atoms in the unit cells may make bonds and other arrangements which all should be included in atomistic modeling of substance. Atomistic modeling in the cement industry has many applications, some of the main achievements will be reviewed in the following chapters. The classical atomistic simulation techniques, based on classic mechanics using empirical force fields are energy minimization and molecular dynamics along with enhanced sampling methods such as Metadynamics simulations are used in this thesis. These will be discussed in more detail in a chapter 3 of the thesis and used therein to gain better understanding of CH and C-S-H interfaces under conditions akin to early hydration of cement.

1.3. The objectives of the thesis

The objectives of this thesis are as follow:

- To develop a general force field which can be used for the study of the adsorption of calcium, hydroxyl, sulfate, and gluconate on the surface of cement hydrates.
- To better understand phenomena behind the adsorption of ions and molecules on portlandite and C-S-H surfaces, specifically, calcium, hydroxyl, sulfate and gluconate.

1.4. Organization of thesis

The thesis is divided into eight chapters.

Chapter 1 - General overview of cement and introduction to thesis structure

Chapter 2 - Methods -brief description of simulation methods used in this work

Chapter 3 - State of art -literature review of selected studies on atomistic simulation of cementitious materials

Chapter 4 - ERICA Force Field details of the developed force field in this work

Chapter 5 - Study of adsorption of Ca and OH onto 00.1 CH surface and 00.1 Ca terminated C-S-H surface using molecular dynamics and metadynamics

Chapter 6 - Study of adsorption of gluconate and ions into C-S-H surfaces and 00.1 Ca terminated C-S-H surface, using molecular dynamics and metadynamics

Chapter 7 – Study of adsorption of sulfate onto 00.1 CH ,10.1 CH surfaces and 00.1 Ca terminated C-S-H surface, using molecular dynamics and metadynamics

Chapter 8 - Conclusions and outlook

Annexes – supplementary information from the submitted publication in chapter 4 and other details of simulations carried out in the thesis.

1.5 References

1. Scrivener KL, John VM, Gartner EM. Eco-efficient cements: Potential economically viable solutions for a low-CO₂cement-based materials industry. *Cem Con Res.* 2018,114, 2-26;
2. Taylor HFW. *Cement Chemistry*, 2th edition. 1997.
3. Gallucci E, Scrivener K. Crystallization of calcium hydroxide in early age model and ordinary cementitious systems. *Cem Concr Res.* 2007, 37, 92–501.
4. S. Diamond. Calcium hydroxide in cement paste and concrete-a microstructural appraisal. *Mater Sci Concr Spec.* 200.1,12,37–58.
5. Glasser, F. P. The Role of Ca(OH)₂ in Portland Cement Concretes. *Materials of Science and Concrete, Calcium Hydroxide in Concrete* 200.1, 36, 11-36
6. Chen JJ, Sorelli L, Vandamme M, Ulm FJ, Chanvillard G. A coupled nanoindentation/SEM-EDS study on low water/cement ratio portland cement paste: Evidence for C-S-H/Ca(OH)₂ nanocomposites. *J Am Ceram Soc.* 2010,93,1484–93.
7. Berger R. L., McGregor J. D. Effect of Temperature and Water-Solid Ratio on Growth of Ca(OH)₂ Crystals Formed During Hydration of Ca₃SiO₅. *J Am Ceram Soc.* 1973,56,73–9.

8. Groves G. W. Microcrystalline calcium hydroxide in Portland cement pastes of low water/cement ratio. *Cem Concr Res.* 1981,11,713–8.
9. S. Galmarini, A. Aimable, N. Ruffray, P. Bowen, Changes in portlandite morphology with solvent composition: Atomistic simulations and experiment, *Cem. Conc. Res* 2011, 41,1330-13380
10. R. S. Gollop, H.F.W.Taylor, Microstructural and microanalytical studies of sulfate attack. I. Ordinary portland cement paste. *Cem Concr Res.* 1992,41, 1027–38.
11. Androniuk I, Landesman C, Henocq P, Kalinichev A. G. Adsorption of gluconate and uranyl on C-S-H phases: Combination of wet chemistry experiments and molecular dynamics simulations for the binary systems. *Phys Chem Earth.* 2017, 9, 194–203.

Chapter 2 – Methods

2.1-Potentials

To investigate materials at the atomic scale we can use different methods such as quantum mechanics (QM) methods or the so-called classical methods based on Newton's laws of motion. We examine both nuclei and electrons in the QM technique. In classical mechanics approaches atoms are defined as point charges. As a result, the degree of freedom is reduced, and we can investigate larger systems in less time than using QM methods. In this thesis the main classical methods used are Energy Minimization (EM), Molecular Dynamics (MD) and Metadynamics (MTD). All the methods use empirical force fields to describe the force between atoms in the system of interest.

The force field is a set of equations and constants that are used to simulate the molecular geometry and properties of tested structures via their interatomic forces. The suitability of the force field to describe the properties of a material (e.g. crystal structure) is tested by comparison with experimental data, or in the case of a lack of experimental data with results from QM methods. Because the accuracy of the generated findings is dependent on the force field that we employ, it is critical to select a thorough and appropriate force field for a simulation. A comprehensive force field has been built in this thesis, which will be examined in detail in chapter 4. The force field was developed in 3 steps, ERICA FF1, FF2 and FF3. ERICA FF1 is a force field that starts with potentials that includes Ca, OH, sulfate, and water. ERICA FF2 adds to it Al, Si, O, and ERICA FF3 adds Na, K, and Cl. The name ERICA FF was chosen to recognize financing of the research from the Marie Curie project "Engineered Calcium Silicate Hydrates for Application (ERICA)."

In general, there are two sorts of interactions. One is intramolecular interaction which is responsible for preserving the molecule's overall structure and includes things like covalent bonds. In intramolecular interaction, we talk about angles and dihedrals in the molecule. Covalent bonds, metallic bonds, and ionic bonds are all used in intramolecular interactions. The physical properties of molecules, such as their boiling point, melting point, density, and enthalpies of fusion and vaporization, are determined by intermolecular forces, which are much

weaker than intramolecular forces of attraction. There are three types of intermolecular interactions: dipole-dipole interaction, hydrogen bonding, and London dispersion interactions. Columbic interaction, on the other hand, can be classified as both intramolecular and intermolecular interactions.

$$E = 4\epsilon\left[\left(\frac{\sigma}{r}\right)^{12} - \left(\frac{\sigma}{r}\right)^6\right] \quad (\text{eq.1})$$

$$E = 4\epsilon\left[\left(\frac{\sigma}{r}\right)^9 - \left(\frac{\sigma}{r}\right)^6\right] \quad (\text{eq.2})$$

$$E = Ae^{\frac{-r}{\rho}} - \frac{C}{r^6} \quad (\text{eq.3})$$

Many body potentials are used to define intermolecular interactions. Only the 2-body van der Waals interaction, which can be characterized using the Lennard Jones (LJ) 12-6, Lennard Jones 9-6, and Buckingham potentials, was considered in this thesis, using equations 1-3.

The equation 1 reflects a Lennard Jones 12-6 potential, which has both a long-range and a short-range attractive van der Waals interaction. The depth of the energy well between atoms i and j is e, and the distance at the minimum potential is s in this equation and r is the distance between atom i and j (1). Equation 2 reflect an L-J 9-6 potential and equation 3 shows a Buckingham potential where A, ρ and C are constant values.

Long-range columbic forces, can be represented by equation 4.

$$E = \frac{CQ_iQ_j}{r_{ij}} \quad (\text{eq4})$$

Q_i and Q_j are the charges of two atoms, while r_{ij} is the distance between the atoms and C is a coulombic constant.

We shall describe the methodology for developing a force field for cementitious systems with the atoms of current interest in Chapter 4 of the thesis. It's worth noting that in order to build these

force fields, we gathered several Lennard Jones and Buckingham potentials from various studies and used them as a basis for ERICA FF with certain modifications for our systems of interest.

2.1.1 Periodic boundary conditions

The atoms are arranged in a unit cell in the crystal structure, and the unit cell structure of atoms is shown in the structure files from various crystallographic databases (e.g. cif files). It includes data on the unit cell's length in three directions as well as angles between cell vector. It is not a good idea to perform molecular dynamic simulation on a unit cell, and it is preferable to deal with a bigger volume than the unit cell, more representative of the bulk. The bulk environment is reached by repeating the unit cell in one, two, or three directions, forming what we call a super cell. We used OVITO software to construct bulk structures in this thesis. When the bulk is formed, the next step is to explore an imaginary situation in which the bulk is repeated in all directions towards an infinite value by creating periodic boundary conditions (PBC). This means that pieces in all directions of a bulk can be treated the same way. Consider Figure 3.1 for a schematic representation of the situation in 2D. Most simulations in this thesis has used full 3D PBCs.

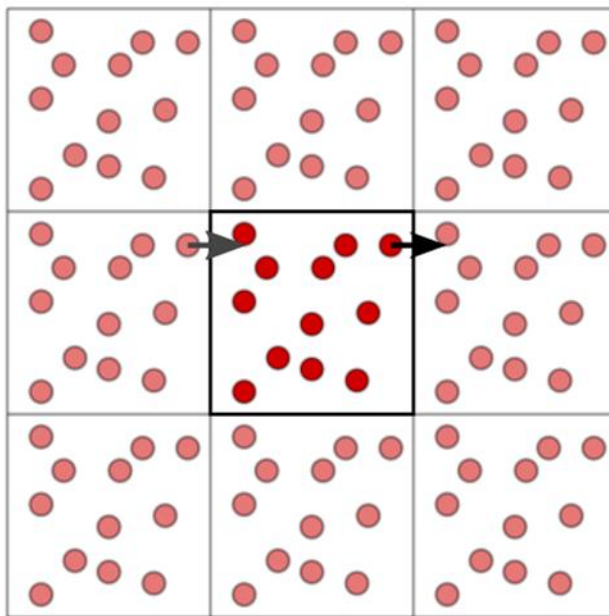


Figure 2.1 Schematic diagram illustrating periodic boundary conditions (2D).

For the long-range electrostatic interactions, a cut-off radius r_c is employed. Only interactions between couples that are closer than the cut-off radius are explicitly calculated. Outside the cut-off, the pair interaction is either ignored or simulated using a different method. In the case of periodic boundary conditions, the Ewald summation is commonly employed to approximate interactions outside the cut-off radius, as used in this thesis. After specifying a cut off radius r_c , the electrostatic interaction is estimated in reciprocal space using the Ewald summation method for values greater than the cut off (2).

2.2 Energy minimization

Energy minimization (EM) is a basic technique of atomistic simulation methods to find the minimum energy for a certain arrangement of atoms (e.g. crystal structure). The total energy of the system will be searched for in energy minimization. In comparison to molecular dynamics simulations and other computer approaches, energy minimization is a highly rapid method. To completely examine these systems, molecular dynamics should be used. However, in a system like an ionic crystal, where temperature has only a small effect on structural properties, bulk and interfacial properties may be calculated directly (3). In EM, there is no dynamics, atomic vibrations, or temperature. A force field is used to simulate the interatomic interaction in EM.

It's worth noting that EM's minimum is often a local one rather than a global one. It has the advantage of examining the metastable structure, but the disadvantage is that the final outcome is very dependent on the initial system configuration, with the starting state normally being closer to the local minimum than the global minimum. As a result, rather than reaching the final minimum during EM, one may reach a local minimum. The number of starting configurations required to find the most stable state structure is quite large (3), since we must analyze several initial conditions to reach a global minimum (most stable state). We employed EM for molecular dynamic and metadynamics simulations in this thesis, and thus we started with a low-energy setup to do molecular dynamic simulations.

Because surfaces are so crucial in so many applications, this thesis often focuses on the interaction of molecules and ions with the surface, and how the surface is generated will now be briefly described.

2.2.1 Surface cell construction

A supercell that comprises many unit cells in all directions can be sliced to resemble a surface in the direction of particular lattice planes. Different surface terminations can be obtained depending on the depth of cleavage (7). The construction of the surface is well discussed in (7) and only briefly described here. Fig 3.2 shows showing how to cleave a supercell in a specific direction and build a slab.

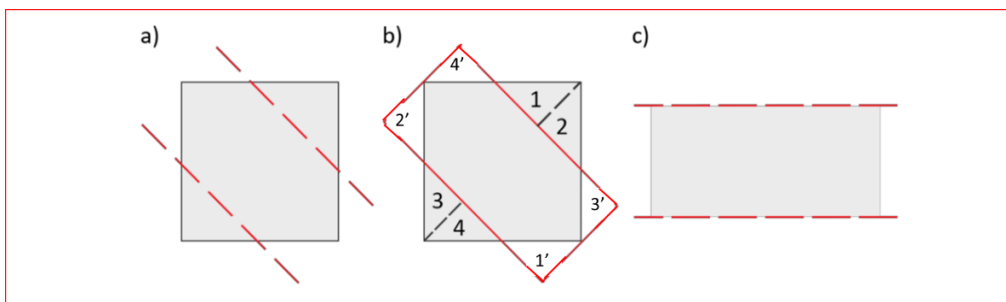


Figure 2.2. A diagram showing how to cleave a supercell in a specific direction and build a slab. a) A supercell that must be split in a specific direction, such as the red dashed line, b) the transformation necessary, and c) the end slab in the desired direction.(3)

The thickness of a slab is limited. The thickness of the slab in surface construction should not allow for considerable interaction between the slab's upper and lower faces. This thickness should also be chosen so that the material in the slab's core part reacts similarly to the bulk.

2.3 Molecular dynamics

In a classical system, the position and momentum of all particles are frequently required to fully characterize the system's behavior. As a result, we need q and p to express the system's behavior, with p describing the phase space of each point and q momentum. A trajectory can be created by dumping the evolution of q and p over time. A trajectory can be utilized to debug simulation problems, as well as for a variety of other uses. An ensemble is a fictitious collection of each state or phase point of a system. In molecular dynamic simulations, we can get various properties of the system. For example, we can acquire an average of properties throughout time to get some properties to compare with other studies and experiment.

The average of the A property can be determined using the calculation below.

$$A = \frac{1}{N} \sum_i^N A(q, p, t_i) \quad (\text{eq5})$$

Time is denoted by t , and the number of measurements taken at different times is denoted by N . In the case of unlimited time and continuous sampling, the above equation becomes:

$$A = \lim_{t \rightarrow \infty} \frac{1}{t} \int_{t_0}^{t_0+t} A(t) dt \quad (\text{eq6})$$

For a given number of atoms (N) in a volume (V) and at constant energy, the ergodic hypothesis says that all accessible states are equally likely over a long period, regardless of the starting time, initial positions (q), and momenta (p) for an isolated system at equilibrium (E). At equilibrium, the property average across time and the ensemble average are equal (5).

All parameters in a molecular dynamic simulation can be determined using locations (q) and momenta (p). Consider the case when we need to figure out the system's density. To calculate density, we must keep track of the number of particles in a given volume over time. The same is true for other quantities. The equipartition principle is used to calculate temperature in molecular dynamics:

$$\frac{1}{2} m v_i^2 = \frac{1}{2} k_B T \quad (\text{eq7})$$

At any given time, only the locations (q) and the momenta (p) must be known. The particles in the system move according to Newton's standard motion equation:

$$F_i = m \cdot \frac{\partial^2 q_i}{\partial t^2} \quad (\text{eq8})$$

To integrate the given equation, the forces on each particle must be computed. To integrate Newton's equation, many algorithms have been created. They all have their own set of benefits and drawbacks. Some of them (4) include issues with energy conservation, energy drifts, reversibility, large dependences on the beginning point, and the need for short time increments. The Verlet algorithm (5) is the most widely used because to its simplicity and performance. The initial velocities are frequently modified to a desired (kinetic) energy value while maintaining zero

total momentum. Each particle's coordinates are first extended in a Taylor series around the fourth term, in both "directions," backward ($t - t$) and forward ($t+ t$). When both equations are added together, we get:

$$q(t + \Delta t) = 2q(t) - q(t - \Delta t) + \frac{F(t)}{m} \Delta t^2 \pm O(\Delta t^4) \quad (\text{eq9})$$

q denotes the particle's position, F denotes the forces acting on it, m denotes the particle's mass, t is the current time, and Dt denotes the time step. Only the forces, along with the current and previous positions, are required to calculate the next positions.

Other algorithms, such as the Euler, Leap Frog, and velocity Verlet algorithms, are alternatives to the Verlet scheme. Higher-Order techniques, such as the predictor correction algorithm, use information from the Taylor expansion's higher-order derivatives. Reference (5) provide a full discussion of algorithms and their capabilities.

2.3.1 Ensembles

The Microcanonical (NVE) ensemble, Canonical ensemble (NVT), and iso thermal-Iso baric ensemble (NPT) are the three most used ensembles in molecular dynamic modeling.

The system is separated from changes in moles (N), volume (V), and energy (E) in the microcanonical ensemble (E). It's the same as an adiabatic process with no heat transfer. A microcanonical molecular dynamics trajectory can be thought of as an exchange of potential and kinetic energy that conserves total energy. The amount of material (N), volume (V), and temperature (T) are all conserved in the canonical ensemble. Endothermic and exothermic processes' energy is exchanged with a thermostat in NVT.

A number of thermostat algorithms are available for adding and removing energy from the limits of an MD simulation in a more or less realistic manner, emulating the canonical ensemble. Velocity rescaling, the Nosé–Hoover thermostat, Nosé–Hoover chains, the Berendsen thermostat, the Andersen thermostat, and Langevin dynamics are all popular ways of controlling temperature. The amount of material (N), pressure (P), and temperature (T) are all conserved in

the isothermal–isobaric ensemble. A barostat is required in addition to a thermostat. It most nearly resembles a laboratory setting, with a flask at room temperature and pressure.

It's worth noting that in this thesis, we mostly employed the NPT ensemble for bulk calculations and the NVT ensemble for all simulations involving surface calculations, such as the computation of surface energy and the interaction of molecules and ions with the surface.

2.4 Metadynamics

In molecular dynamic modeling, the system may become stuck in a local minimum potential energy state. The rate at which it seeks to escape from such minimum k_e (eq 10) and t_c is a timescale process, according to the harmonic transition state theory (8). For oxides, a frequency of 6.21 Hz is typical, and the highest available timescale is in the range of 1 hour (7). We can simulate the system with a maximum energy difference of F_{\max} 0.23 eV using these settings. We must use alternative methods, such as metadynamics, to sample rare events for systems with a longer characteristic period.

$$k_e = \frac{1}{t_c} = \nu e^{-\Delta F_e / K_b T} \quad (\text{eq10})$$

$$\Delta F_{\max} = k_b T \ln(\nu t_{\max} 2) \quad (\text{eq11})$$

We can examine the energy landscape using the collective variable. The system's collective variables are a small set of properties. It should be a function of atom positions explicitly. It could be anything from the distance between two atoms to the distance between two groups of atoms, and so on. We employed distance from the surface as a collective variable in this thesis, and we'll go over it in depth in Chapter 5. The probability distribution $P_b(s)$ of the system state with respect to the vector of collective variables $s = (s_1, s_2, s_d)$ is solely determined by the system's total free energy $F(s)$. The initial free energy of the system is calculated by integrating over the partition function of the energy of all systems with the same value.

$$P_b(s) = \frac{e^{-F(s)/T}}{\int e^{-F(s)/T} ds} \quad (\text{eq12})$$

$$F_{Sys}(s) = -T \cdot \ln \left(\int e^{-\frac{V_{sys}(r)}{T}} \delta(s - S(r)) \cdot dr \right) \quad (\text{eq13})$$

The metadynamics technique is based on the addition of a modest repulsive Gaussian bias potential to the system at intervals $n G$, $n (1, 2, 3, \dots)$. $V(s, t)$ is the entire metadynamics bias potential.

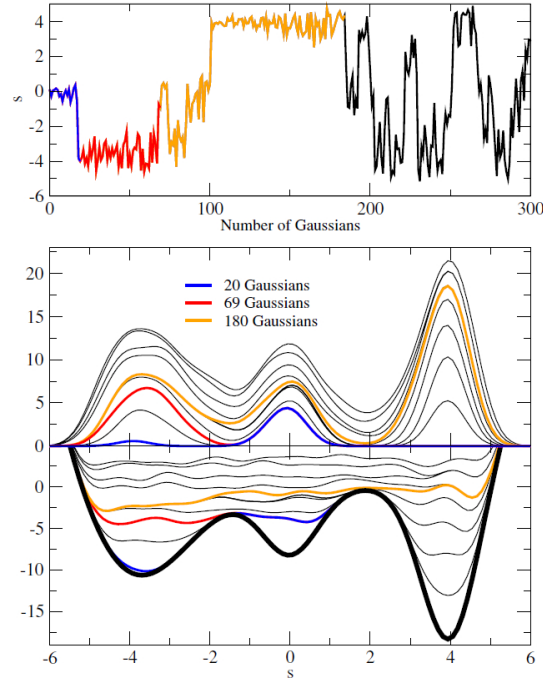


Figure 2.3: During a metadynamics simulation on the 3- potential minima shown in the lower panel, the trajectory of the collective variable s for a one-dimensional system. The metadynamics parameters are $s = 0.4 \text{ \AA}$, $w = 0.3 \text{ eV}$, and $G = 300 \text{ ps}$. Time evolution of the metadynamics bias potential V_G in the middle panel. V_G when the first minimum is filled and the system ‘escapes’ to the second minimum; red line: V_G when the second minimum is also filled; orange line: V_G when the full profile is filled. Lower panel: the sum of the metadynamics potential V_G and the system’s intrinsic potential V_{sys} with time. A thick black line represents the final V_{sys} . Take from (6)

The bottom of the potential well is filled first in metadynamics, and it fills gradually, allowing the system to escape the lowest energy well. Figure 3.3 depicts a schematic depiction of the metadynamic filling process for the energy well. At that point, the free energy $F(s, t_{fill}) = F_{sys}(s) + V_G(s, t_{fill})$ will essentially be constant for all values of s , and the system will diffuse freely throughout the entire energy landscape, i.e. the probability distribution $P_b(s, t) | t > t_{fill}$. This

indicates that the bias potential finally equals the system's free energy plus a dependent shift (7). As a result, we can conclude that the bias potential can be utilized to estimate the free energy landscape.

2.4.1. Choice of collective variables

The selection of appropriate collective variables must be done with great care. The results of metadynamics simulations are highly reliant on the collective variables chosen.

According to Galmarini (7), there are four key considerations for selecting collective variables.

1-collective variables should represent system properties and should be able to differentiate between all states of interest (6). It means that when studying the production of two ion pairs, for example, the interatomic distance between two atoms must be considered.

2-All slow modes relevant to the system should be described by the collection of collective variables (6). If one of the system's slow modes is ignored, the system may gradually overestimate the transition barrier.

3- The variables in the ~~molecular aggregate~~ molecular ensembles should be independent of one another. For instance, in the case of ion adsorption to the surface of portlandite, one collective variable may be the ion's vertical distance from the surface, while another could be the radius distance from the adsorption site. These two collective variables are unrelated to one another and can be used to represent the system well.

4-The number of collective variables d should be kept to a minimum. When a large number of collective variables are used to explore the free energy profile, the step number increases, making convergence slower and increasing computational cost.

Here a brief overview of the main techniques used in the thesis have been generally described. More detailed information for each situation will be described in the relevant chapters.

2.5 References

1 A. Rahman, Correlations in the Motion of Atoms in Liquid Argon. Phys Rev.1964, 136,405–11.

2. P. P. Ewald. Die Berechnung optischer und elektrostatischer Gitterpotentiale. *Ann Phys.* 1921, 369, 253–87.
3. A. Yazdan Yar, Atomistic simulation of bio-relevant ionic and organic species interacting with rutile - Towards the understanding of apatite formation. EPFL Thesis no. 8872, 2018.
4. D. Frenkel BS. Understanding molecular simulations: from algorithms to applications. 2000
5. L. Verlet. Computer experiments on classical fluids. I. Thermodynamical properties of Lennard-Jones molecules. *Phys Rev.* 1967,32,159-169.
6. A. Laio and F. Gervasio. Metadynamics: a method to simulate rare events and reconstruct the free energy in biophysics, chemistry and material science. *Reports Prog Phys.* 2008,71,126601-126608.
7. Galmarini S. Atomistic Simulation of Cementitious Systems. EPFL Thesis No. 5754, 2013.
8. Vineyard H. Frequency factors and isotope effects in solid state rate processes. *J Phys Chem Solids.* 1957, 3,121–7.

Chapter 3

State of the Art – general overview of atomistic simulations in cementitious systems

Force fields accessible for water and sulfate will first be discussed in this chapter since this force fields are base of our developed FF (ERICA FF) in chapter 4. Then, some of the many types of force fields that are available for cementitious systems will be described, as well as an overview of how to apply current force fields to cementitious systems.

More specific details will be given in each separate chapter which focus on separate topics.

3.1 - Potentials for Water

Many prospective water models have been developed over the last three decades. There are three types of water models: rigid, flexible, and polarizable (1). The O-H distance and H-O-H angle are fixed in rigid models. The distance (stretching) and angles are permitted to vary in flexible water models. Polarizable models include an explicit polarization model that should improve the capacity to replicate water in various phases and their interactions. SPC (rigid), SPC/E (rigid), SPC/Fw (2)(flexible), and TIP4P2005 (3)(rigid) are only a few of the most commonly used water models.

The SPC/E and SPC/Fw water models were produced as modifications to the SPC model(4). Compared to the original SPC model, the SPC/E model re-parameterizes the SPC model and improves density, radial distribution function, and diffusion coefficient. Water was simulated by four trial versions in order to get the SPC/E model and for re-parameterization of the SPC model. The best result came from the fourth model. Three point masses with an OH distance of 0.1 nm and an H-O-H angle of 109.5 degrees characterize the SPC/E model. The SPC model was given more flexibility by Wu et al. (2) to produce the SPC/Fw model a flexible model. They looked at the effect of intramolecular degrees of freedom on water system liquid characteristics. According to their findings, the diffusion constant is particularly sensitive to the equilibrium bond length, and this effect is primarily related to the strength of intermolecular hydrogen bonds. They also discovered that the dielectric constant is highly dependent on the equilibrium bond angle. The equilibrium link length and angle are used to optimize bulk diffusion and dielectric constant to

experimental values in this flexible, simple point charge model (SPC/Fw). They believe that their model is superior to the rigid SPC model in terms of performance, and that it is at least equivalent to, if not better than, the rigid SPC/E model.

The TIP4P 2005 (3) model performs well for condensed phases of water. It's a four-site rigid model with three charged fixed points and a Lennard-Jones site. The parameterization was based on a fit of the temperature of maximum density, which was calculated indirectly from the melting point of hexagonal ice, as well as the stability of different ice polymorphs and other factors. A range of thermodynamic parameters of the liquid and solid phases, the phase diagram involving condensed phases, melting and vaporization properties, dielectric constant and pair distribution function, and self-diffusion coefficient are among the estimated properties. The model is applicable at temperatures ranging from 123 K to 573 K, as well as pressures up to 40000 bar. This potential can be regarded as the most precise approximation of the phase diagram up to this point.

Table 3.1 summarizes the main parameters and properties of these various water models. The SPC/Fw model has been used in this work because of its simplicity and it is used in the work of Gale's group (5) for a non-polarizable sulphate force field as discussed in the following section.

Table 3.1. Main parameters and properties of various water models.

	Liquid Water	SPC	SPC/E	SPC/Fw	TIP4P	TIP4P2005
$q_O(e)$	-	-0.82	-0.84	-0.82	-1.11	-1.11
$q_H(e)$	-	+0.41	0.42	0.41	0.55	0.55
$d_{OH}(\text{\AA})$	0.9584	1.00	1.00	1.012	0.95	0.97
HOH angle	104.54	109.47	109.47	113.24	104.52	104.52
$D (10^{-9} \text{ m}^2/\text{s})$	2.3	4.22	2.50	2.32	2.08	2.08
$\rho (\text{g}/\text{cm}^3)$	0.997	0.971	0.998	0.998	0.99	0.99
$C_p (\text{Cal}/\text{mol}/\text{K})$	17.99	23.40	19.43	27.37	19.30	18.90

3.2 Potentials for Sulfate

In this section, we will focus on the two most recent potentials for the sulfate: a nonpolarizable sulfate model proposed by the Gale group (5) and a polarizable sulfate model proposed by Duvail et al (1). The thermodynamics of ion pair production between Ca^{2+} and SO_4^{2-} have been computed by the Gale group using a stiff ion force field, the AMOEBA polarizable force field, and ab-initio molecular dynamic simulations. They produced two new rigid ion force fields (FF1 and FF2) that target the solvation free energy of sulfate. The strongest solvation free energy is more plausible, according to the features of solvated anions and the pairing free energy. They employed the SPC/Fw model for water and Lamberet et al sulfate-water interaction parameters in their simulation(6). The parameters for calcium ions are derived from the AMOEBA09 library. Using the anhydrite structure, they performed relaxed fitting to determine calcium-sulfate interaction parameters. They claim that the FF 1 (notation from their work) can accurately capture the structure of water around the sulfate ion and is comparable to the polarizable model results and those from the ab-initio calculations (Fig 3.1)

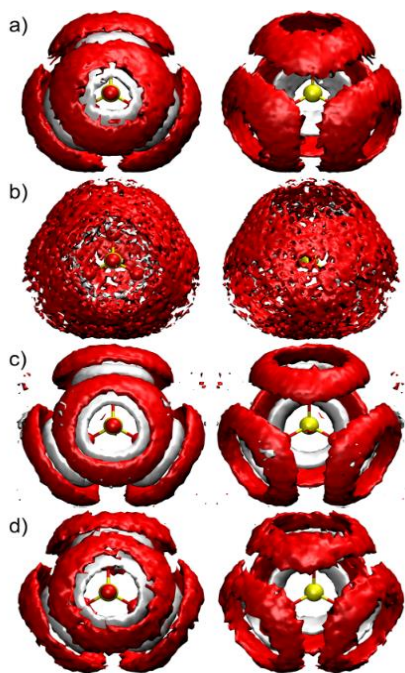


Figure 3.1. Representations of the 3D water structure around the sulfate ion as calculated with FF1 (a), FF2 (b), AMOEBA (c), and BLYP-D3 (DFT) (d). Iso-surfaces for O and H atoms of water are represented in red and white, respectively. The oxygen and sulfur atoms of sulfate

are shown in ball and stick representations, colored in red and yellow, respectively. Image taken from Gale (5)

They also suggest that FF1, rather than FF2, can better describe the solvation structure of sulfate in water and the ion pairing of sulfate and calcium.

The work of Duvail et al. is another force field that accurately depicts SO_4^{2-} behavior in water and ion pair formation (1). To mimic the structural and thermodynamic features of the aqueous phase, they built a polarizable force field for sulfate anions (expanded from a nonpolarizable model). Two force fields were investigated and employed with molecular dynamics simulations, each with differing atomic partial charges on S and O. In addition, the potential of the mean force of sulfate electrolytes has been computed using simulations of sulfate anions in aqueous solutions. Their findings are in good agreement with those of the experiments. The non-polarizable force field of Gale's group (5) was chosen for its simplicity and the fact that the main interest in the thesis is sulphate in solution which is well described and less computationally expensive than the polarizable model.

3.3 Force fields for Cementitious systems

There are many aspects of cement and concrete behavior that would benefit from a better understanding at the atomistic level (7), i) Dissolution of the anhydrous clinker and growth of the solid hydrous cement phases ii) Interaction of chemical additives with anhydrous and hydrous cement phases iii) Influence of replacing clinker with locally available materials (clays, waste materials and recycled materials) which influences the chemistry, hydration dynamics, effect on microstructure development iv) Degradation mechanisms in cement and concrete (corrosion of steel re-inforcements, freeze thaw and sulfate attack) v) Mechanism of waste/cement interactions (storage of radioactive and non-radioactive waste) vi) Understanding the dependence of mechanical and fracture characteristics due to anisotropy, hardness, dislocation dynamics, porosity and impurities, etc. In this section the 5 most popular force fields used in cementitious material modelling are described, highlighting the reasons behind their development. In the cemff review paper(7) more quantitative comparisons of their application can be found highlighting their strong and weak points but will not be included here.

3.3.1 *ClayFF force field*

ClayFF was created in response to a pressing need for a reliable and adaptable force field for molecular simulations of mineral/water interactions, particularly clay and clay-related phases such as metal (oxy-) hydroxides and layered double hydroxides (LDHs)(8). Because the solid material substrate is typically inadequate or poorly defined in terms of crystal structure and composition, computational molecular modeling of such interactions is particularly difficult. They have big unit cells, little symmetry, and a lot of varied composition, and they're usually just microns to sub-micron in size. Because most cementitious materials share the same compositional and structural problems, this force field was quickly applied to molecular simulations of numerous cement-related phases (9). There are two techniques to realistically add the required mobility and flexibility of such complicated hydrated solid without jeopardizing the calculation's accuracy by assuming a fully stiff or frozen surface. In addition to the typically employed electrostatic and van-der-Waals (vdW) terms of the force field, a set of bound interaction terms can be explicitly introduced. This method requires identifying and evaluating all primarily covalent links for each conceivable local interatomic coordination (10). The application of this approach to systems with complicated covalent bond structures, on the other hand, may be difficult due to a lack of experimental data to restrict all of the parameters required for a complete description of the bound interactions. To be easily transferable between models and simulations, the force field parameters must be thermodynamically consistent, that is, they must reproduce structures and surface energies. The force field parameterization's general structure must be basic enough to allow modeling of extremely disordered systems with huge numbers of atoms and to properly capture their complicated and often cooperative behavior. ClayFF's empirical parameters were designed to properly mimic the crystal structures of simple and well-characterized oxides, hydroxides, and oxyhydroxides, such as brucite, portlandite, quartz, and kaolinite (8). Individual atoms do not have their full formal charges in this method; instead, they have so-called partial atomic charges, which experimentally account for electron transport in actual covalent bonds. Partially charged oxygen atoms, for example, have a partial charge of 0.8 to 1.1. They were empirically tuned, along with the van der Waals (vdW) parameters, based on the experimental crystal structure refinements of the above model phases. Water molecules, hydroxyl groups, and bridging and substitution environments all affect the

charge of oxygen and hydroxyl. ClayFF was simplified in that the vdW terms centered on all types of O atoms in crystal structures were assumed to be equivalent to those of the SPC water oxygen, while those centered on the H atoms of structural OH groups were omitted for agreement with the SPC water model (8).

3.3.2 - Interface Force Field

IFF (10) is the classical modeling platform for the construction of inorganic, organic, and biological nanostructures on the 1–10.00 nm scale. For organic and inorganic components, it is based on the thermodynamic consistency of classical Hamiltonians. By employing the same functional form and combination rules, the INTERFACE force field parameterizations have been validated for multiple potential energy expressions, including the COMPASS(11), CHARMM(12), AMBER (13), allowing simulations of inorganic-organic and inorganic-biomolecular interfaces. Chemically significant atomic charges and van-der-Waals parameters are emphasized in IFF parameterization, which is thoroughly validated by observed atomic-scale and surface properties(14) The reasons for this are twofold: chemical bonding is reproduced by a chemically realistic balance of covalent versus ionic bonding, which allows for reactive extensions (10), and it satisfies the requirement for an accurate quantum mechanical Hamiltonian that reproduces structures (X-ray data), energies (e.g. surface energy), and energy derivatives (elastic constants, thermal properties). The investigation of chemical bonding is the first step in developing force field parameters, followed by the confirmation of structural and energetic features that must be consistent with experimental data (10). It entails a thorough examination of inorganic minerals' structural, interfacial, mechanical, and thermal characteristics in order to determine the accuracy of atomistic force field models and the computation of such critical properties under varied processing conditions. In most cases, the confirmation of structure and energy is sufficient for the other quantities to follow without needing to be adjusted further. The atomistic model based on IFF parameters provides a wide range of properties, including lattice constants, densities, surface energies, solid water interface tensions, anisotropies of interfacial energies of different crystal facets, structural properties (IR and Raman spectra), and thermal and elastic constants.

3.3.3 *Cement Force Field (Cement FF)*

The cement force field is notable for its application to all cementitious systems. The force field is created by merging and adapting the potential generated for similar atomic species systems. The calcium oxygen interaction is based on an adaption by Freeman et al. (15) of the force field first constructed by Lewis and Catlow using the formulation of Schroeder et al. (16). Except for the hydroxyl groups, these interactions are based on Buckingham functional forms, and the species have full formal charges (OH). Furthermore, Freeman et al. (15) used TIP3P for the water model, which has been superseded by Abascal and Vega's TIP4P/2005 potential (3), which affords better agreement with the physical and thermodynamic features of water. Freeman et al did not cover silicate-containing systems. The potential values for the silicon–oxygen and oxygen–oxygen interactions are taken from Leeuw and Parker (17), which used polarizable oxygen shells. These were adapted in accordance with the work of Freeman et al. (15) resulting in the Si-O-Si angle being straightened. An Si-O-Si harmonic angle potential was created to remedy this, with the parameters set to fit the empirically reported Si-O-Si angle in quartz. The force field now includes an additional harmonic angle potential that describes the Si-O-H angle. All other atoms, with the exception of water and hydroxyl, have full formal charges. This has the significant advantage of removing the need for particular consideration of model flaws such as surfaces, where partial charges may vary, as well as ion adsorption from the solution. At solid-water interfaces, a complete atomic charge force field is thought to cause excessive restructuring and water density fluctuations. However, there is no evidence of such excessive re-structuring (18) when comparing water density fluctuations at the (0 0 1) surface of portlandite estimated with the current and the partial atomic charge employed in the ClayFF force field(8). Lime, portlandite, alite (triclinic crystal), quartz, tobermorite 9Å and tobermorite 14 Å have all been examined with the resulting force field (19). Validation of the force field's applicability to cementitious systems is based on its ability to reproduce the structure of solvated calcium and hydroxyl ions. Additional validation was obtained by calculating the reaction enthalpies of many chemical reactions involving the above-mentioned minerals/phases and various aqueous species, which were found to be in good agreement with experimental values (19). Empirical formulas for the estimated error in structure and enthalpies have been constructed based on these results.

3.3.4. *Reactive Force Field (ReaxFF)*

ReaxFF is a reactive force field that was originally developed by A.C.T van Duin and coworkers to study combustion processes (20) and was quickly adapted to study inorganic materials (21).

The total potential energy of the system E is calculated in ReaxFF using: bond, angle, torsion, over van der Waals, and Coulombic energies and specific energies. The first four terms in the total energy expression ($E_{\text{bond}}+E_{\text{angle}}+E_{\text{torsion}}+E_{\text{over}}$) (20) explain short-range interactions between bound atoms and correspond to the interatomic two-body bonding energy, three-body angular energy, four-body torsion energy, and a penalty energy to prevent over-coordination. ReaxFF, unlike typical force fields, does not use constant functions to relate interatomic distances or angles to bonding interaction potential energy. The potentials are continuous bond-order dependent functions. That is to say, the bond-order is a quantity that quantifies the electron density in the region between two atoms (22) thereby indicating the strength of their bond. The bond-order is computed from the atomic position and inserted into the potentials at each stage of the simulation, balancing the interaction. When the bond-order between two atoms falls, the interaction energy lowers as well, until it reaches zero, at which point the bond between them effectively breaks. The non-bonded van der Waals and Coulomb energies are represented by the following two terms (E_{vdW} and E_{Coulomb}), while the final term, E_{specific} , includes specific energy terms for special systems, such as hydrogen bonding and ion pairs in water molecules, or conjugation in hydrocarbons. Due to atomic charges, the Coulombic energy is a long-range interaction. An electronegativity equalization technique (EEM) is used in ReaxFF to calculate atomic charges at each simulation step (23). This makes it possible to describe the polarization effects of molecules in various contexts. Finally, each atom has a unique identity, which is a critical feature of the ReaxFF formalism, which is required to perform chemical reactions. For example, whether it is part of a water molecule, tricalcium silicate, or the C-S-H gel, there is only one form of oxygen atom, and it can migrate from one type to another if chemical reactions occur. This is in contrast to non-reactive force fields, in which an atom can have different "identities" depending on the chemical environment. For example, water oxygen and silicate oxygen are not interchangeable and each has its own set of empirical parameters and atomic charge. In fact, the ReaxFF formalism allows for a considerable amount of flexibility when describing molecular properties, but it also allows for accurate simulation of chemical reactions and determination of transition states (24). In comparison to DFT or semi-empirical approaches,

this permits simulation of chemical reactions in much bigger systems (25). The parameterization of the Ca/O/H set by Manzano et al. (26) made it easier to apply ReaxFF to cement research. This set was combined with the existing Si/OH/set (27), resulting in the Si/Ca/O/H set, which may now be used to investigate the most important phases of cement, calcium silicates, and their hydration products (28)

3.3.5 CSH force field (CSH-FF)

CSH-FF is a force field potential for hydrated calcium-silicates that was derived by utilizing structural and elasticity data (9). Because it is designed to predict both structural data and high-order qualities, it is an upgraded version of the core-only model ClayFF(8) (i.e. elastic constants). CSH-FF is less computationally expensive than other force fields like core-shell potentials (29) making it more efficient for bigger systems. The CSH-prediction FF's powers have been extensively tested against first-principles results for two tobermorite polymorphs distinguished by their basal spacing and thus water content: 14 Å tobermorite (30) and 11 Å tobermorite (31). Note that tobermorite polymorphs differ in chemistry in terms of Ca/Si ratio: Merlino's 14 Å tobermorite has a Ca/Si ratio of 0.83, whereas Hamid's 11 Å tobermorite has a Ca/Si ratio ranging from 0.67 to 1, with the one with a ratio of 1 being used. ClayFF has several limitations in predicting higher order qualities like elastic constants because it was meant to predict structural data. ClayFF's low transferability for complicated hydrated calcium-silicate materials necessitates a boost in second-order prediction capabilities (32). CSH-FF is derived via equal weight fitting of 29 parameters (Lennard-Jones parameters + atomic charges) to 29 observable input data. The fitting process is described in greater detail in (9).

Table 3.2 shows examples of the use of these different force fields for simulation of structural cementitious systems

Table 3.2. Examples of the use of different force fields for simulation of structural parameters for some cementitious systems

Mineral	Force field type	Method	Cell dim.	a (nm)	b (nm)	c (nm)	α (°)	β (°)	γ (°)	V (nm ³)	ρ (g/cm ³)	% Error
Portlandite (trigonal)		Experiment [152]	1 × 1 × 1	0.3589	0.3589	0.4911	90	90	120	0.0548	2.246	0
	DFT [158]	EM ^b	1 × 1 × 1	0.369	0.369	0.497	90	90	120	0.0586	2.10	6.48
	ClayFF [44]	MD	1 × 1 × 1	0.357	0.357	0.491	90	90	120	0.0542	2.27	1.09
	IFF ^a	MD	1 × 1 × 1	0.375	0.375	0.438	90	90	120	0.0533	2.30	2.74
	CementFF [46]	MD	1 × 1 × 1	0.368	0.367	0.481	90	90	120	0.0564	2.18	2.92
	ReaxFF [45]	EM	1 × 1 × 1	0.366	0.366	0.486	90	90	120	0.0564	2.18	2.92
Tricalcium silicate (monoclinic)		Experiment [151]	1 × 1 × 1	1.2235	0.7073	0.9298	90	116.31	90	0.7213	3.154	0
	IFF [49]	MD	1 × 1 × 1	1.224	0.704	0.934	90	116.2	90	0.7230	3.15	0.23
	CementFF	MD	1 × 1 × 1	1.243	0.719	0.957	89.7	115.6	90	0.7710	2.98	6.93
	ReaxFF [58]	EM	1 × 1 × 1	1.217	0.708	0.933	90	117.2	90	0.7150	3.18	0.87
Tobermorite-11 Å (monoclinic)		Experiment [153]	1 × 1 × 1	0.6735	0.7385	2.2487	90	90	123.25	0.9354	2.460	0
	DFT [138]	EM	1 × 1 × 1	0.660	0.740	2.313	90	90	123.6	0.9407	2.45	0.57
	ClayFF	MD	1 × 1 × 1	0.677	0.733	2.451	91.1	90	123.1	1.0145	2.27	8.45
	IFF	MD	1 × 1 × 1	0.685	0.737	2.257	90	90	122.5	0.9605	2.40	2.68
	CementFF	EM	1 × 1 × 1	0.687	0.729	2.348	90	88.3	121.8	0.9988	2.30	6.78
	ReaxFF	EM	1 × 1 × 1	0.681	0.765	2.308	90	90	123.9	0.9981	2.31	6.70
Tobermorite-14 Å (monoclinic)		Experiment [134]	1 × 1 × 1	0.6735	0.7425	2.7987	90	90	123.25	1.1704	2.227	0
	DFT [138] ^c	EM	1 × 1 × 1	0.687	0.743	2.849	90	90.1	123.47	1.2131	2.15	3.65
	ClayFF	MD	1 × 1 × 1	0.687	0.737	2.855	89.2	90	122.69	1.2164	2.14	3.93
	IFF [51]	MD	1 × 1 × 1	0.677	0.735	2.785	90	90	122.55	1.1673	2.23	0.26
	CementFF	MD	1 × 1 × 1	0.686	0.727	2.741	88	91	123	1.1520	2.27	1.57
	ReaxFF [33]	EM	1 × 1 × 1	0.668	0.750	2.833	91.1	89.4	124.32	1.1720	2.22	0.14
	CSH-FF [43]	EM	1 × 1 × 1	0.67	0.741	2.870	90	89.8	123.77	1.1909	2.19	1.75

^a Reproduction of lattice parameters has been done using supercell of $\sim(1.5 \times 1.5 \times 1.5 \text{ nm}^3)$. Parameters have been normalized to make it compatible to compare with others

In conclusion, the many types of force field used for cementitious systems are more or less specific for particular systems, interfaces, property prediction or limited in their atom types. There still seems to be a need for a more general or universal forcefield that is easily transferable and useable for the many different types of systems and interfaces of interest in cementitious materials. This was the initiator for the ERICA force field developed in this thesis in chapter 4. It may not yet be universal but can become a good solid starting point.

3.4 Applications force field for molecule and ion adsorption on cementitious systems.

In this section, some of the applications of the various force fields in cementitious systems are highlighted. Concentrating on the surfaces of cement hydrates portlandite (CH) and C-S-H, in particular the adsorption of ions such as calcium, hydroxyl, sulfate and silicate. For the case of small organic molecules (e.g. gluconate) of interest in cementitious systems has been left for chapter 6 of the thesis.

3.4.1 interaction of ions with CH interaction

By modelling the adsorption of Ca^{2+} and OH^- at different portlandite surfaces, Galmarini et al. (18) examined the growth of portlandite in aqueous systems using Cement FF. Both molecular dynamics, conventional and well-tempered metadynamics calculations were performed. Different adsorption sites were detected depending on the structure of the portlandite–water interface. They were able to propose an atomistic mechanism for portlandite growth in various crystallographic directions based on these findings. Different species govern growth in different directions, according to the hypothesized mechanism, which is compatible with experimental findings in the literature. The morphology of portlandite particles precipitated from lime solutions is equiaxed rather than dominated by the 00.1 surface, which is a perfect cleavage plane, according to the experimental section of their work. This is due to the creation of a network of firmly bonded surface water at the 10.1 and 10.0 surfaces, which stabilizes those surfaces both energetically and kinetically, according to conventional atomistic molecular dynamics models. They were able to gain a better understanding of the growth process of portlandite at various portlandite–water interfaces thanks to MTD simulations. They hypothesize that:

- dehydration and adsorption of the Ca^{2+} ion at the (00.1) surface; and
- desorption of strongly bound surface water and subsequent adsorption of OH at the (10.1) surface are the rate-determining steps for growth in distinct directions.
- desorption of highly bound surface water and subsequent adsorption of Ca^{2+} at the (10.0) surface is the key step here; another mechanism for this would be the transfer of a proton from the water to a nearby hydroxyl in solution, but such a process would have to be examined by an alternate approach as the classical methods used cannot take these interactions into account.

Based on these conclusions, they proposed growth mechanisms to explain changes in portlandite morphology with changing Ca/OH ratios observed experimentally(33), where an increase in pH was observed to lead to an increased aspect ratio of 10.1/00.1, whereas an increase in relative calcium concentration led to elongated particles dominated by 00.1 surfaces.

Galmarini et al. (19)) also used atomistic simulations to provide evidence and offer a method for understanding the relationship between CH and CSH growth, again using Cement FF. They evaluated the adsorption of silicate species at three different portlandite surfaces ([00.1], [10.1], and [10.0]) using atomistic-scale simulations to acquire a better understanding of portlandite formation in cementitious systems. The charge neutral $\text{CaSiO}_2(\text{OH})_2$ complex and the $\text{SiO}_2(\text{OH})_2^{2-}$ ion were examined as the two primary silicate species indicated by thermodynamic modeling. Metadynamics simulations validated the stability of the CaSi complex, which had previously been questioned. The estimated free energy of complex formation agreed reasonably well with the energy found experimentally. Both species adsorb on the portlandite surfaces via hydrogen bonding, with one or both of the hydroxyl groups contributing a hydrogen bond to surface oxygen atoms, according to metadynamics calculations. The neutral CaSi complex, however, has a substantially longer residence period than the silicate ion, indicating that the CaSi complex has greater interaction with the portlandite surfaces. Both silicate species appear to retain some mobility while remaining adsorbed on atomically flat surfaces ([00.1] and [10.1]). While at the [10.0] surface a more tightly bonded adsorption site exists as well, where the silicate species remains immobile. The silicate species adsorb to the step-like exposed Ca ions on the [10.1] as it is a Ca terminated surface. The adsorption free energy profiles determined for the [00.1] surface revealed that the neutral $\text{CaSiO}_2(\text{OH})_2$ complex had dramatically different energy profiles than the $\text{SiO}_2(\text{OH})_2^{2-}$ ion. There were two distinct minima for the CaSi complex, but none for the silicate ion. The stability of the mobile CaSi complex at the surface was confirmed by the free energy profile and unconstrained MD simulations. This showed that the CaSi combination adsorbs preferentially compared to calcium and hydroxyl ions, which had previously been examined. These findings led to the discovery of a mechanism for reduced portlandite growth and poisoning in the presence of silica, in which the CaSi complex preferentially adsorbs compared to the growth species and can travel along surfaces until they reach a step-like growth feature, where they are immobilized. The hypothesized mechanism can account for previously observed experimental results. Finally, the combined use of molecular dynamics, well-tempered metadynamics, and conventional metadynamics has provided a deeper understanding of the interaction of silicate species with portlandite surfaces, and how these interactions may influence growth and, as a result, cement hydration kinetics.

3.4.2 interaction of ions with C-S-H interaction

Hou et al. (34) investigated the microstructure of Portland cement paste (PC) and PC with granulated blast furnace slag (PC-GBFS) curing in both water and the sulfate sodium solution for 365 days using ^{29}Si and ^{27}Al MAS NMR spectroscopy combined with SEM-EDS methods. They used molecular dynamics to analyze the molecular interactions between sulfate ions and the C-A-S-H gel using the CLAY FF force field. For the PC system the sulfate ions dragged interface Ca^{2+} ions into the pore solution, forming ionic clusters of Ca-SO_4 and causing the C-A-S-H gel to decalcify. With a lower Ca/Si ratio in PC-GBFS the Si-O-Ca bonding is more stable in the C-A-S-H gel with an intact alumino-silicate chain structure, and the Ca ions can stay in the C-A-S-H gel for longer.

Elaknesweran et al. (35) looked at the surface charge mechanism of cement hydrates and how it relates to chloride adsorption, using MD. Physical binding is caused by ionic adsorption on the surface, while chemical binding is caused by the reaction of chloride with the hydrated cement phase (i.e. Friedel's salt production). By dissociation, Portlandite and Friedel's salt have positively charged surfaces and can physically adsorb chlorides. C-S-H, on the other hand, dominates the physical adsorption of chlorides in HCP. The chloride adsorption on the C-S-H surface was accurately predicted using a surface complexation model. Chlorides adsorb physically onto the surface of C-S-H, resulting in a negative surface charge.

Kalanichev et al. (36) studied the structure and dynamical behavior of chloride and related cations at the interfaces between aqueous solutions and portlandite ($\text{Ca}(\text{OH})_2$), Friedel's salt ($[\text{Ca}_2\text{Al}(\text{OH})_6]\text{Cl}_2\text{H}_2\text{O}$), tobermorite ($\text{Ca}_5\text{-Si}_6\text{O}_{16}(\text{OH})_2$), and ettringite ($\text{Ca}_6[\text{Al}(\text{OH})_6](\text{SO}_4)$). In their simulations, they employed CLAY FF. Their main focus was on the structure at and near the solution/solid interfaces, as well as the molecular mechanisms of aqueous Cl^- , Na^+ , and Cs^+ ion adsorption on a neutral portlandite surface and comparisons to Cl^- sorption behavior on Friedel's salt's positively charged surface. Also estimated were molecular motion power spectra for bulk and surface species, diffusion coefficients for Cl^- , Na^+ , and Cs^+ ions in various surface-related settings, and mean residence periods on surface sites. They discovered the diffusion coefficients of Cl^- in an inner-sphere surface complex are lowered by nearly an order of magnitude compared to those in bulk solution; those in outer-sphere complexes are reduced less, and the coefficients

for both types are reduced more for Friedel's salt than for portlandite. On tobermorite, there was no Cl^- adsorption, while on ettringite, there was just a small amount. Experimental sorption and ^{35}Cl NMR analyses were in good qualitative agreement with the simulated results. The MD data adds to the growing body of evidence that chloride binding on C-S-H is related to sorption on surface locations that are identical to those found on portlandite. The MD simulations show how important it is to account for the mobility and flexibility of the surface OH groups when modeling realistic local electrostatic conditions conducive to cation and anion adsorption on hydroxides. The bending and stretching of hydrogen bonds established among the anions, surface hydroxyls, and surrounding water molecules drive the dynamics of the translational motions (low-frequency vibrations) of Cl^- absorbed on the surfaces of portlandite and Friedel's salt. They claim that a well-developed H-bonding network forms across the aqueous phase-calcium hydroxide interface, whereas the formation of such a tetrahedrally ordered network of H-bonds is prevented in the interfacial region of the Ca_2Al double hydroxide (Friedel's salt) due to the polarizing effect of its structural charge. The chloride-binding capacity in their MD simulation showed a decreasing trend in the following order Friedel's salt > portlandite > ettringite > tobermorite. Their research emphasized the good agreement of the simulated parameters with existing experimental data for the systems.

Tu et al. (37) investigated coupled ion transport in the two primary hydration products of aluminum-doped cement-based materials, namely calcium aluminate-silicate hydrate (C-A-S-H) gel and calcium hydroxide (CH). In three different solutions (1 mol/L NaCl, 0.5 mol/L NaCl + 0.5 mol/L Na_2SO_4 , and 1 mol/L Na_2SO_4), each material was simulated using MD. Sulfate ions were discovered to stimulate the aggregation of other ions in solution to create ion clusters that block the nanopores of the materials and prevent their degradation. Because the ion clusters in the C-A-S-H gel are adsorbed at the interface, causing "necking," whereas in CH, they flow with the solution and are not adsorbed at the material's surface, the degree of this reduction is substantially greater. Sodium ions bind to C-A-S-H gels more strongly than chloride ions, whereas the reverse is true for CH. As a result, the two hydration products have significantly different impacts on ion transport.

To better understand the nanoscale mechanism of the composite material subject to chemical attack, Hou et al. (38) used molecular dynamics to investigate the capillary adsorption of NaCl

and Na_2SO_4 solutions in the nanometer channel of the calcium silicate hydrate (C-S-H) coated with epoxy employing the CLAY FF force field. Anion-cation couples are formed when SO_4 and Cl ions combine with Na and Ca ions. The creation of an interfacial chemical bond and an ionic pair in the solution reduces the ion transport rate even more. The ions and water in the gel pore, on the other hand, can gradually infiltrate the interfacial region between the epoxy molecule and the C-S-H substrate, causing the Ca ions to diffuse away from the substrate, part of the epoxy chains to dissociate from the silicate chains, and the interfacial connection to weaken.

Molecular dynamics simulations were used to explore the adsorption mechanisms of cesium at calcium-silicate-hydrate surfaces by Bu et al. (39). The calcium-silicate-hydrate analogues investigated were – tobermorite 9 Å, tobermorite 14 Å, and jennite. Their research shed light on the significance of distinct calcium-silicate-hydrate phases in the immobilization of radionuclides in cementitious materials, revealing that the charge and structure of the solid surface layer had a significant impact on the immobilization mechanisms. The following is a summary of the main findings:

- Cs^+ ions, prefer to be adsorbed as inner-sphere complexes on the tetrahedral SiO_4 and octahedral CaO_6 surfaces of tobermorite 9 Å and tobermorite 14 Å

-The competition for surfaces between water molecules and Cs^+ ions altered the mechanisms of Cs^+ ion adsorption as inner-sphere or outer-sphere complexes, e.g. hydrogen bonding at the surfaces of jennite was predicted to reduce Cs^+ ion adsorption and favor outer-sphere adsorption.

3.5 Summary and conclusion

There are many force fields that can be used to mimic cementitious systems, but their accuracy is highly dependent on the experimental data that was utilized in the force field development. In this thesis, we attempt to create a new force field that is very general and capable of performing well in a variety of situations. We believe that more research is needed in the cement industry to develop a force field that is more suited than current force fields. In order to model all cementitious systems, the created force field must be generic and contain enough interaction parameters. Second, it must be reasonably precise, particularly when calculating reaction enthalpies.

3.6 References

1. Duvail M, Villard A, Nguyen TN, Dufrêche JF. Thermodynamics of Associated Electrolytes in Water: Molecular Dynamics Simulations of Sulfate Solutions. *J Phys Chem B*. 2015;119(34):11184–95.
2. Wu Y, Tepper HL, Voth GA. Flexible simple point-charge water model with improved liquid-state properties. *J Chem Phys*. 2006;124:1–12.
3. Abascal JLF, Vega C. A general purpose model for the condensed phases of water: TIP4P/2005. *J Chem Phys*. 2005;
4. H.J.C.Berendsen, J.R, Grigera T. S. the missing term in effective pair potentials. *Phys Chem*. 1987;91:6269–71.
5. Byrne EH, Raiteri P, Gale JD. Computational Insight into Calcium-Sulfate Ion Pair Formation. *J Phys Chem C*. 2017;121(46):25956–66.
6. Lambrecht DS, Clark GNI, Head-Gordon T, Head-Gordon M. Exploring the rich energy landscape of sulfate-water clusters $\text{SO}_4^{2-}(\text{H}_2\text{O})_n$, $n=3-7$: An electronic structure approach. *J Phys Chem A*. 2011;41:11438–54.
7. Mishra RK, Mohamed AK, Geissbühler D, Manzano H, Jamil T, Shahsavari R, et al. cemff: A force field database for cementitious materials including validations, applications and opportunities. Vol. 102, *Cement and Concrete Research*. 2017. p. 68–89.
8. Cygan RT, Liang JJ, Kalinichev AG. Molecular models of hydroxide, oxyhydroxide, and clay phases and the development of a general force field. *J Phys Chem B*. 2004;108:1255–66.
9. Shahsavari R, Pellenq RJM, Ulm FJ. Empirical force fields for complex hydrated calcio-silicate layered materials. *Phys Chem Chem Phys*. 2011;
10. Heinz H, Lin TJ, Kishore Mishra R, Emami FS. Thermodynamically consistent force fields for the assembly of inorganic, organic, and biological nanostructures: The INTERFACE force field. *Langmuir*. 2013;
11. Sun H. COMPASS: an ab initio force-field optimized for condensed-phase applications -

- overview with details on alkane and benzene compounds. *J Phys Chem B*. 1998;102:7338–64.
12. MacKerell AD, Bashford D, Bellott M, Dunbrack RL, Evanseck JD, Field MJ, et al. All-atom empirical potential for molecular modeling and dynamics studies of proteins. *J Phys Chem B*. 1998;
 13. J.M. Wang, R.M. Wolf, J.W. Caldwell, P.A. Kollman DAC. Development and testing of a general amber force field. *J Comput Chem*. 2004;25:1157–74.
 14. Heinz H, Vaia RA, Farmer BL, Naik RR. Accurate simulation of surfaces and interfaces of face-centered cubic metals using 12-6 and 9-6 lennard-jones potentials. *J Phys Chem C*. 2008;
 15. Freeman CL, Harding JH, Cooke DJ, Elliott JA, Lardge JS, Duffy DM. New forcefields for modeling biomineralization processes. *J Phys Chem C*. 2007;111(32):11943–51.
 16. G.V. Lewis CRAC. Potential Models for Ionic Oxides. 1985;1149–61.
 17. Leeuw NH, Parker SC. Effect of Chemisorption and Physisorption of Water on the Surface Structure and Stability of alpha-Alumina. *J Am Ceram Soc*. 2004;82(11):3209–16.
 18. Galmarini S, Bowen P. Atomistic simulation of the adsorption of calcium and hydroxyl ions onto portlandite surfaces - Towards crystal growth mechanisms. *Cem Concr Res*. 2016;81:16–23.
 19. Galmarini S, Kunhi Mohamed A, Bowen P. Atomistic simulations of silicate species interaction with portlandite surfaces. *J Phys Chem C*. 2016;120(39):22407–13.
 20. Van Duin ACT, Dasgupta S, Lorant F, Goddard WA. ReaxFF: A reactive force field for hydrocarbons. *J Phys Chem A*. 2001;
 21. Van Duin ACT, Strachan A, Stewman S, Zhang Q, Xu X, Goddard WA. ReaxFFSiO reactive force field for silicon and silicon oxide systems. *J Phys Chem A*. 2003;
 22. A.D. McNaught AW. *Compendium of Chemical Terminology*. 1997;
 23. P. Bultinck, W. Langenaeker, P. Lahorte, F. De Proft, P. Geerlings, M. Waroquier JT. The

- electronegativity equalization method I: parametrization and validation for atomic charge calculations. *J Phys Chem A*. 2002;106:7887–94.
24. Yeon J, Van Duin ACT. ReaxFF Molecular Dynamics Simulations of Hydroxylation Kinetics for Amorphous and Nano-Silica Structure, and Its Relations with Atomic Strain Energy. *J Phys Chem C*. 2016;
 25. Plimpton SJ, Thompson AP. Computational aspects of many-body potentials. *MRS Bull*. 2012;
 26. H. Manzano, R.J.M. Pellenq, F.-J. Ulm, M.J. Buehler ACT van D. Hydration of calcium oxide surface predicted by reactive force field molecular dynamics. *Langmuir*. 2012;28:4187–97.
 27. J.C. Fogarty, H.M. Aktulga, A.Y. Grama, A.C. Van Duin SAP. A reactive molecular dynamics simulation of the silica-water interface. *J Chem Phys*. 2012;132:174704.
 28. H. Manzano, S. Moeini, F. Marinelli, A.C. Van Duin, F.-J. Ulm RJ-MP. H. Manzano, S. Moeini, F. Marinelli, A.C. Van Duin, F.-J. Ulm, R.J.-M. Pellenq. *J Am Chem Soc*. 2012;123:2208–15.
 29. Gale JD. Empirical potential derivation for ionic materials. *Philos Mag B Phys Condens Matter; Stat Mech Electron Opt Magn Prop*. 1996;
 30. Bonaccorsi E, Merlino S, Kampf AR. The crystal structure of tobermorite 14 Å (plombierite), a C-S-H phase. *J Am Ceram Soc*. 2005;88:505–12.
 31. Hamid SA. The crystal structure of the 11 Å natural tobermorite $\text{Ca}_{2.25}[\text{Si}_3\text{O}_7.5(\text{OH})_{1.5}]\text{H}_2\text{O}$. *Zeitschrift fur Krist - New Cryst Struct*. 1981;
 32. R. Shahsavari, L. Chen LT. Edge dislocations in dicalcium silicates: experimental observations and atomistic analysis. *Cem Concr Res*. 2016;90:80–8.
 33. Gallucci E, Scrivener K. Crystallisation of calcium hydroxide in early age model and ordinary cementitious systems. *Cem Concr Res*. 2007;37:492–501.
 34. Ding Q, Yang J, Hou D, Zhang G. Insight on the mechanism of sulfate attacking on the cement paste with granulated blast furnace slag: An experimental and molecular dynamics

- study. *Constr Build Mater.* 2018;169:601–11.
35. Y.ElakneswaranT.NawaK.Kurumisawa. Electrokinetic potential of hydrated cement in relation to adsorption of chlorides. *Cem Concr Res.* 2005;39:340–4.
 36. Kirkpatrick AGK and RJ. Molecular Dynamics Modeling of Chloride Binding to the Surfaces of Calcium Hydroxide, Hydrated Calcium Aluminate, and Calcium Silicate Phases. *Chem Mater.* 2002;8:3539–3549.
 37. Y.Tu, R.Wen QY. Molecular dynamics study on coupled ion transport in aluminum-doped cement-based materials. *Constr Build Mater.* 2021;295:123645.
 38. Hou D, Search author for Hou D, , Li, Dengke, Yu, Jiao, Zhang P. Insights on Capillary Adsorption of Aqueous Sodium Chloride Solution in the Nanometer Calcium Silicate Channel: A Molecular Dynamics Study. *J Phys Chem C.* 2017;121:13786–97.
 39. J.Bu, R.Gonzalez, Teresa, K.G.Brown FS. Adsorption mechanisms of cesium at calcium-silicate-hydrate surfaces using molecular dynamics simulations. *J Nucl Mater.* 2019;515:35–51.

Chapter 4

Molecular dynamic simulations of cementitious systems using a newly developed force field suite ERICA FF

This chapter has been submitted as a paper to the International Journal of Cement and Concrete Research the premier journal in cement and concrete science. At the time of writing the thesis it is currently under review. The paper deal with the development of the ERICA force field suite ERICA FF1, FF2 and FF3 and their validation which extends and further develops previous force fields used by our group as described in detail here.

4.0 Abstract

A force field suite, ERICA FF has been developed for the simulation of cementitious systems. It has been validated for structural, energetic and mechanical properties. It covers the species Ca, OH, sulfate, water, Si, Al, Na, K and Cl. We have simulated structural properties of 19 cementitious systems. Results show that all errors are acceptable with less than 6% on length parameters and 5 degrees on angles. Furthermore, we have validated the suite with the simulation of 16 reaction enthalpies, again with reliable results. Also, hydration enthalpies of ions of interest for transport properties using the flexible SPC/Fw water model have been evaluated. Good correspondence between experiment and simulation, for the mechanical properties of several systems were found; namely, lime, portlandite, quartz, tricalcium silicate, and tobermorite. The results obtained show that the ERICA FF suite demonstrates a very good all-round performance for simulation of cementitious systems.

Keywords: Cement, Molecular simulation, Force field (FF), Cementitious systems, Molecular dynamics

4.1 Introduction

It has been more than 2000 years that cement has been used in concrete for construction purposes [1]. Concrete is the largest material by volume produced by humans and it is expected that its quantity will double in the next 30 years. Consequently, much research has been carried out on the development of high-performance sustainable materials towards the reduction of carbon dioxide produced by the cement industry [2]. At the moment 6 to 8 % CO₂ emission in the world

is due to the cement industry [3]. About 60 percent of CO₂ emission in the cement industry is due to the decomposition of limestone which makes up almost 80 percent of the raw material used to produce cement. The reduction of CO₂ can be obtained by using new alternative materials, supplementary cementitious materials (SCMs), such as calcined clays, limestone, fly ash, slag, and silica fume [4-7]. Poor early age strength and poor knowledge of atomistic scale mechanisms of cement hydration reactions and microstructure formation that contribute to early age strength, limit the amount of SCMs that can substitute the basic Portland cement.

Understanding cement at the atomistic scale can help us to better understand the molecular mechanisms at play in cement hydrate formation. Atomistic simulations have already been shown to help understand certain aspects of the hydration and atomic structural features, in particular for the main hydration phase of calcium-silicate hydrate (C-S-H) [8-15] and the interaction of ions with portlandite [16,17] and tricalcium silicate [18].

An important prerequisite for atomistic simulations is the availability of reliable classical atomistic force fields and many force fields for cementitious systems have been reported in literature [2]. Most of these force fields include a set of potentials for materials involving Calcium, Hydroxide, Silicon, Oxygen, Aluminum and water, the main constituents of cementitious materials. As Mishra et al. [2] highlighted in their recent paper, it is often difficult to compare the strengths and weaknesses of different force fields for cementitious systems, motivating the development of the cemff database. The cemff database (<https://www.cemff.org/>) provides an online platform of user-contributed force fields, calculation input files, and benchmarking data, targeted to be able to give a quick comparison of how each force field performs in a given situation. The library takes the form of a web-application with a simple user interface allowing consultation and editing of the different items stored in the database. The authors reviewed the most widely used potentials and generally speaking, each force field performs reliably in the simulations it has been validated for. Therefore, it can be noted that there is no force field which performs well in all conditions. For example, CSH-FF is fitted to several ab-initio-based lattice parameters and elastic constants of tobermorite, thus it does a good job in predicting equilibrium and mechanical properties of C-S-H phases. However, it cannot predict reactive phenomena, whereas the REAXFF can account for reactivity but is less accurate than say the IFF for mechanical properties [2] [19]. ClayFF [20] is a very general force field with low computational cost, but does not give satisfactory results for 14 Å tobermorite [2]. The Cement

FF force field was found to be very versatile for the different cementitious systems of interest although sometimes less accurate than say IFF [12], but is a good alternative for exploratory simulations, where the specificity of IFF can be difficult to implement [2]. The IFF captures the structural behavior more accurately and has also the advantage of compatibility with force fields used for organic materials [19]. However, it also has limitations as it is not validated with respect to the energetics and thus the transferability of parameters from one system to another similar system is limited when compared to more general force fields.

In the current work, we will describe the development of the ERICA force field which is an extension of the Cement FF type forces fields [2,11,12,17]. The ERICA FF has been developed for use in LAMMPS [21] for wide accessibility. The aim of the new force field development is to extend the applicability by including Al^{3+} , SO_4^{2-} , K^+ , Na^+ , and Cl^- , thus providing a very versatile force field with well characterized accuracy and includes all the major chemical elements in cement chemistry.

4.2. Methods

In this section, the approach used to develop the force field will be highlighted before discussing the detailed results and validation in the subsequent sections. A schematic of the approach used is given in Figure 4.1. Please note that in this flowchart by refinement I mean changing potential parameters in order to get simulated results closer to experimental values. This was carried out by changing parameters manually in order to get the desirable results. For example, we decreased the A parameter of Buckingham potential between Ca-Osi manually in order to get 7-fold coordination of Ca in the main layer in tobermorite. Due to the extensiveness of the complete force field, it will be described in three different parts:

- The core consisting of calcium, hydroxide, water, and sulfate (ERICA FF1).
- An extension of the force field to include silicates and aluminates (ERICA FF2).
- An extension of the force field to include different solvated ions i.e. Na, K, Cl (ERICA FF3).

Four different interaction types between atomic species are considered in the force field: Coulombic (electrostatic) interactions, short-range Van der Waals interactions (VdW), bonded pair-wise and angle interactions. For most ion-ion pairs, Van der Waals interactions are only

considered for species of opposite charges, as those are the ones that can enter in close contact (details and exceptions can be found in the Annex 1). Bonded species interact via harmonic and Morse potentials and for some bonded interactions like $\text{H}_{\text{OH}}-\text{O}_{\text{OH}}$ there are short and long -range interactions in addition to bonded interactions. A short-range cutoff of 8.5 Å was used and the long-range interactions were calculated via periodic boundaries and the Ewald summation. The full force field equations can be found in section S1-4 of the Annex 1.

Before the production run, the equilibration of the system was monitored by plotting the total energy of system with respect to the time of simulation. The system was considered in equilibrium if the energies and unit cell parameters (in the anisotropic NPT ensemble) fluctuated around a constant value for at least 150 ps. The thus determined equilibration times were approximately 200 ps. The production run was then done for 800 ps. In all simulations, a time step of 0.0007 ps was used in the absence of adiabatic shells (ERICA FF1) and 0.0002 ps for calculations with adiabatic shells (for silica oxygen in ERICA FF2, see section 4.3.1-tobermorite). All calculations were done at constant pressure and temperature, with flexible angles and simulation cell parameters in the case of solids (anisotropic NPT ensemble) and with constant cell geometry in the case of liquids (isotropic NPT ensemble), using a Noose Hoover thermostat barostat.

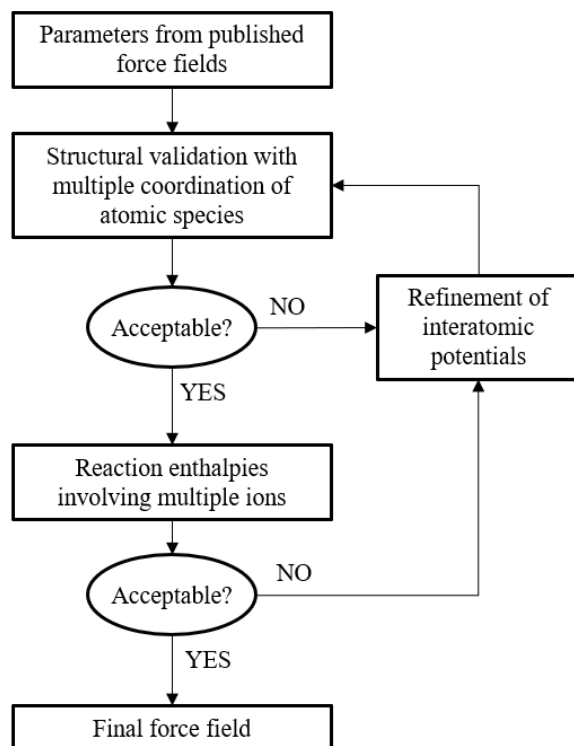


Figure 4.1. Flow diagram of developing a force field

4.2.1 Ca, OH, water, sulfate force field core (ERICA FF1)

The core of the ERICA force field are parameters for calcium, sulfate, hydroxyl ions and water molecule. The idea behind developing this force field was to extend the Cement FF suite to include sulfate containing systems as sulfate has a significant effect on the morphology of portlandite [22]. All parameters are shown in the supporting information (SI-S4). ERICA FF1 is a combination of parameters from three Force Fields. It uses SPC/Fw [23] potential for water and for sulfate it uses potentials developed by Byrne et al. [24]. For portlandite it uses Cement FF1 [2,17]. For the interaction of portlandite with water we have adjusted the potential of Cement FF1 (which uses TIP4P/2005 for water) since the charges of H and O in two water models are different. We fitted Buckingham potentials for ERICA FF1 to the Lennard-Jones potentials of Cement FF1. ERICA FF1 has parameters for portlandite ($\text{Ca}(\text{OH})_2$), calcium, sulfate, hydroxyl and water

The simple SPC/Fw [22] model used for water is very similar to the SPC and SPC/E [25] water models. Bonds and angles are flexible in this model and for transport properties, such as

diffusion coefficients, it gives better results in comparison to all different versions of SPC and TIP4P and TIP3P [26]. It contains only three sites to represent the behavior of water and its simplicity and good performance make it a very suitable model.

Byrne et al. [24] in their recent paper developed two non-polarizable force fields for Sulfate to simulate Calcium and Sulfate ion pair formation, using the SPC/Fw water model. They compared the results of the force field used with the polarizable AMOEBA FF [27] force field as well as with DFT simulations. They found that the force field used here is remarkably consistent with both DFT and available experimental data such as the solvation enthalpy of sulfate and the water coordination number around the sulfate ion. These results motivated our choice of this force field for ERICA FF1.

4.2.2 Silicate-Aluminate extension (ERICA FF2)

After developing the sulfate parameters in the simple ERICA FF1, we then included the parameters for silicon and aluminum, which are key atoms in cementitious systems. As for Cement FF2 [12] we used a polarizable core-shell oxygen potential for oxygen bonded to silicon [28]. All sets of parameters can be found in the Annex 1-S1 and S2).

We already briefly reviewed Cement FF1 in the introduction which gives good general results for portlandite interfaces and their interaction with different ions [16,17,21]. Cement FF2 is a modification of Cement FF1 which uses a polarizable shell for oxygens attached to silicon [29]. An improved version of Cement FF2 with added aluminum interactions from de Leeuw and Parker [30] was successfully used to simulate the bulk structure of C-A-S-H [12]. de Leeuw and Parker [30] presented a set of potentials for aluminum and silicon. They studied chemisorption and physisorption of water onto the [00.1], [10.1], [112], and [243] surfaces of α -alumina using potentials that were verified against the structures of hydrated β -alumina and diaspore. The calculated energies of both physisorption and chemisorption agree well with experimentally obtained hydration energies. The accuracy of their model to represent physisorption and chemisorption shows that their model is carefully developed and validated from energetic and structural points of view.

ERICA FF2 uses the adiabatic core-shell model from Mitchell and Fincham for polarizability, since the limitation of classical empirical force fields is in how the charge distribution of the

molecules is treated [31]. In order to use the model correctly we strictly followed the equilibration procedure from Mitchell and Fincham [31], whereby we decouple the motion of the core-shell pairs and use the Berendsen thermostat to rescale the velocities in combination with the NVE ensemble as the integrator. With this we achieve the adiabatic behavior of shells since thermal energy is not introduced into the core-shell pairs. This special treatment of the core-shells needs to be performed at the start of the equilibration for only 10.000 steps. However, we monitor the kinetic energy of the core-shell pairs through the whole simulation run, to ensure a continuous adiabatic behavior, since any additional amount of kinetic energy could result in failed polarization and rising temperature of the system. For a detailed explanation of the adiabatic core shell model, we refer the reader to the paper from Mitchell and Finchman [31].

4.2.3 Hydrated ions extension (Na, K, Cl; ERICA FF3)

ERICA FF3 is a further extension of ERICA FF2 using parameters based on those of Predota et al. [32] and CLAY FF [20] to include potentials for Na, K, and Cl. These ions are of particular interest for transport properties in cementitious materials as described in more detail in the Annexe1- SI and S4 [33]. We have previously briefly introduced CLAY FF [20], which is a very powerful low cost force field. Predota et al. [32] developed a force field on the basis of ab-initio calculations to be able to calculate the electric double layer at the rutile (110) surface. This allowed them to evaluate the structure of rutile surfaces and interfacial water using molecular dynamics. We have modified slightly the parameters for the systems investigated to get closer to experimental results and to take into account the different water models used. Details are given in Annexe 1

4.2.4 Structural properties

First energy minimization was used in all simulations followed by approximately 150-240 ps molecular dynamic simulation for equilibration and then approximately 750 ps was used for the generation of results. The anisotropic NPT ensemble with Noose-Hover thermostat was used in all simulations where angle and cell dimension were allowed to change during the simulation. For more details on the structural validation, the reader is referred to the Annexe 1-S7.

4.2.5 Energetic validation

A series of chemical reactions involving various species and compounds of interest were used for validation of the energetics. To estimate the errors on reaction enthalpies, an empirical error estimation was used [22], which allows us to better evaluate our force fields from an energetic point of view. More details on the calculation of reaction enthalpies and the error estimate can be found in S6 of the Annex 1.

4.2.6 Hydration enthalpies

For solvation of ions in water in order to validate the force field the enthalpy of a box of water was compared to the enthalpy of box of water containing an ion. This was as successfully used by Dang et al. [34] to give results very close to those found experimentally, supporting their assumption that the energy of the charged background is negligible.

4.2.7 Surface energies

The calculation of surface energies in vacuum is possible with energy minimization only, as finite temperature effects play a minor role [22]. To calculate the vacuum surface energies, we have used a surface region that was allowed to relax in contact with a fixed bulk region and periodic boundary conditions parallel to the surface. The energy of the surface was then compared to the energy of a pure bulk region. If different non-polar surface terminations existed for one surface, the surface termination with the lowest energy was considered. Please note that for portlandite-vacuum surfaces, ERICA FF1 is equivalent to Cement FF1. For calculation of portlandite-water interfacial energies, we compared the energy of a portlandite slab presenting the surface in question in contact with water on one side with the half the energy of a twice as large, equivalent portlandite and the energy of a twice as large, equivalent water slab. We used the NVT ensemble with Noose Hoover thermostat together with a cut of 8.5 Å. The more detailed methodology for calculation of surface energies can be found in [22].

4.2.8 Mechanical property calculation

The ability to predict the mechanical properties of selected structures is an important aspect for the validation of a force field since mechanical properties describe the materials behavior under loading. In this section we describe the methodology that we used to validate Erica FF2 based on overall bulk elastic properties of selected cementitious systems.

We carried out elastic constant calculations at finite temperature as implemented in the LAMMPS code. There are two different approaches for calculating the elastic constants. The first one is to use an isothermal-isobaric (anisotropic NPT) ensemble where it relates the strain tensor fluctuations in the system to the elastic stiffness tensor by statistical mechanics as formulated by Shinoda et al. [35]. The second approach applies small deformations in the linear regime to the simulation box in the canonical (NVT) ensemble. We used the second approach (the canonical ensemble), after observing the heavy dependency of the NPT results on the mass of the barostat. This effect has been observed previously by Clavier et al. [36], where the authors compare different elastic constant calculation methods, confirming our current choice of method.

The calculation protocol was as follows. First, we performed energy minimization, which was followed by an equilibration run for at least 1 ns in the anisotropic NPT ensemble to relax the structure. Afterwards we used the resulting structure of the equilibration run as the starting structure for the elastic constant calculation, which was done for 3.38 ns. During the calculation we carried out 13 cycles, which consisted of 200 ps equilibration, followed by 60 ps of production, in which we carried out positive and negative box displacements, from which the resultant changes in stress are used to compute the elastic stiffness tensor. To validate our calculation protocol, we did a sensitivity analysis and found no change in the final results with an increase in the equilibration run time, production run time, and/or the number of cycles. All calculations were carried out at 300 K, with a time step of 0.0002 ps, and deformation magnitude of 2%.

4.3 Result and Discussion

Results from atomistic simulations are very dependent on the force field used. It is therefore very important to validate the force field carefully. In this work we have first validated the different parts of the ERICA FF from structural and energetic points of view. For further validation, we have then used the force field to simulate the water-portlandite interface and compared the [00.1], [10.0] and [10.1] surface energy in vacuum and water. In addition, we have employed the force field to predict mechanical properties of selected components of cementitious materials including portlandite and tobermorite.

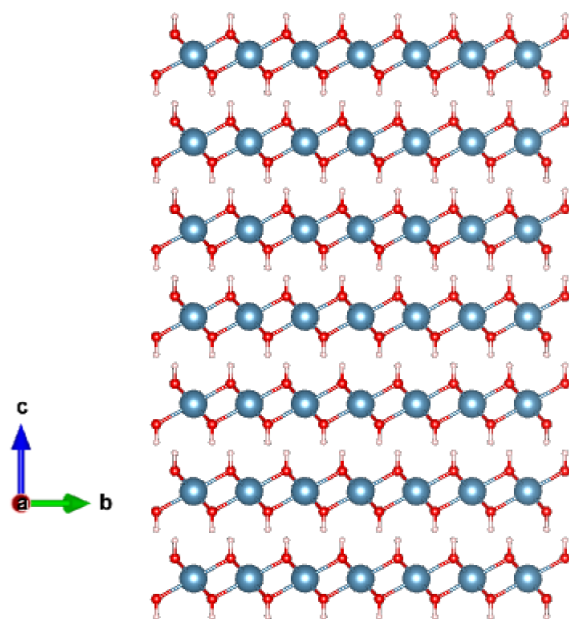
To facilitate their use by other interested parties, the different parts of the ERICA force field (FF1-3) have been introduced into the cemff database (<https://www.cemff.org/>) along with the corresponding LAMMPS scripts.

4.3.1 Structural Validation

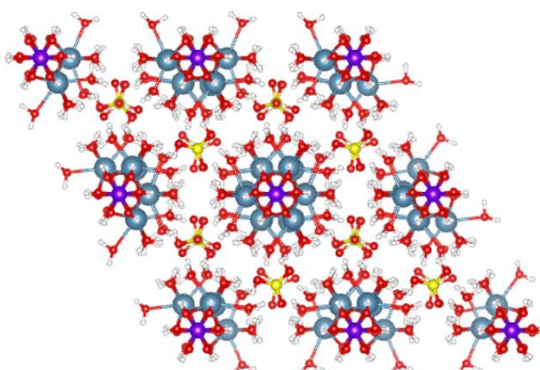
ERICA FF1 and FF2 were used to simulate structural properties of 19 known crystal structures relevant for cementitious systems. The structures were chosen to cover the whole range of components of interest i.e. calcium, silicate, aluminate, hydroxyl, sulfate, and water. Table 4.1 provides a summary of the molecular dynamic results and a comparison to experimental results. All angles of the crystalline unit cells were within 5.2° and the length of the unit cell vectors within 5.2 % of the experimental values. It is out of the scope of this manuscript to discuss structural details of all compounds considered, however we will do so for some of the most important compounds for cementitious systems, namely portlandite, ettringite, 14 Å tobermorite and gypsum.

Portlandite. Portlandite is one of the main products of cement hydration and its structure is quite simple. A super cell of 6x6x6 crystalline unit cells was considered (Figure 4.2 (a)) and as you can see from Table 4.1 there is good agreement between experimental and MD simulated cell parameters and a maximum relative error ($\sim 2\%$) was observed in a and b directions.

Ettringite. Ettringite is an interesting cementitious material with a complex structure (Fig. 4.2(b)). The formula of this compound is $(\text{Ca}_6\text{Al}_2(\text{SO}_4)_3(\text{OH})_{12}\cdot 26\text{H}_2\text{O})$ and some water molecules have partial occupancy in the unit cell structure. We first adjusted the structure to deal with partial occupancy of the water molecule. There are two equivalent positions (top and bottom) in the unit cell containing six water molecules with half occupancy. Although many combinations are possible within a bulk supercell, we considered three water molecules on top and another three sets of water molecules in the bottom position ensuring that all the types of water sites are present according to its occupancy in the structure. The structure of ettringite was important for the validation of the sulfate-hydroxyl interactions, which is present in its structure. As you can see from Table 1, ERICA FF2 performs well with the maximum error of less than 2 % compared to the experimental data.



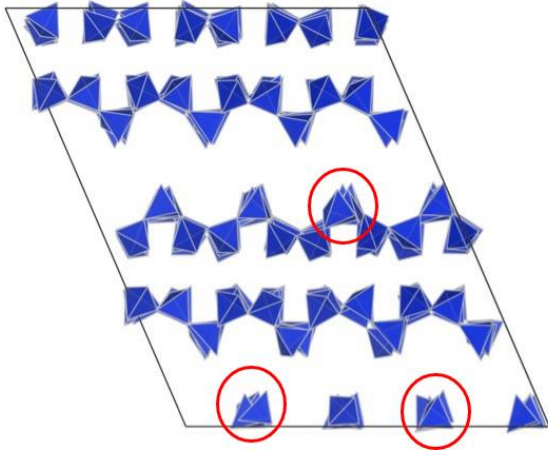
(a)



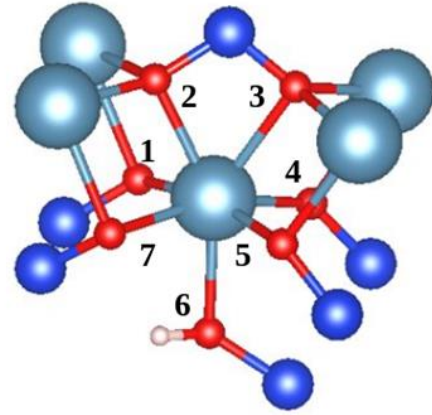
(b)

Figure 4.2. Bulk structure of (a) Bulk structure of portlandite (6x6x6 supercell) and (b) bulk structure of ettringite (2x2x1 supercell). Color code Light Blue: Ca, Purple: Al, Red: O, White: H, yellow: S. Using the ERICA FF (FF1 core for (a) and FF2 extension for (b)).

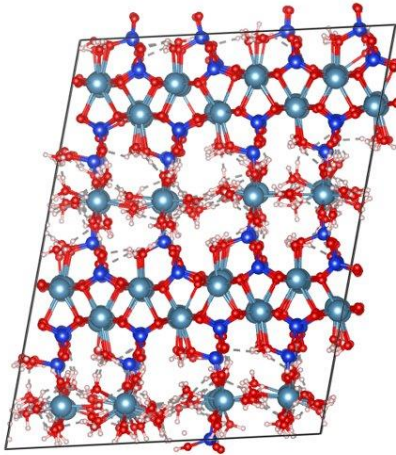
Gypsum. For gypsum, one of the highest errors on the crystalline unit cell vectors is observed (5.21 % in a direction). The only other structure with similar errors is calcium sulfate anhydrate (error of 5.2 % for both a and b unit cell vectors). A reason for the slightly higher deviations for those two structures might be the non-polarizable nature of the oxygens in the sulfate. To get a better impression of the accuracy of the force field, we have also analyzed the different bond



(a) Misorientation of silica tetrahedra in 14 Å tobermorite before final adjustment of the Si-O_w parameters



(b) Structural detail for 14 Å tobermorite showing 7-fold coordination of Ca in the main layer.



(c) Final 14 Å tobermorite structure with final ERICA FF2 forcefield

Figure 4.3. Bulk structure and unit cell of tobermorite 14 Å – after adjustment of Ca-O_{Si} bond and before adjustment of Si-O_w parameters (a) distortion- rotation of Si-O tetrahedra before Si-O_w adjustment (b) 7-fold coordination (c) bulk structure after Si-O_w adjustment. Colour code Ca; turquoise, Si: dark blue, H_{OH}: white O_{Si}: red, O_w: red, H_w: white

lengths in gypsum obtained by MD. The results for sulfur-sulfate oxygen (S-O_s), calcium-water oxygen (Ca-O_w), calcium-sulfate oxygen (Ca-O_s), and hydroxyl hydrogen – water oxygen (H-O_w) are all within 2 percent of the experimental values (table 4.2). In addition, the other sulfate containing structures (ettringite and millosevichite) are described with better

accuracy. Consequently, we considered that the additional computational cost due to a core-shell description of the sulfate oxygens would not be justified by a potential gain in accuracy.

Table 4.1. Comparison between experimental and simulated values of different bond types in gypsum, (O_s – oxygen of sulfate, O_w – oxygen of water).

Bond Type	Bond Length (Å)		Error %
	Experimental	MD	
S- O_s	1.47	1.49	1.36
Ca- O_w	2.36	2.40	1.69
Ca- O_s	2.37	2.41	1.68
H- O_w	1.01	1.03	1.89

14 Å Tobermorite. Tobermorite is of particular interest as its structure is similar to the main hydration product of cement i.e. Calcium-Silicate-Hydrate (C-S-H). For tobermorite, a supercell of 4x4x2 crystalline unit cells [37] was used. The reader should note that at first, we tried to simulate the structure of tobermorite using a non-polarizable oxygen attached to silicon $Si-O_{Si}$ (CEMENT FF1 [2]). However, without a polarizable silicate oxygen we failed to produce 7-fold Coordination of Ca in the main layer of tobermorite based on Experimental evidence [37] shows that Ca in the main layer of 14 Å tobermorite is coordinated with six oxygens of silicon and one oxygen of a hydroxyl or water molecule, so in total seven oxygen atoms.

When observing the structure in more detail we found distortion and rotation of most Si-O tetrahedra (see figure 4.3(a)). Additionally, the calculated Si-O coordination number was slightly above the expected 4.0, a consequence of water molecules coordinating to the bridging silicon tetrahedra in the interlayer. Also, while we managed to obtain the 7-fold coordination of Ca-O in the main layer (Fig 4.4(b), the majority was still 6-fold coordinated, with an exception of one 8-fold coordinated Ca-O, which does not occur in tobermorite 14Å. The reason for this was a slight planar shift of the main layer, which resulted in the calcium and silicon atoms not being vertically aligned.

The problem was solved by using the Si- O_w interaction from Cement FF2 [12] instead of the one from de Leeuw and Parker [30], where the A parameter of the Buckingham potential is

larger, preventing the water molecules from easily coordinating to the silicon. The rotation of Si-O tetrahedra was prevented by switching to a harmonic angle description instead of the three-body non-bonded harmonic potential. This leads to an average Si-O bond length of 1.61 Å. At the same time, the coordination number of Ca-O improved, and is mostly 7-fold in the main layer (6.8 at 3.05 Å cutoff for all calcium in the system, which is in agreement with Bonaccorsi et al. [36]), without any 8-fold coordinated Ca-O in the main layer, as observed experimentally. The calculated radial distribution function for Ca-O shows the first peak is ranging from 2.08 Å to 2.77 Å, with the maximum value at 2.42 Å. The resulting structure is shown in figure 4.6(c) and the coordination number as a function of Ca-O bond length in Fig S1 of the Annex 1.

4.3.2 Energetic validation

To validate the force field from the energetic point of view, the reaction enthalpy of a series of reactions simulated in this work was calculated and compared to experimental results. Due to the different description of water molecules and hydroxyl groups in our force field, for some reactions we need to add a correction term for the dissociation of water ($\text{H}_2\text{O} + \text{O} \rightleftharpoons 2 \text{OH}$). This correction, calculated by estimating the average difference of the calculated to the reported experimental enthalpies of a series of reactions (see more details in Annexe 1 SI 5), was estimated to be 10.4 +/- 0.9 eV. The error on the calculated reaction enthalpies was estimated based on the previously developed error estimation (reference and details in Annex 1 S6). The calculated values can be found in table 4.3 and in figure 4.4. As one can see in figure 4.4, there is a clear correspondence between calculated and experimental reaction enthalpies. Care has to be taken with reactions involving aqueous species where proton exchange within the hydration shell are likely to play an important role (circled in red in figure 4.4). The proton exchange cannot be described with the current force field and its absence in the simulations clearly leads to additional errors.

Table 4.2. Structural validation of ERICA FF for 19 materials of interest. The figure in brackets () after the crystallographic direction from the MD results (a, b, c) is the percentage relative deviation with respect to experimental values (Exp)

No	Name	a (Å)	b (Å)	c (Å)	$\alpha(^{\circ})$	$\beta(^{\circ})$	$\gamma(^{\circ})$	Ref
1	14 Å tobermorite	6.88 (2.3)	7.51 (1.2)	31.28 (2.2)	113.5	92.5	122.46	[37]
	Exp ($\text{Ca}_3\text{Si}_6\text{O}_{16}(\text{OH})_2 \cdot 26\text{H}_2\text{O}$)	6.73	7.42	30.65	111.3	87.3	123.25	
2	Corundum	4.71 (1.0)	4.71 (1.0)	12.94 (0.3)	89.9	90	120.06	[38]
	Exp (Al_2O_3)	4.76	4.76	12.99	90	90	120	
3	Alite	12.37(1.1)	7.15 (1.1)	9.44 (1.5)	90	115.8	90	[39]
	Exp (Ca_3SiO_5)	12.24	7.07	9.3	90	116	90	
4	Gibbsite	8.84 (1.1)	5.18 (1.4)	9.91 (1.1)	90	94.6	90	[40]
	Exp ($\text{Al}(\text{OH})_3$)	8.74	5.11	9.8	90	94.5	90	
5	Millosevichite	8.34 (4.0)	8.34 (4.0)	22.14 (3.7)	90	90.7	120.8	[41]
	Exp ($\text{Al}_2(\text{SO}_4)_3$)	8.02	8.02	21.35	90	90	120	
6	Böhmite	3.59 (3.0)	12.16(4.9)	2.75 (4.2)	90.1	90.1	90.1	[42]
	Exp ($\text{AlO}(\text{OH})$)	3.7	12.22	2.87	90	90	90	
7	Tricalcium aluminate	15.34(0.6)	15.34(0.6)	15.34 (0.6)	90	90	90	[43]
	Exp ($\text{Ca}_3\text{Al}_2\text{O}_6$)	15.26	15.26	15.26	90	90	90	
8	Hydrogarnet	12.63(0.5)	12.63(0.5)	12.63(0.55)	90	90	90	[44]
	Exp ($\text{Ca}_3\text{Al}_2\text{O}_{12}\text{H}_{12}$)	12.56	12.56	12.56	90	90	90	
9	Lime	4.85(0.83)	4.85(0.83)	4.85 (0.83)	90.1	90.1	90.1	[45]
	Exp (CaO)	4.81	4.81	4.81	90	90	90	
10	Ettringite	11.45(1.9)	11.45(1.9)	21.68 (0.9)	89.9	89.9	120.5	[46]
	Exp ($\text{Ca}_6\text{Al}_2(\text{SO}_4)_3(\text{OH})12 \cdot 26\text{H}_2\text{O}$)	11.23	11.23	21.49	90	90	120	
11	Gypsum	6.6 (5.21)	15.5 (2.1)	5.61 (0.8)	89.5	113	90.5	[47]
	Exp ($\text{CaSO}_4 \cdot 2\text{H}_2\text{O}$)	6.27	15.18	5.66	90	114.3	90	
12	Anhydrate	7.35 (5.2)	7.35 (5.2)	6.45 (3.2)	90	90	90	[48]
	Exp (CaSO_4)	6.99	6.99	6.25	90	90	90	
13	Portlandite	3.67 (2.2)	3.67 (2.2)	4.85 (0.4)	89.7	89.9	120	[49]
	Exp ($\text{Ca}(\text{OH})_2$)	3.59	3.59	4.87	90	90	120	
14	Quartz	4.99 (1.6)	4.99 (1.6)	5.48 (1.5)	90	90	120	[50]
	Exp (SiO_2)	4.91	4.91	5.4	90	90	120	
15	Sodium Chloride	5.64 (4.0)	5.64 (4.0)	5.64 (4.0)	90	90	90	[51]
	Exp (NaCl)	5.41	5.41	5.41	90	90	90	
16	Potassium Chloride	3.63 (2.2)	3.63 (2.2)	3.63 (2.2)	90	90	90	[52]
	Exp (KCl)	3.71	3.71	3.71	90	90	90	
17	Sodium Hydroxide	3.39 (3.2)	11.33 (2.0)	3.38 (2.9)	90	90	90	[53]
	Exp (NaOH)	3.5	11.56	3.48	90	90	90	
18	Potassium hydroxide	3.96 (2.0)	3.99 (0.7)	5.73 (0.5)	90	104.2	90	[54]
	Exp (KOH)	3.85	4.02	5.76	90	105	90	
19	Calcium chloride	6.24 (2.0)	6.43 (2.7)	4.2 (2.6)	90	90	90	[55]
	Exp (CaCl_2)	6.11	6.25	4.31	90	90	90	

Overall, the results do give reasonable confidence in the validity of the force field but calculations of energetics with the force field must consider the limitations described above.

Table 4.3. Validation of energetics via the simulation of reaction enthalpies ΔH with ERICA FFs.

Reaction	ΔH (Exp) eV	ΔH (MD) eV	Estimated error *	Difference Exp-MD eV	Ref
1 $\text{Ca(OH)}_2 \rightarrow \text{Ca}^{2+}(\text{aq}) + 2\text{OH}(\text{aq})$	-0.19	-0.55	0.20	0.36	[57]
2 $\text{CaSO}_4 \cdot 2\text{H}_2\text{O} \rightarrow \text{Ca}^{2+}(\text{aq}) + \text{SO}_4^{2-}(\text{aq}) + 2\text{H}_2\text{O}$	-0.18	-1.25	0.16	1.07	[46]
3 $\text{CaSO}_4 \rightarrow \text{Ca}^{2+}(\text{aq}) + \text{SO}_4^{2-}(\text{aq})$	1.11	2.49	0.24	1.38	[46]
4 $2\text{H}_2\text{O} + \text{SiO}_2 \rightarrow \text{Si(OH)}_4(\text{aq})$	6.27	3.81	2.18	2.46	[58]
5 $\text{Ca(OH)}_2 + \text{SiO}_2 \rightarrow (\text{CaSiO}_4\text{H}_2)(\text{aq})$	2.44	3.36	0.51	0.92	[58]
6 $(\text{Ca} + 2\text{OH})(\text{aq}) + \text{Si(OH)}_4 \rightarrow$ $(\text{CaSiO}_4\text{H}_2)(\text{aq}) + 2\text{H}_2\text{O}$	-3.62	0.09	2.06	3.71	[58]
7 $\text{AlOOH} + \text{H}_2\text{O} \rightarrow \text{Al(OH)}_3$	-0.11	0.56	1.00	0.67	[58]
8 $\text{Ca}_3\text{Al}_2\text{O}_6 + 6\text{H}_2\text{O} \rightarrow \text{Ca}_3\text{Al}_2(\text{OH})_{12}$	-2.71	-3.93	5.74	1.22	[58]
9 $3\text{CaOH}_2 + 2\text{Al(OH)}_3 \rightarrow \text{Ca}_3\text{Al}_2(\text{OH})_{12}$	-0.42	-0.49	0.37	0.07	[58]
10 $3\text{CaO} + 2\text{Al(OH)}_3 \rightarrow \text{Ca}_3\text{Al}_2\text{O}_6 + 3\text{H}_2\text{O}$	-0.67	0.60	3.00	1.27	[58]
11 $3\text{CaO} + \text{Al}_2\text{O}_3 + 6\text{H}_2\text{O} \rightarrow \text{Ca}_3\text{Al}_2(\text{OH})_{12}$	-2.50	-1.02	5.56	1.48	[58]
12 $3\text{CaO} + 2\text{Al(OH)}_3 + 3\text{H}_2\text{O} \rightarrow \text{Ca}_3\text{Al}_2(\text{OH})_{12}$	-5.00	-3.33	3.13	1.67	[58]
13 $\text{Al}_2\text{O}_3 + 3\text{H}_2\text{O} \rightarrow 2\text{Al(OH)}_3$	-0.46	2.31	2.94	2.77	[58]
14 $\text{Al}_2(\text{SO}_4)_3 + 3\text{Ca(OH)}_2 \rightarrow 2\text{Al(OH)}_3 + 3\text{CaSO}_4$	-4.86	-4.93	0.53	0.07	[58]
15 $3\text{CaO} + \text{Al}_2\text{O}_3 \rightarrow \text{Ca}_3\text{Al}_2\text{O}_6$	0.21	2.91	0.62	2.70	[58]
16 $\text{Ca(OH)}_2 \rightarrow \text{CaO} + \text{H}_2\text{O}$	0.66	0.95	0.96	0.29	[58]

*See Section S6-Annex 1

4.3.3 Validation of ERICA FF3 from Hydration enthalpies

In this work, we further validated ERICA FF3 by looking at the hydration enthalpy of ions. In the table 4.4 we compared our result with the result of Yazdan Yar [59]. All results are very satisfactory confirming that the force field can be used with confidence for transport properties, e.g. chloride ingress [60] (i.e. the chloride ion as well as the most common counter ions Na and K should give accurate results).

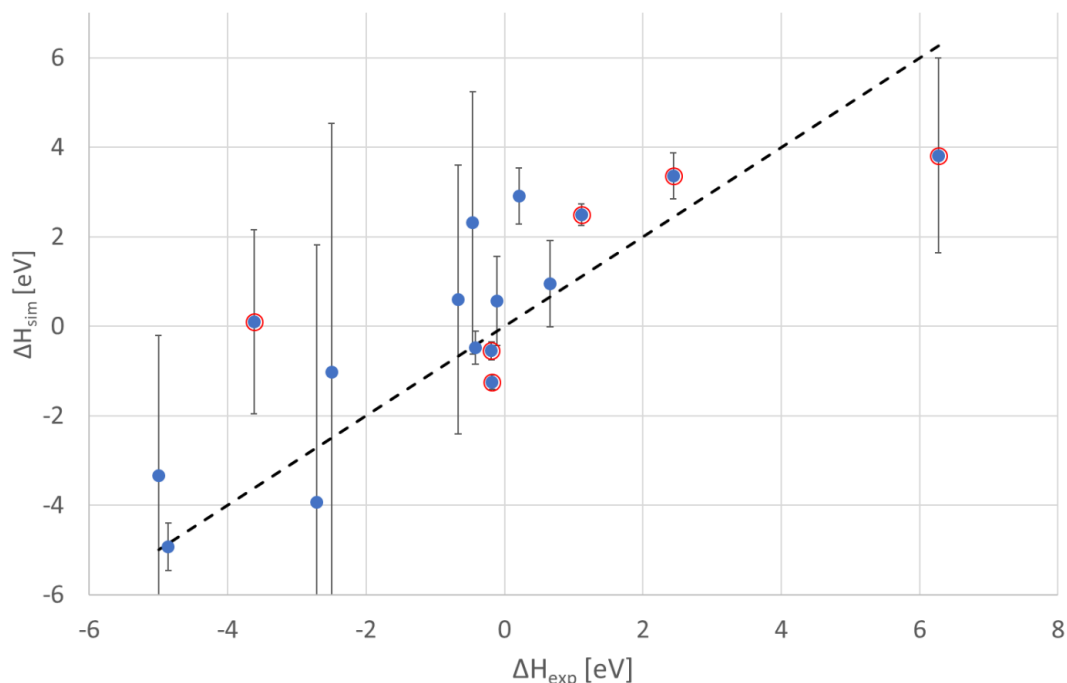


Figure 4.4. Simulate reaction enthalpies vs. experimental reaction enthalpies for the reactions in table 4.3. The black dotted line is one-to-one relationship between experimental and calculated reaction enthalpies and the error bars are the estimated error based on eq. S10 in Annex (values reported in table 4.3). Results circled in red are for reactions involving aqueous species where proton transfer in the hydration shell is likely to play some role.

Table 4.4. Hydration Enthalpies from comparing energy of box of water and box of water and ion.

Ion	This work (eV)	Dang et al. (eV) [59]	Exp (eV)	Ref (Exp)
Na	-4.24	-3.55	-4.40	[61]
K	-3.57	-2.64	-3.30	[61]
Ca	-15.05	-15.09	-15.32	[62]
Cl	-3.20	-3.26	-3.35	[62]

4.3.4 Portlandite surface energies

Portlandite is a major component of hydrated cement, which means understanding the mechanisms behind morphological changes is important. Here we carried out both energy

minimization and molecular dynamics simulations to understand the change of portlandite morphology in water with respect to vacuum. The calculated values are reported in Table 4.5 for a series of surfaces shown to be present experimentally for pure portlandite systems [17]. Also shown is a comparison with previous results by Galmarini et al. [17,21] using Cement FF1. Compared to Cement FF1 we have changed the water model from TIP4P/2005 to the SPC/Fw water model. Both force fields give very similar results: the surface energy of the [00.1] surface, which has already a very low energy in vacuum, seems to be influenced only slightly by the presence of water. The surface energies of both the [10.0] surface and the [10.1] surface were reduced noticeably by the presence of water but the effect is much more marked for the [10.1] surface. The [10.1] surface, which has the highest surface energy in vacuum and does not appear in the portlandite-vacuum morphology, has a similar energy to the [00.1] and the [10.0] surface in water and becomes part of the calculated portlandite-water equilibrium morphology (see Fig. S2 of the Annexe 1). However, compared to Cement FF1, the ERICA FF predicts a stronger water-portlandite interaction for the hydroxyl terminated [10.0] surface and less with the calcium terminated [10.1] surface. Consequently the [10.0]/[00.1] surface energy ratio is lower (more in the range of the experimental values) and the [10.1]/[00.1] surface energy ratio higher (less in range of experimental values) compared to Cement FF1 (Table 4.5). However all differences are well within the estimated errors on the force fields [63].

Table 4.5. Simulation of surface energies of different facets of portlandite by ERICA FF1 and CEMENT FF1 [17,22]; comparison with available experimental data on surface energy ratios.

FF	[00.1]	[00.1]	[10.0]	[10.0]	[10.1]	[10.1]	[10.0]/[00.1]		[10.1]/[00.1]	
	J/m2	J/m2	J/m2	J/m2	J/m2	J/m2	Wat		Wat	
	Vac.	Wat.	Vac.	Wat.	Vac.	Wat.	MD	Exp[64]	MD	Exp[64]
Cement FF1	0.073	0.11	0.55	0.13	0.92	0.09	1.1	0.58-0.75	0.81	0.65-0.73
ERICA FF1	0.073*	0.16	0.55*	0.10	0.92*	0.14	0.62	0.58-0.75	0.87	0.65-0.73

*Please note that for vacuum calculations ERICA FF1 reduces to Cement FF1

4.3. 5 Mechanical Properties

With the calculation of elastic constants, we provide the final validation for the ERICA FF. We have chosen systems of increasing complexity from simple cubic to layered minerals [36]. In the case of layered structures the behavior of layers is expected to be very anisotropic [65]. The results are presented in table 5.6, where we show the elastic tensor coefficients in Voigt notation (C_{ij}) for portlandite, lime, and quartz. In Table 4.7, we present the overall elastic properties for tricalcium silicate and 14 Å tobermorite.

Table 4.6 summarizes the simple systems, where we see that ERICA FF replicates the bulk modulus within reasonable deviations (12.6% for portlandite and 4.1% for quartz). The individual components of the elastic tensor are well replicated in the case of portlandite. In particular as portlandite exhibits a large elastic anisotropy in compressional (C_{11} and C_{33}) and shear elastic coefficients (C_{66} and C_{44}), which corresponds to a larger stiffness and rigidity in the basal plane with respect to the axial direction, the results are particularly reassuring [66]. For lime we see a 15% deviation for compressional (C_{11}) and shear (C_{44}) elastic coefficients, while the off-diagonal constant C_{12} differs by 40%. In quartz we replicate the bulk modulus, and C_{11} very well, while all other elastic tensor coefficients do not perform well, which could be attributed to the tendency of slight rotations of the silicon tetrahedra in our structures. The individual components (C_{ij}) of the elastic tensor give a better estimation of the accuracy of the force field than the overall bulk properties and could be used for further force field improvements [36]. However, for generalized force fields as Erica FF the risk of overfitting for one system to the detriment of another must be taken carefully into consideration. Additionally, the reliability of experimental values is not always clear as one can observe large discrepancies already between experimental measurements with the same technique. Speziale et al. [66] for example reported a discrepancy of C_{13} by 253% for portlandite.

Since there is no experimental data of the elastic tensor coefficients for tricalcium silicate and tobermorite 14Å, we present in table 4.7 the overall elastic properties. We report two values for the shear modulus and Young's modulus, since the shear modulus can be calculated in two ways: $G_1 = (C_{44} + C_{55} + C_{66})/3$, or $G_2 = (C_{11} + C_{22} + C_{33} - C_{12} - C_{13} - C_{23})/6$, and the literature cited do not state which way it was calculated. The Young's modulus is calculated as $E = 2G(1 + \nu)$, where E is the Young's modulus, G the shear modulus, and ν the Poisson ratio.

Table 4.6. Elastic tensor coefficients in Voigt definition (C_{ij}) and the bulk modulus (K) for portlandite, lime, and quartz. TS – this study, C_{ij} units are [GPa].

System	C_{11}	C_{12}	C_{13}	C_{14}	C_{33}	C_{44}	C_{66}	K [GPa]
Portlandite [TS]	118.04	33.31	11.79	-5.06	31.76	10.54	37.08	41.65
Exp [66]	102±2.0	32±1.0	8.4±0.4	4.5±0.2	33.6±0.7	12.0±0.3	35.0±1.1	36.4±0.4
DFT [67]	99.39	30.78	7.36	~ 0	36.29	7.88	34.31	-
Lime [TS]	259.30	97.30	94.00	-1.20	261.20	96.20	94.90	149.40
Exp [68]	220.53	57.67	-	-	-	81.43	-	-
Exp [69]	222.34	59.34	-	-	-	81.00	-	-
Quartz [TS]	82.64	16.84	27.73	8.37	69.69	36.1	30.99	38.60
Exp [70]	86.60	6.74	12.40	17.80	106.40	58.00	-	37.00
Exp [71]	87.26	6.57	11.95	-17.18	105.8	57.15	40.35	-

Erica FF replicates the bulk modulus of tricalcium silicate with a deviation of 13%, while, if considering the lower value of the shear modulus, we are in the 30% range of the shear and Young's modulus if compared to the results of Boumiz et al. [72], and within 10% to the results of Valez et al. [73]. In comparison to the interface force field (IFF), which is not a general force field, and is finely adjusted for its application, Erica FF performs very well (~10-15% deviation), and at the same time much better than ClayFF, which is one of the most popular force fields for cementitious systems. Our MD calculation is also comparable to the force field method calculation with GULP from Manzano et al. [74]. The comparison of the elastic tensor coefficients between Erica FF, IFF and ClayFF is shown in Annex 1-S9.

The bulk modulus of 14Å tobermorite is in very good agreement with the experimental value from Oh et al. [75], which is impressive since tobermorite is a heterogeneous layered material.

The DFT studies were reported using two different simulation packages (Dharmawardhana et al. [76] used VASP, while Kuhni Mohamed et al. [12] and Shahsaveri et al. [77] used Quantum Espresso) and are in good accordance with experimental data for the bulk modulus. Depending on which shear modulus we take, we are in good agreement with both DFT studies, which suggests that Erica FF is also successful in replicating the elastic constants of complex materials with good accuracy. The elastic tensor coefficients for 14Å tobermorite are reported in Annexel-S9.

In conclusion, we showed that Erica FF can replicate the mechanical properties of simple and complex systems with satisfactory precision, although special care needs to be taken when comparing the results, since calculating and measuring elastic constants is not a trivial task. As mentioned above to facilitate their use by other interested parties, the ERICA force field has been introduced into the cemff database (<https://www.cemff.org/>) along with the corresponding LAMMPS scripts.

Table 4.7. Elastic properties for tricalcium silicate and tobermorite 14Å. K, E, and G stand for bulk, Young’s, and shear modulus. TS – this study, FF – force field.

System	K [GPa]	E [GPa]	G [GPa]	Poisson ratio (ν)
Tricalcium silicate [TS]	120.1	188.0 155.0	76.0 62.7	0.24
FF ClayFF [78]	53.9	83.2	33.5	0.24
FF IFF [78]	104.7	139	54.3	0.28
FF Gmira[74]	103.0	138.9	54.5	0.28
Exp[73]	-	147-135	-	0.3
Exp [72]	105.2	117.68	44.6	0.314
Tobermorite 14Å [TS]	49.93	85.50 58.30	35.23 24.00	0.21
DFT [76]	56.42	80.00	31.65	0.26
DFT [77]	35.91	51.9	20.61	-
DFT [12]	49.00	-	-	-
FF Gmira [74]	44.80	19.00	49.94	0.31
Exp [75]	47± 4	-	-	-

4.4. Conclusions

In this work, we have described and validated a force field (ERICA FF) developed in three parts (ERICA FF1, 2 and 3) to simulate structural properties, reaction enthalpies, and mechanical properties of various cementitious systems. Results are generally in very good agreement with experimental findings and show that these force fields can be used with good accuracy to simulate cementitious systems. In the case of structural properties, 19 cementitious materials were simulated with relative errors on distances all below 5.2 %. From an energetic perspective, we have provided an error estimate for the force field able to estimate the confidence interval of calculated reaction enthalpies within certain limitations. Namely, care has to be taken with systems where proton transfer might play an important role. We have further validated the ERICA FF from calculations of hydration enthalpies of ions in water. We also simulated mechanical properties for 5 cementitious materials which all are in very good agreement with experimental values. These findings demonstrate that ERICA FF can be implemented to simulate cementitious materials with good reliability.

Acknowledgments:

The authors would like to thank, Marie Skłodowska-Curie - Innovative Training Network (ITN) programme under EU Horizon 2020 and the Swiss National Foundation for financing the contribution of Masood Valavi and Ziga Casar (grant no. 179076) respectively. The authors also thank the SCITAS at EPFL for giving access to HPC computing resources.

The various authors made the following contributions

Masood Valavi: overall development of the force field, structural and energetics validations and writing of the original draft. **Ziga Casar:** fine tuning of force field for tobermorite structural validation, mechanical property simulations, partial contribution to original draft. **Aslam Kunhi Mohamed:** supervision, reviewing and editing, **Paul Bowen:** supervision, reviewing and editing and **Sandra Galmarini:** supervision, reviewing and editing.

4.5. References

- [1] U. Angst, B. Elsener, C.K. Larsen, Ø. Vennesland, Critical chloride content in reinforced concrete - A review, *Cem. Concr. Res.* 39 (2009) 1122–1138.
- [2] R.K. Mishra, A.K. Mohamed, D. Geissbühler, H. Manzano, T. Jamil, R. Shahsavari, A.G. Kalinichev, S. Galmarini, L. Tao, H. Heinz, R. Pellenq, A.C.T. van Duin, S.C. Parker, R.J. Flatt, P. Bowen, cemff: A force field database for cementitious materials including validations, applications and opportunities, *Cem. Concr. Res.* 102 (2017) 68–89.
- [3] UN environment, K.L. Scrivener, V.M. John, E.M Gartner, Eco-efficient cements: Potential economically viable solutions for a low-CO₂ cement-based materials industry, *Cem. Concr. Res.* 114 (2018) 2-26
- [4] E. Gartner, H. Hirao, A review of alternative approaches to the reduction of CO₂ emissions associated with the manufacture of the binder phase in concrete, *Cem. Concr. Res.* 78 (2015) 126–142.
- [5] B. Lothenbach, K. Scrivener, R.D. Hooton, Supplementary cementitious materials, *Cem. Concr. Res.* 41 (2011) 1244–1256.
- [6] I. Androniuk, C. Landesman, P. Henocq, A.G. Kalinichev, Adsorption of gluconate and uranyl on C-S-H phases: Combination of wet chemistry experiments and molecular dynamics simulations for the binary systems, *Phys. Chem. Earth.* 99 (2017) 194–203.
- [7] M.J. Tapas, L. Sofia, K. Vessalas, P. Thomas, V. Sirivivatnanon, K. Scrivener, Efficacy of SCMs to mitigate ASR in systems with higher alkali contents assessed by pore solution method, *Cem. Concr. Res.* 142 (2021) 1063–1071.
- [8] M.J. Abdolhosseini Qomi, K.J. Krakowiak, M. Bauchy, K.L. Stewart, R. Shahsavari, D. Jagannathan, D.B. Brommer, A. Baronnet, M.J. Buehler, S. Yip, F.J. Ulm, K.J. Van Vliet, R.J.M. Pellenq, Combinatorial molecular optimization of cement hydrates, *Nat. Commun.* 67 (2014) 681–689.

- [9] R.J.-M. Pellenq, A. Kushima, R. Shahsavari, K.J. Van Vliet, M.J. Buehler, S. Yip, F.-J. Ulm, A realistic molecular model of cement hydrates, *Proc. Natl. Acad. Sci.* 38 (2009) 26102–16107.
- [10] A. Kumar, B.J. Walder, A. Kunhi Mohamed, A. Hofstetter, B. Srinivasan, A.J. Rossini, K. Scrivener, L. Emsley, P. Bowen, The Atomic-Level Structure of Cementitious Calcium Silicate Hydrate, *J. Phys. Chem. C.* 121(32) (2017) 17188-17196.
- [11] A. Kunhi Mohamed, S.C. Parker, P. Bowen, S. Galmarini, An atomistic building block description of C-S-H - Towards a realistic C-S-H model, *Cem. Concr. Res.* 107 (2018) 221–235.
- [12] A. Kunhi Mohamed, P. Moutzouri, P. Berruyer, B.J. Walder, J. Siramanont, J. Siramanont, M. Harris, M. Negroni, S.C. Galmarini, S.C. Parker, S.C. Parker, K.L. Scrivener, L. Emsley, P. Bowen, The Atomic-Level Structure of Cementitious Calcium Aluminate Silicate Hydrate, *J. Am. Chem. Soc.* 142 (2020) 11060–11071.
- [13] F. Puertas, M. Palacios, H. Manzano, J.S. Dolado, A. Rico, J. Rodríguez, A model for the C-A-S-H gel formed in alkali-activated slag cements, *J. Eur. Ceram. Soc.* 31 (2011) 2043–2056.
- [14] G. Kovačević, B. Persson, L. Nicoleau, A. Nonat, V. Veryazov, Atomistic modeling of crystal structure of $\text{Ca}_{1.67}\text{SiH}_x$, *Cem. Concr. Res.* 59 (2015) 68–79.
- [15] G. Kovačević, L. Nicoleau, A. Nonat, V. Veryazov, Revised atomistic models of the crystal structure of C-S-H with high C/S ratio, *Zeitschrift Fur Phys. Chemie.* 20 (2016) 134–42.
- [16] S. Galmarini, A. Kunhi Mohamed, P. Bowen, Atomistic simulations of silicate species interaction with portlandite surfaces, *J. Phys. Chem. C.* 120 (2016) 22407–22413.
- [17] S. Galmarini, P. Bowen, Atomistic simulation of the adsorption of calcium and hydroxyl ions onto portlandite surfaces - Towards crystal growth mechanisms, *Cem. Concr. Res.* 81 (2016) 16–23.
- [18] E. Pustovgar, R.K. Mishra, M. Palacios, J.B. d’Espinoze de Lacaille, T. Matschei, A.S. Andreev, H. Heinz, R. Verel, R.J. Flatt, Influence of aluminates on the hydration kinetics of tricalcium silicate, *Cem. Concr. Res.* 10.0 (2017) 245–262.

- [19] H. Heinz, T.-J. Lin, R.K. Mishra, F.S. Emami, Thermodynamically consistent force fields for the assembly of inorganic, organic, and biological nanostructures: the INTERFACE force field, *Langmuir* 29 (2013) 1754–1765
- [20] R.T. Cygan, J.J. Liang, A.G. Kalinichev, Molecular models of hydroxide, oxyhydroxide, and clay phases and the development of a general force field, *J. Phys. Chem. B.* 108 (2004) 1255–1266.
- [21] S. Plimpton, Fast parallel algorithms for short-range molecular dynamics, *J. Comput. Phys.* 117 (1995) 1–19.
- [22] S. Galmarini, A. Aimable, N. Ruffray, P. Bowen, Changes in portlandite morphology with solvent composition: Atomistic simulations and experiment, *Cem. Concr. Res.* 41 (2011) 1330–1338.
- [23] Y. Wu, H.L. Tepper, G.A. Voth, Flexible simple point-charge water model with improved liquid-state properties, *J. Chem. Phys.* 124 (2006) 1–12.
- [24] E.H. Byrne, P. Raiteri, J.D. Gale, Computational Insight into Calcium-Sulfate Ion Pair Formation, *J. Phys. Chem. C.* 121 (2017) 25956–25966.
- [25] P. Mark, L. Nilsson, Structure and dynamics of the TIP3P, SPC, and SPC/E water models at 298 K, *J. Phys. Chem. A.* 105 (2003) 9954–9960.
- [26] W.L. Jorgensen, J. Chandrasekhar, J.D. Madura, R.W. Impey, M.L. Klein, Comparison of simple potential functions for simulating liquid water, *J. Chem. Phys.* 79 (1983) 926–934.
- [27] J.W. Ponder, C. Wu, P. Ren, V.S. Pande, J.D. Chodera, M.J. Schnieders, I. Haque, D.L. Mobley, D.S. Lambrecht, R.A. Distasio, M. Head-Gordon, G.N.I. Clark, M.E. Johnson, T. Head-Gordon, Current status of the AMOEBA polarizable force field, *J. Phys. Chem. B.* 114 (2010) 2549–2564.
- [28] N. de Leeuw, S. Parker, Molecular-dynamics simulation of MgO surfaces in liquid water using a shell-model potential for water, *Phys. Rev. B - Condens. Matter Mater. Phys.* 58 (1998) 13901–13910. <https://doi.org/10.1103/PhysRevB.58.13901>.

- [29] A.K. Mohamed, Atomistic Simulations of The Structure of Calcium Silicate Hydrates: Interlayer Positions, Water Content And A General Structural Brick Model, , EPFL Thesis, No. 8840, 2018.
- [30] N.H. Leeuw, S.C. Parker, Effect of Chemisorption and Physisorption of Water on the Surface Structure and Stability of alpha-Alumina, *J. Am. Ceram. Soc.* 82 (2004) 3209–3216.
- [31] P.J. Mitchell, D. Fincham, Shell model simulations by adiabatic dynamics, *J. Phys. Condens. Matter.* 5 (1993) 1031-1042.
- [32] M. Předota, A. V. Bandura, P.T. Cummings, J.D. Kubicki, D.J. Wesolowski, A.A. Chialvo, M.L. Machesky, Electric double layer at the rutile (110) surface. 1. Structure of surfaces and interfacial water from molecular dynamics by use of ab initio potentials, *J. Phys. Chem. B.* 108 (2004) 12049–12059. <https://doi.org/10.1021/jp037197c>.
- [33] V. Baroghel-Bouny, Water vapour sorption experiments on hardened cementitious materials. Part II: Essential tool for assessment of transport properties and for durability prediction, *Cem. Concr. Res.* 37 (2007) 438–454.
- [34] L. X. Dang, J.E. Rice, J. Cadwell, P.A. Kollman, Ion solvation in aqueous in polarizable water: molecular dynamic simulation, *J. Chem. Soc.* 113 (1991) 2481–2486.
- [35] W. Shinoda, M. Shiga, & M. Mikami, Rapid estimation of elastic constants by molecular dynamics simulation under constant stress, *Phys. Rev. B*, 69 (2004) 134103.
- [36] G. Clavier, N. Desbiens, E. Bourasseau, V. Lachet, N. Brusselle-Dupend & B. Rousseau, Computation of elastic constants of solids using molecular simulation: comparison of constant volume and constant pressure ensemble methods, *Mol. Simul.*, 43(17), (2017) 1413-1422.
- [37] E. Bonaccorsi, S. Merlino, A.R. Kampf, The crystal structure of tobermorite 14 Å (plombierite), a C-S-H phase, *J. Am. Ceram. Soc.* 88 (2005) 505–512.
- [38] J. Lewis, D. Schwarzenbach, H.D. Flack, Electric field gradients and charge density in corundum, α -Al₂O₃, *Acta Crystallogr. Sect. A.* 38 (1982) 733–739.
- [39] D.L. Bish, S.A. Howard, Quantitative phase analysis using the Rietveld method, *J. Appl. Crystallogr.* 21 (1988) 86–91.

- [40] E. Balan, M. Lazzeri, G. Morin, F. Mauri, First-principles study of the OH-stretching modes of gibbsite, *Am. Mineral.* 91 (2006) 115–119.
- [41] T. Dahmen, R. Gruehn, Beiträge zum thermischen Verhalten von Sulfaten: IX. Einkristallstrukturverfeinerung der Metall(III)-sulfate $\text{Cr}_2(\text{SO}_4)_3$ und $\text{Al}_2(\text{SO}_4)_3$, *Zeitschrift Für Krist. - Cryst. Mater.* 32 (2014) 40–54.
- [42] R.J. Hill, Hydrogen atoms in boehmite: a single crystal X-ray diffraction and molecular orbital study., *Clays Clay Miner.* 29 (1981) 435–445.
- [43] P. Mondal, J.W. Jeffery, The Crystal Structure of Tricalcium Aluminate, $\text{Ca}_3\text{Al}_2\text{O}_6$, *Acta Crystallogr.* 31 (1975) 689–697.
- [44] G.A. Lager, T. Armbruster, J. Faber, Neutron and X-ray diffraction study of hydrogarnet $\text{Ca}_3\text{Al}_2(\text{OH}_4)_3$, *Am. Mineral.* 72 (1987) 756–765.
- [45] G. Fiquet, P. Richet, G. Montagnac, High-temperature thermal expansion of lime, periclase, corundum and spinel, *Phys. Chem. Miner.* 27 (1999) 103–111.
- [46] F. Goetz-Neunhoeffler, J. Neubauer, Refined ettringite ($\text{Ca}_6\text{Al}_2(\text{SO}_4)_3(\text{OH})_{12} \cdot 26\text{H}_2\text{O}$) structure for quantitative X-ray diffraction analysis, *Powder Diffr.* 21 (2006) 4–11.
- [47] P. Comodi, S. Nazzareni, P.F. Zanazzi, S. Speziale, High-pressure behavior of gypsum: A single-crystal X-ray study, *Am. Mineral.* 93 (2008) 1530-1537.
- [48] F. C. Hawthorne, R.B. Ferguson, Anhydrous sulphates. II. Refinement of the crystal structure of anhydrite, *Can. Mineral.* 13 (1975) 289-292.
- [49] D.M. Henderson, H.S. Gutowsky, A nuclear magnetic resonance determination of the hydrogen positions in $\text{Ca}(\text{OH})_2$, *Am. Mineral.* 47 (1962) 24-32.
- [50] L. Levien, C.T. Prewitt, D.J. Weidner, C.T. Prewitt, D.J. Weidner, Structure and Elastic Properties of Quartz at Pressure, *Am. Mineral.* 65 (1980) 920–930.
- [51] D. Walker, P.K. Verma, L.M.D. Cranswick, R.L. Jones, S.M. Clark, S. Buhre, Halite-sylvite thermoelasticity, *Am. Mineral.* 89 (2004) 204–210.
- [52] G. Will, Energiedispersion und Synchrotronstrahlung: eine neue Methode und eine neue Strahlenquelle für die Röntgenbeugung., *Fortschritte Der Mineral.* 59 (1981) 31–94.

- [53] Y. Liu, H. Hu, X-ray diffraction study of bamboo fibers treated with NaOH, *Fibers Polym.* 9 (2008) 735–739.
- [54] B. Mach, H. Jacobs, W. Schäfer, Bindungsverhältnisse in kristallinen Phasen von Kaliumdeuterhydroxid, KOD, ZAAC - *J. Inorg. Gen. Chem.* 553 (1987) 187–195.
- [55] L. Krastanow, I.N. Stranski, Crystallisation of alkali halogen salts on fluorite, *Zeitschrift fuer Krist. Krist. Krist. Krist.* 43 (1938) 17–30.
- [56] P. Maksyutenko, T.R. Rizzo, O. V. Boyarkin, A direct measurement of the dissociation energy of water, *J. Chem. Phys.* 125 (2006) 18110.1–181110.
- [57] J.W. Bullard, E. Enjolras, W.L. George, S.G. Satterfield, J.E. Terrill, A parallel reaction-transport model applied to cement hydration and microstructure development, *Model. Simul. Mater. Sci. Eng.* 18 (2010) 133–140.
- [58] G.D. Miron, T. Wagner, D.A. Kulik, C.A. Heinrich, Internally consistent thermodynamic data for aqueous species in the system Na-K-Al-Si-O-H-Cl, *Geochim. Cosmochim. Acta.* 187 (2016) 41–78.
- [59] L.X. Dang, J.E. Rice, J. Caldwell, P.A. Kollman, Ion Solvation in Polarizable Water: Molecular Dynamics Simulations, *Journal of the American Chemical Society.* 113 (1991) 2481–2486.
- [60] JM Marangu, JK Thiong'o, JM Wachira, Chloride Ingress in Chemically Activated Calcined Clay-Based Cement, *J. Chem.* 12 (2018) 1–8.
- [61] A. Grossfield, P. Ren, J.W. Ponder, Ion Solvation Thermodynamics from Simulation with a Polarizable Force Field, *J. Am. Chem. Soc.* 125 (2003) 15671–15682
- [62] Y. Marcus, A simple empirical model describing the thermodynamics of hydration of ions of widely varying charges, sizes, and shapes, *Biophys. Chem.* 51 (1994) 111–127.
- [63] S. Galmarini, Atomistic Simulation of Cementitious Systems, EPFL Thesis. No. 5754 (2013).
- [64] S. Brunauer, D. L. Kantro, and C. H. Weise, The surface energies of calcium oxide and calcium hydroxide, *Can. J. Chem.* 34 (1956) 729–742.

- [65] B. Carrier, M. Vandamme, R.J-M Pellenq & H. Van Damme, Elastic Properties of Swelling Clay Particles at Finite Temperature upon Hydration, *J. Phys. Chem. C*. 118 (2014) 8933–8943.
- [66] S. Speziale, H.J. Reichmann, F.R. Schilling, H.R. Wenk, P.J.M. Monteiro, Determination of the elastic constants of portlandite by Brillouin spectroscopy, *Cem. Concr. Res.* 38 (2008) 1148–1153.
- [67] J.L. Laugesen, Density functional calculations of elastic properties of portlandite, *Cem. Concr. Res.* 35 (2005) 199–202.
- [68] P.R. Son, R. Bartels, CaO and SrO Single Crystal Elastic Constants and Their Pressure Derivatives, *J. Phys. Chem. Solids*. 33 (1972)17-25.
- [69] H. Oda, Measurement of Elastic Properties of Single-Crystal CaO up to 1200K, *Phys. Chem. Miner.* 19 (1992)64-73.
- [70] J. Wang, Z. Mao, F. Jiang, T.S Duffy, Elasticity of single-crystal quartz to 10GPa, *Phys. Chem. Mater.* 42 (2005) 203–212.
- [71] P. Heyliger, Elastic constants of natural quartz, *J. Acoust. Soc. Am.* 114 (2003) 644–650.
- [72] A. Boumiz, D. Sorrentino, C. Vernet, F. Cohen Tenoudji, Modelling the development of the elastic moduli as a function of the hydration degree of cement pastes and mortars, in: *Second Int. RILEM Symp. Hydration Setting*, (1997)295–316.
- [73] K. Valez, S. Maximilien, D. Damidot, G. G.Fantozzi, F.Sorrentino, Determination by nanoindentation of elastic modulus and hardness of pure constituents of Portland cement clinker, *Cem. Concr. Res.* 31 (200.1) 551–561.
- [74] H. Manzano, J.S. Dolado, A. Ayuela, Elastic properties of the main species present in Portland cement pastes, *Acta Materialia* 57 (2009) 1666-1674
- [75] J.E. Oh, S.M.Clark, H.R Wenk, P.J.M Monteiro, Experimental determination of bulk modulus of 14 AA tobermorite using high pressure synchrotron X-ray diffraction, *Cem. Concr. Res.* 42 (2) (2012) 397–403.

- [76] C.C. Dharmawardhana, A Misra, S. Aryal, P.Rulis, W.Y.Ching, Role of interatomic bonding in the mechanical anisotropy and interlayer cohesion of CSH crystals, *Cem. Concr. Res.* 52 (2013) 123–130.
- [77] R. Shahsavari, M.J. Buehler, R.J.Pellenq, F.J Ulm First-Principles Study of Elastic Constants and Interlayer Interactions of Complex Hydrates Oxides: Case Study of Tobermorite and Jennite, *J. Am. Ceram. Soc.* 10 (2009) 2323–2330.
- [78] J. Claverie, S. Kamali-Bernard, J.M.M. Cordeiro & F. Bernard, Assessment of mechanical, thermal properties and crystal shapes of monoclinic tricalcium silicate from atomistic simulations, *CCR* 140 (2021) 106269

Chapter 5: Adsorption of Calcium and Hydroxyl ions onto portlandite and C-S-H surfaces

5.1 Introduction

The morphology of portlandite in cementitious systems is affected by the cement composition, temperature, and water-to-solid ratio (1). However, it is yet unclear how these aspects affect portlandite growth and, as a result, the ultimate morphology of portlandite (CH). Furthermore, the role of portlandite during the induction period of cement hydration, which occurs before the cement sets, has yet to be fully understood. Experimental access to the atomistic mechanisms at solid-solution interfaces is difficult. Also, interaction of ions with the surface of C-S-H is crucial in order to understand phenomena behind precipitation of C-S-H. We used traditional atomistic simulation approaches to investigate the characteristics of portlandite–water surfaces with various crystallographic orientations. Also, the interaction of calcium and hydroxide ions with these interfaces and the interaction of Ca^{2+} with a C-S-H surface were made in the current study. We employed the newly developed Force field ERICA FF2 in this work, as described in detail in Chapter 4. Simulations are made using, both molecular dynamics (MD) and metadynamics (MTD). The detailed method of calculation is presented in the next section. Then, the structure of water above the 00.1, 10.0, and 10.1 CH surfaces via MD is presented comparing results using the SPC/FW water model of ERICA FF and the TIP4P 2005 model used in a previous study by Galmarini et al [2,5]. The results of the MTD simulations investigating Ca^{2+} and OH^- adsorption onto portlandite surfaces will then be discussed. Then, based on our findings of surface dissolution issues an MD study was necessary to better examine the interaction of Ca^{2+} and OH^- ions on the 00.1 CH surface. Finally, we will present a preliminary study of MTD simulations on the interaction of Ca^{2+} with a 00.1 Ca terminated C-S-H surface. The chapter has been written in publication style to facilitate writing of an expected publication, hence a little bit of repetition of previous sections may be apparent.

5.2 Simulation details

The challenge in reproducing solid–water interactions in molecular dynamics stems from the solid and liquid's vastly differing mechanical characteristics. In an NPT calculation, differing mechanical qualities result in significantly different pressure fluctuations. The root means squared pressure fluctuations in water are on the order of 0.2–0.5 katm, but the pressure fluctuations in portlandite are on the order of 1–3 katm. The barostat would account for these discrepancies in

separate simulations, but in a mixed simulation, both phases are considered identically. As a result, the simulation is subjected to artificial stresses. For two reasons, anisotropic NPT is not a viable solution to the problem. To begin with, in simulations of a pure liquid phase, the angles are poorly defined and will begin to change uncontrollably. Second, the solid and liquid phases are still considered as one parallel to the interface. As a result, the setup adopted for this study was an NVT simulation of a portlandite–water slab with periodic boundaries separated by a vacuum gap parallel to the contact (see Chp. 2 and Galmarini et al. (2)). This indicates that the volume of the liquid and the portlandite slab can fluctuate independently perpendicular to the interface, but no volume variations are allowed parallel to the interface. This lessens the problem of artificial stress, but it does not eliminate it. MD calculations were performed using the LAMMPS Code (timestep:0.7 fs, Nosé–Hoover thermostat with goal temperature Text=300°C and relaxation constant T= 0.5 ps). The detailed set-up for each study is described in the sections below (5.2.1).

5.2.1 Simulation details for calculating the structure of water above CH surfaces

An NVT ensemble was used to calculate the structure of water above different surfaces of portlandite. The first 200 ns of the simulation run was deemed to be equilibration; thus, this time was not used for averaging and analysis. Energy minimization before running the Molecular dynamic simulation was made. Fix ave was used in LAMMPS to save the density of water for every 10.00 steps, which is the average of the previous 10.00 steps. The average of all trajectories was then calculated using a MATLAB function.

For analysis a hydrogen bond (HB) length was considered to be equal to or less than 1.8 Å, as in Leeuw and Parker's study (3). Please note that it was only used to qualitatively assess the HB network and I did not count the number of HB or quantify in detail. We first utilized the OVITO software to create photos and snapshots, but because of the difficulty in making high-quality images, we switched to an in-house code to move the dump file from LAMMPS (4) production to the VESTA visualization program. This code saves the most recent trajectory generated by LAMMPS and converts it to a txl file that can be read by VESTA Software.

5.2.2 Details of MTD simulations for adsorption of Ca and OH ions onto 00.1 CH surface.

The PLUMED software was used to calculate the interaction of Ca and OH ions with the 00.1 surface of portlandite. PLUMED is a program that calculates metadynamic and well-tempered

metadynamic simulations. A COLVAR file was created that holds collective variables as a function of time, as well as a fes.dat file that stores free energy profiles as a function of time. As examples a couple of PLUMED programs for the simulations are given in Annex 2.

ERICA FF1 with a cutoff of 8.5 Å between short and long-range interaction was used. We used this cut off to compare with the results of Galmarini et al. (2) who used the same cut off. The size of the surface is 22 x 26 Å, and a neutral surface was selected for this simulation. With approximately 470 water molecules, the water contains 1 Ca²⁺ and 2 OH⁻ ions. We need to perform two simulations because we are looking for Ca²⁺ and OH⁻ ions adsorption on the 00.1 CH surface. One to use MTD to push Ca²⁺ toward the surface, and the other to push OH toward the surface. Solid slabs are 22 x 26 x 30 Å³, whereas liquid slabs are 22 x 26 x 40 Å³. The vacuum dimension was constructed with dimensions of 22 x 26 x 30 Å³. The reason for the large vacuum gap is to prevent water molecules from moving to the bottom surface. We used the ion of interest distance from the surface as a collective variable (CV). In the first layer of the portlandite slab, the surface was defined to be an oxygen of the hydroxyl that terminates the surface. We used 16 Å as the highest limit for both Ca²⁺ and OH⁻ ions from the surface. This means we build a wall 16 Å from the surface, allowing ions to travel a maximum distance of 16 Å from the surface. The reason for this is to reduce the computing cost of simulation because ions are only allowed to be a particular distance away from the surface. Another limitation is that we defined three confining cylinders' (they were chosen to use entire surface with biggest possible radius for each) perpendicular to the surface, each carrying one ion. This was to prevent the creation of ion pairs, which can influence the interpretation of the free energy profile. Another motivation for preventing ion pair creation is to save simulation time by allowing ions to interact more with the surface instead of spending time forming such ion pairs. Figure 5.1 is a close-up of the 00.1 CH surface with the 3 cylinders indicated. Runs of 60 ns with a time step of 0.007 ps was simulated with the first 2 ns being considered as equilibration. For the MTD, Gaussians with a height of 0.005 eV, a width of 0.3 Å, and a frequency of 0.1 ps was employed for conventional MTD simulations and all MTD simulations were performed with same parameters.

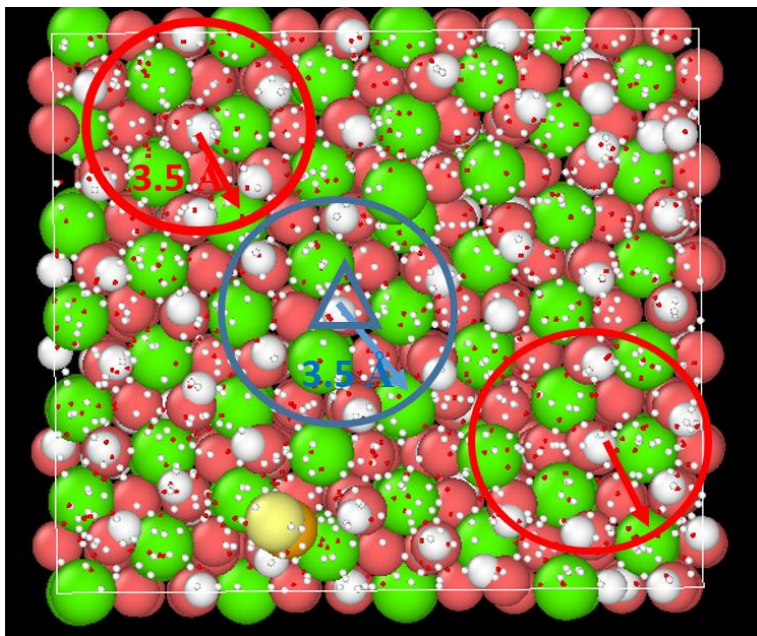


Fig 5.1. Snapshot of 00.1 CH surface with three constraining cylinders defined. The yellow and brown ion shows adsorbing O (OH) and H (OH) respectively. *Green – Ca, red - O, white - H*

5.2.3 Details of MD simulations for adsorption of Ca and OH ions onto 00.1 CH surface.

Details of simulation and constraints for molecular dynamic simulation of adsorption of Ca^{2+} and OH^- into 00.1 Surface of portlandite are very similar to those of the MTD simulations. The only difference is that here we performed MD simulation instead of metadynamic simulation. That is to say the PLUMED program was used but no bias was applied so we do not push ions toward the surface and we let ions interact with the surface via MD only. This was necessary because surface dissolution effects made the MTD simulations difficult to interpret. We monitored the distance of ion from the surface oxygen together with coordination number and internal energy profile as a function of time using the PLUMED software.

5.3 Results

In order to discuss the results, we first refer the reader to the table 5.1 which we provided for a comparison between three water models namely SPC/E, SPC/Fw and TIP4P2005. The main differences are charges of Ow and Hw in models and also predicted diffusion coefficient and heat capacity. However, there are some similarities with the hydrogen bond and density predictions.

Table 5.1. A comparison between different water models.

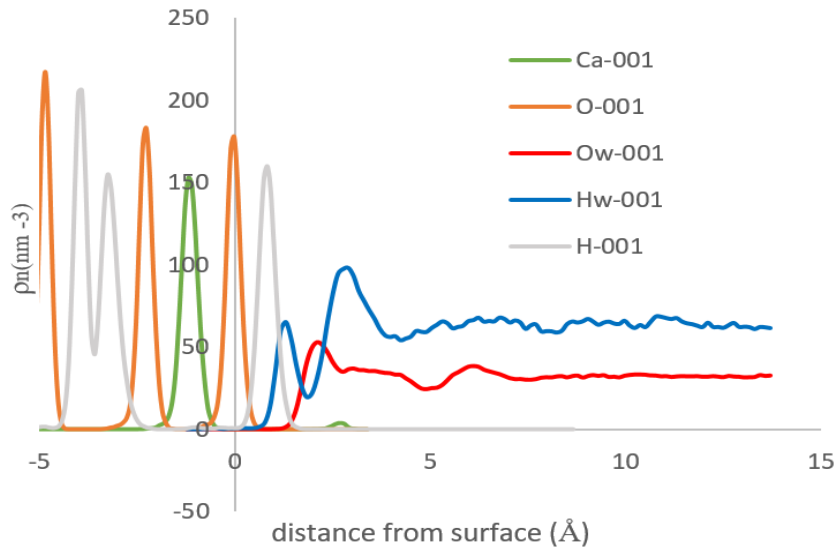
	Liquid Water	SPC/E	SPC/Fw	TIP4P2005
$q_o(e)$	-	-0.84	-0.82	-1.11
$q_H(e)$	-	0.42	0.41	0.55
$d_{OH}(\text{Å})$	0.9584	1.00	1.012	0.97
HOH angle	104.54	109.47	113.24	104.52
$D (10^{-9} \text{ m}^2/\text{s})$	2.3	2.50	2.32	2.08
$\rho (\text{g}/\text{cm}^3)$	0.997	0.998	0.998	0.996
$C_p (\text{Cal}/\text{mol}/\text{K})$	17.99	19.43	27.37	18.90

In the following sections, we will go through an analysis of results for the calculation of the structure of water above different surfaces of portlandite together with metadynamic simulations and molecular dynamic simulations of adsorption of Ca and OH onto the 00.1 CH surface.

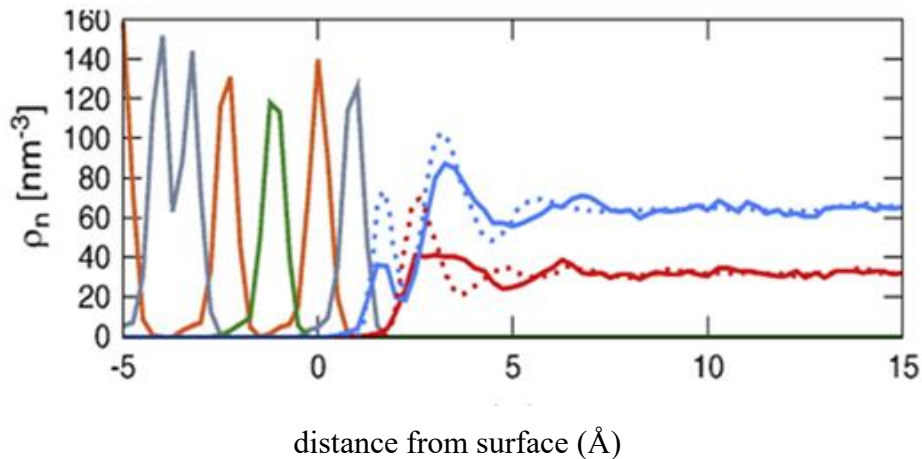
5.3.1(a) Structure of water above 00.1 CH surface

Figure 5.2 (a) shows the structure of water above 00.1 CH surface modeled with the SPC/Fw water model. For comparison, the results obtained by Galmarini et al.(5) using the TIP4P2005 water model is also shown, include here is also the SPC/E water from (6) (Fig. 5.2 (b)). As one can see from figure 5.3 the surface is oriented with OH groups terminating the portlandite surface.

The structure of SPC/Fw water model is very similar to SPC/E work of Kalinichev (6), this is expected since SPC/E and SPC/Fw water model are very similar (the main difference is the HOH angle, Table 5.1) As one can see from this figure the peaks are higher than bulk water in both first and second hydrogen peaks. The first peak is slightly lower than Kalinichev work (6) but it is still higher than TIP4P2005 work of Galmarini et al (5) indicating a more ordered and denser profile than TIP4P2005 but slightly lower than SPC/E. The position of the hydrogen peaks has very similar positions for all three water models. When looking at atomic snapshots (figure 5.3 (a) and (b)), we see two types of water site, b1 and b2. In the b1 site both hydrogens of the water



(a)



(b)

Figure 5.2. (a) structure of water above 00.1 CH surface modeled by SPC/Fw – this work. (b) structure of water above 00.1 CH surface modeled by TIP4P2005 (Galmarini et (5))- with dotted lines corresponding to density profile for SPC/E water model from Kalinichev et al (6)

molecules make hydrogen bonds with O in the surface whereas for the b2 only one hydrogen of the water molecule make hydrogen bond toward the surface. Kalinichev et al. (6) only mentions type b1 but as figure 5.3 shows we can detect both sites as also found by Galmarini et al (5). As one can note there are significant difference in Ow peak since in TIP4P2005 it is very broad peak

but in SPC/Fw it is quite a sharp peak. At 5 Å from the surface both models show a minimum however minimum of Hw is more evident in TIP4P2005 rather than SPC/Fw water model. These all might be due to different parameters of TIP4P2005 and SPC/Fw water models.

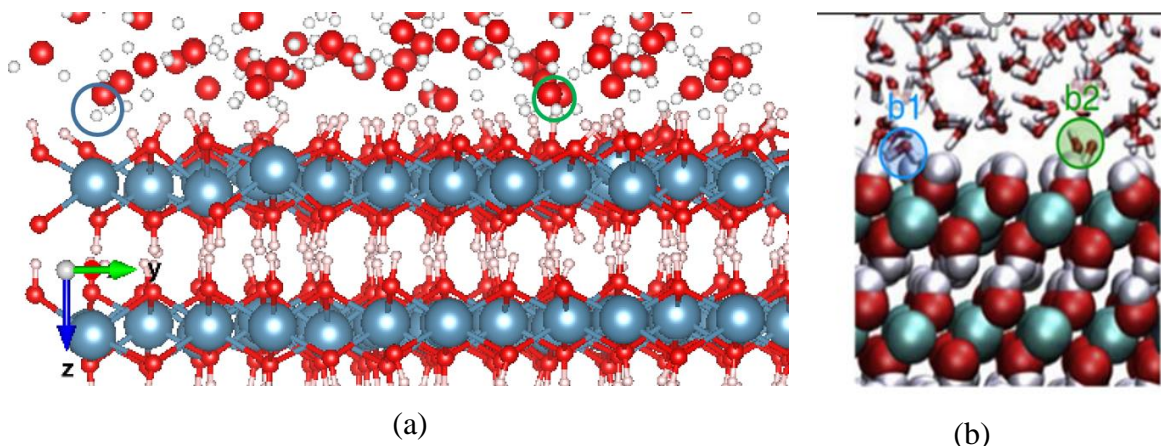
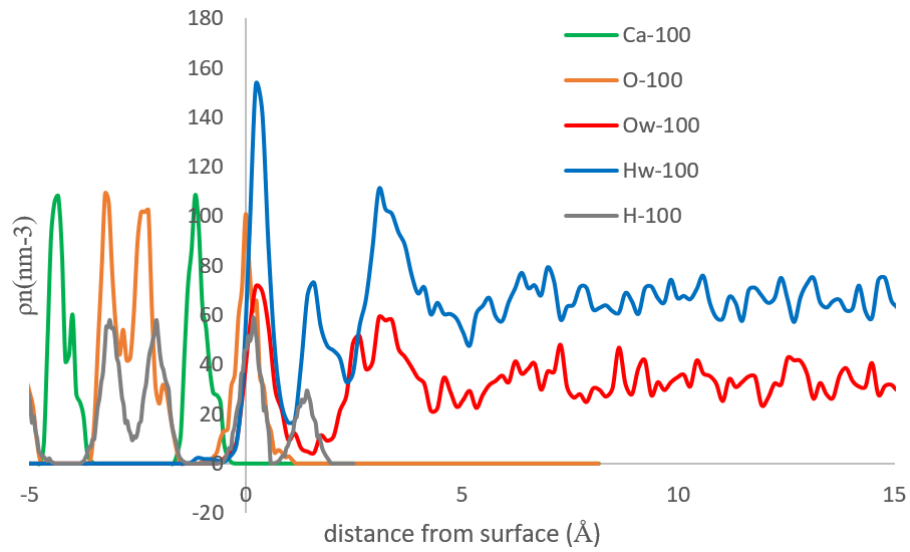


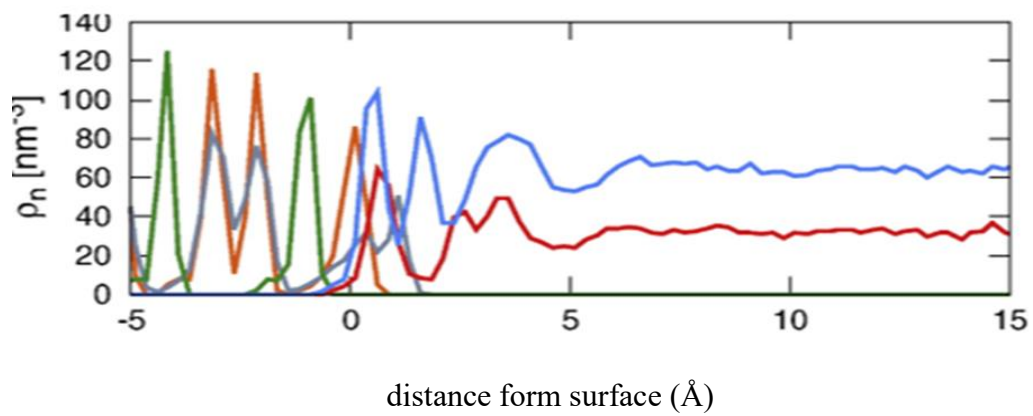
Figure 5.3) (a) snapshot of water above 00.1 CH surface SPC/Fw – this work (b) atomistic snapshot of water above 00.1 CH surface TIP4P2005 (Galmarini et al. (5)) Blue: type 1-Green: type 2

5.3.1(b) Structure of water above 10.0 CH surface

Figure 5.4 (a) shows a structure of water above the 10.0 CH surface modeled with the SPC/Fw water model. A comparison result obtained by Galmarini et al. (5) using TIP4P2005 is also shown (Figure 5.4 (b)). As shown in Figure 5.5 the 10.0 surface is terminated by OH. Again, two different types of bound water sites can be seen b1 and b2. Type b1 is situated at a position close to where the next hydroxyl layer of portlandite may form. The type b1 waters donate two hydrogen bonds to the surface hydroxyl groups. Type b1 is seen to be highly populated.



(a)



(b)

Figure 5.4. (a) structure of water above 10.0 CH surface modeled by SPC/Fw water. (b) structure of water above 10.0 CH surface modeled by TIP4P2005 water

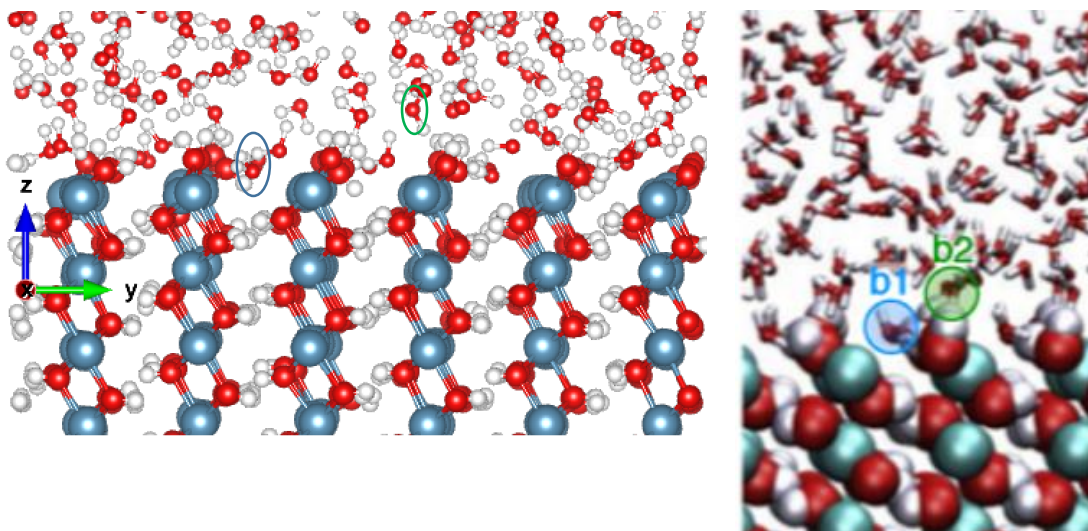


Figure 5.5) (a) snapshot of water above 10.0 CH surface SPC/Fw (b) snapshot of water above 10.0 CH surface TIP4P2005 (from (5)). blue: type b1-Green: type b2

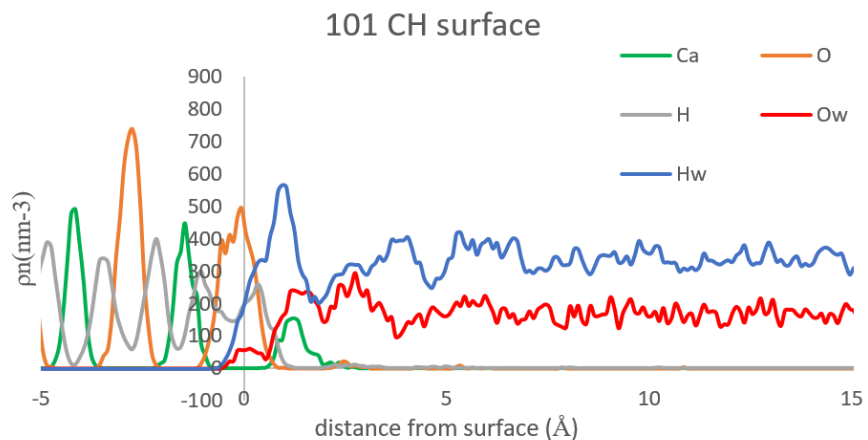
The occupancy of b2 water molecules is similar to one of 00.1 surfaces. According to this figure Ow slightly closer to surface in for SPC/Fw in compare to TIP4P2005. This maybe because of modification of CH hydrogens. According to the water density profile (Fig 5.4(a)) we can see that the population of the water layer at 10.0 surfaces is higher than 00.1 CH surface because of an increase in the type of water sites. Indicating that water is interacting more strongly with the 10.0 CH surface compared to the 00.1 surface. We can in fact see three peaks of Hw and three peaks of Ow at 10.0 surfaces which also means that water at 10.0 CH surface is more structured than the 00.1 CH surface where we only observed two peaks

5.3.1 (c) Structure of water above 10.1 CH surface

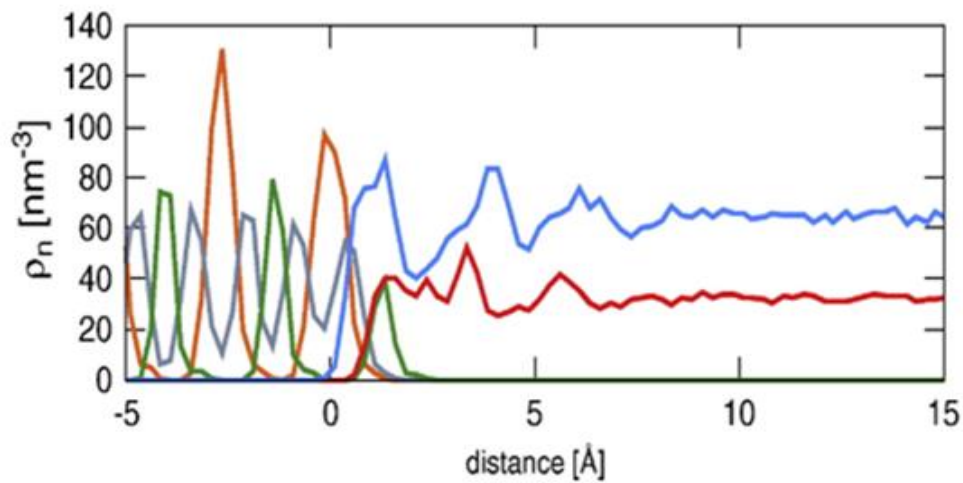
Figure 5.6 and 5.7 show the structure and snapshot for the 10.1 CH surface. The 10.1 surface is terminated by alternating hydroxyl groups and calcium ions. Type b1 and b2 waters are both situated slightly above the two hydroxyl groups with hydrogens pointing toward OH groups, forming hydrogen bonds. In type b1: water molecule is suited between two occupied Ca sites with Ow tilted toward the nearest Ca. In type b2: The Hw is closer to the surface between two empty Ca sites, Figure 5.7 (a).

On this surface, as previously observed by Galmarini et al (5) a type b3 site is observed: the water molecule sits above the surface Ca with Ow toward the Ca (Fig. 5.7 (a) and (b)). The Ow has density peaks at 0, 1.5 and 2.5 Å from surface, the Hw density peaks occur at 1, 2.5, and 3.5 Å

from the surface. The profile of water SPC/Fw is very similar to TIP4P 2005 (Fig. 5.6(b)) except that there is a small peak of Ow at the same position of H of the Hydroxyl of the portlandite surface. The reason for this peak is possibly the dissolution of OH in water for this surface as discussed in the dynamic simulations in the following sections.



(a)



(b)

Figure 5.6. (a)structure of water above 10.1 CH surface modeled by SPC/Fw, this work. (b)structure of water above 10.1 CH surface modeled by TIP4P2005 (from (5)).

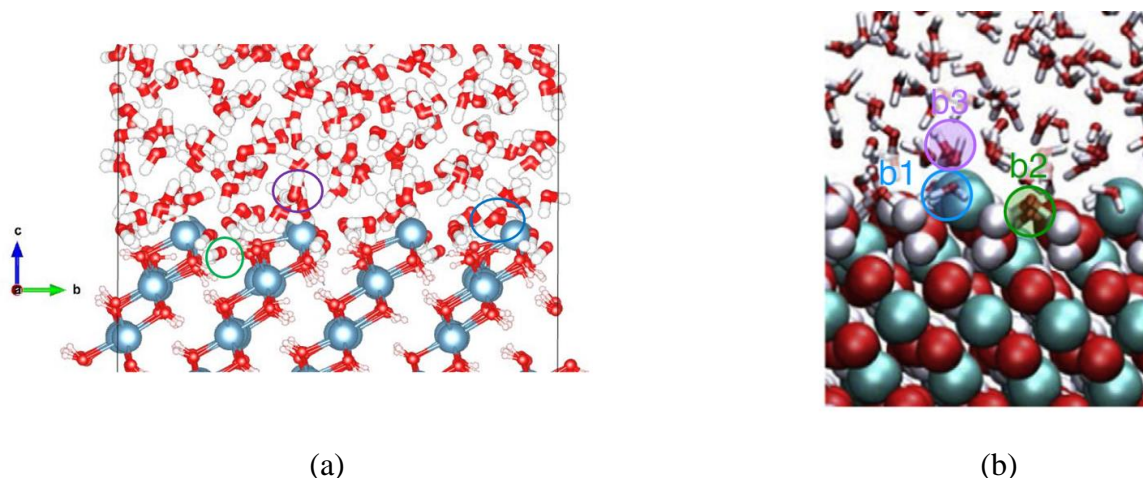


Figure 5.7) (a) snapshot of water above 10.1 CH surface SPC/Fw (b) snapshot of water above 10.1 CH surface TIP4P2005(from (5)). – blue: type b1-Green: type b2 purple: type b3

In conclusion for this section the water structure above the three different portlandite surfaces varies with the surface. Three hydrogen bonded water sites are observed with different frequencies on the different surfaces. The results for the SPC/Fw water model are similar to previous simulations using SPCE (6) and TIP4P2005 (5) but there are differences in the densities of the different water sites. In general, the SPC/Fw water seems to be interacting a little more strongly with the portlandite surfaces studied.

5.4 MTD simulation of adsorption of Ca^{2+} and OH^- onto 00.1 CH surface

We performed MTD simulations of adsorption of Ca^{2+} and OH^- onto the 00.1 CH surface. Simulation details were mentioned in the section 5.2.2. It was observed that in the MTD simulations that both Ca^{2+} and OH^- dissolve from the surface into the water and remain in solution. In the case of Ca^{2+} adsorption after 2.5 ns one Ca^{2+} dissolves from the surface and after 18 ns one OH^- dissolves and remain in solution. In the case of OH^- adsorption after 3 ns 1 Ca^{2+} dissolves and one OH^- dissolves after 8ns, again both remain in solution for the rest of the simulation.

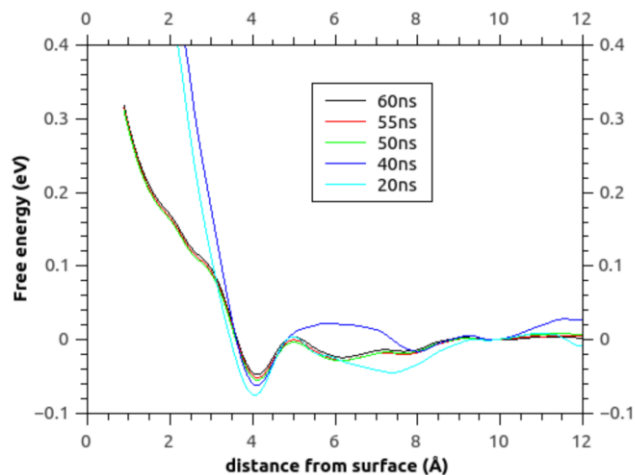
5.4.1 Ca^{2+} adsorption onto 00.1 CH surface

Figure 5.8(a) shows free energy profiles (FEPs) for the MTD simulations of Ca^{2+} adsorption for up to 60 ns, together with the water structure at this surface (Figure 5.8(b)). The FEP's show a significant amount of variation as a function of time, probably influenced by the dissolution of the surface. Please note that this dissolution could happen in real cement systems considering that in

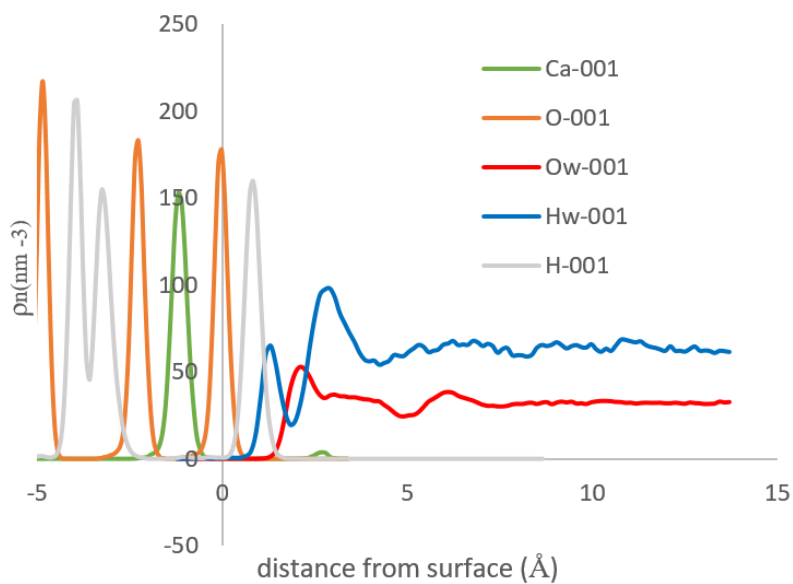
the simulation the concentration of $\text{Ca}(\text{OH})_2$ in our water box is 0.5 mM, which would correspond to a pH of 11.7. At such a pH the expected equilibrium concentration of Ca^{2+} is around 10 mM [12]. Therefore, we would expect dissolution at some stage since the system is undersaturated. However, the final 10 ns shows reasonable consistency, it is difficult to call it convergence as the CV is ill-defined because of the dissolution. The FEPs over the last 10 ns show a clear attractive minimum at 4 Å, a minor minimum at 6 Å, and perhaps a hint of one at around 8 Å. Please note that no averaging was done on the FEPs and the output profile was shifted in order to set zero energy at 10 Å.

A comparison between Figure 5.8.a and 5.8.b shows that Ca diffuses through the water and reaches the minimum at 4 Å, just where the first b2 type water layer ends (Figure 5.8 (b), i.e. suggesting an outer sphere adsorption. The depth of the minima was -0.5 eV at 4Å, -0.2 eV at 6 Å and -0.1 eV at 8 Å. Figure 5.9 shows a Snapshot of MTD Ca adsorption at 4 Å at 10 ns.

As one can see from figure 5.9 Ca^{2+} adsorbs in the middle of a group of 3OH⁻s and in the middle of 2 Ca^{2+} ions in the underlying structure. Figure 5.10 shows the Ca distance and coordination number collective variables as a function of simulation time. As figure 5.10 shows Ca^{2+} ions do not stay for a long time at the surface. Ca^{2+} regularly gets to around 4 Å before the dissolution.



(a)



(b)

Fig5.8. (a)Free energy profile of adsorption of Ca onto the 00.1 CH surface simulated by MTD
 (b) water structure of SPC/Fw water model above 00.1 CH surface

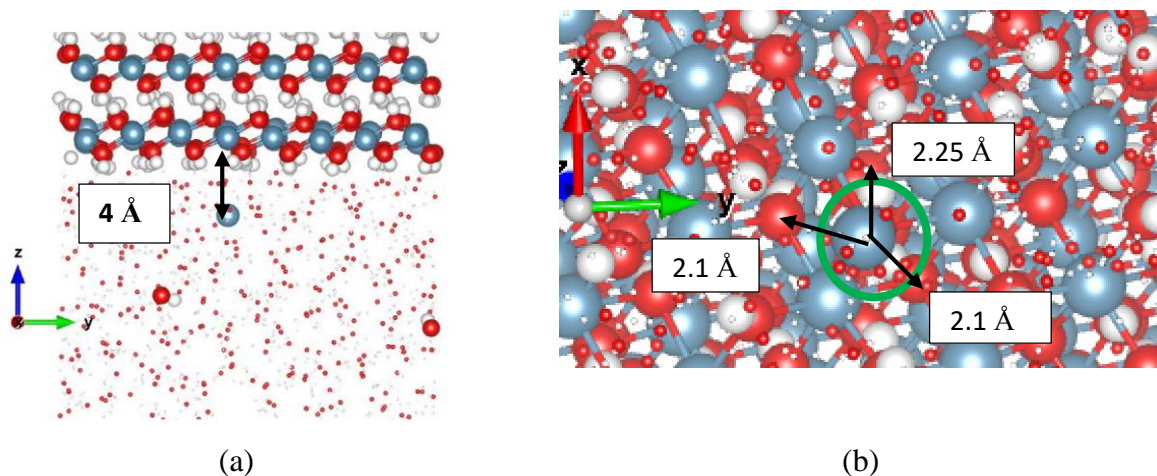


Figure 5.9. Snapshot of adsorption of Ca onto 00.1 CH surface simulated by MTD at 10 ns and minima at 4Å. (a) side view (b) top view (before OH dissolution)

However, because of dissolution we have to be careful not to over interpret as at 18 ns the OH in the central cylinder dissolves in water which makes the CV negative— as this oxygen was the designated surface atom. We have a negative CV from 18 to 25 ns because the designated surface atom is moving in the box. Thereafter the distance CV is ill-defined and cannot be interpreted.

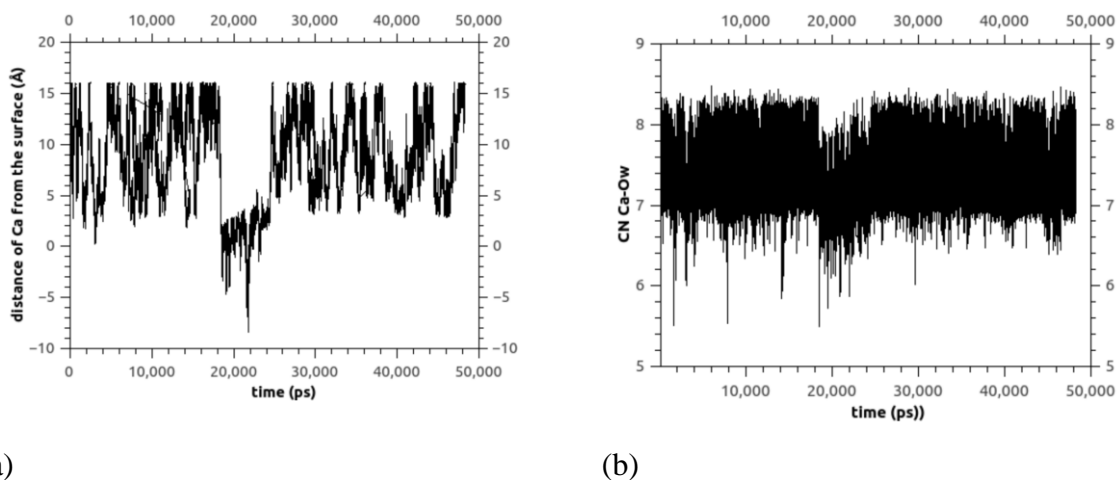


Figure 5.10. (a) distance of Ca^{2+} from the 00.1 CH surface as a function of simulation time by MTD (b) coordination number of Ca-Ow as a function of time simulated by MTD

5.4.2 OH adsorption onto 00.1 CH surface

Figure 5.11 shows FEPs of OH adsorption onto 00.1 CH surface from MTD simulations. When we have dissolved OH, apart from the negative distance CV problem it interacts with the ion of

interest in solution and since it changes its position it affects the free energy profile, which have not converged after 60 ns. Figure 5.12 shows a snapshot of MTD OH adsorption at 4 Å from the 00.1 CH surface at 10 ns, where the OH ion adsorbs close to a group of 3 OH of the underlying portlandite surface.

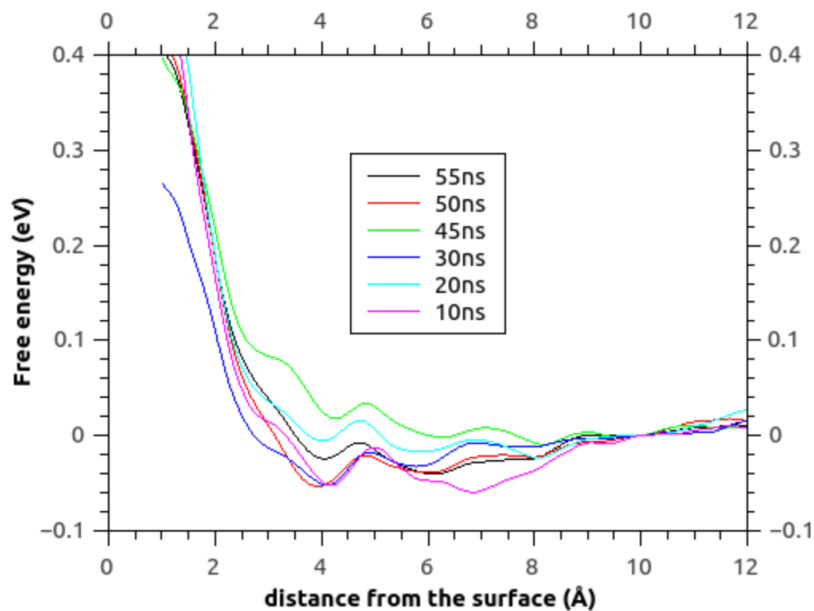


Fig 5.11. Free energy profiles of adsorption of OH onto 00.1 CH surface simulated by MTD at various simulation times

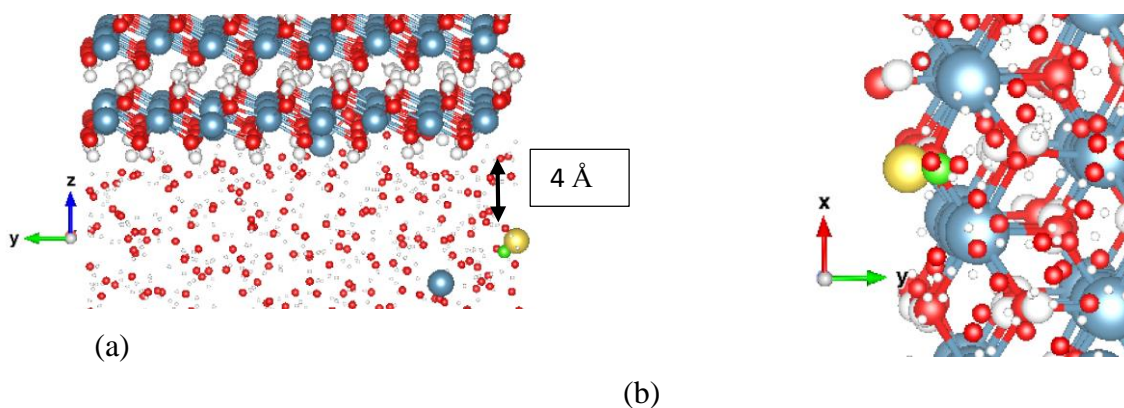
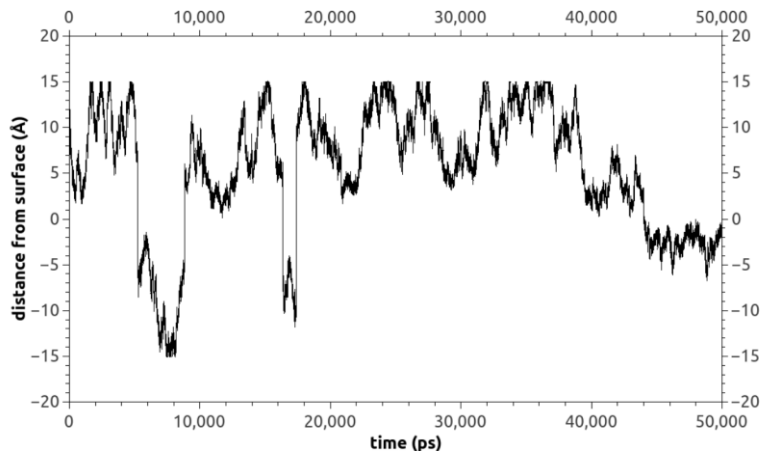
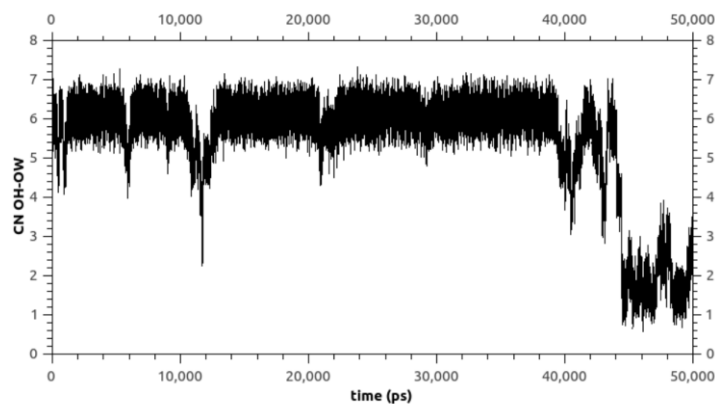


Figure 5.12. Snapshot of adsorption of OH into 00.1 CH surface simulated by MTD – at 10 ns time...and minima at 4 Å (a) side view (b) top view-adsorbed OH - Yellow: O (OH-Ion) green: H (OH-Ion)

As figure 5.13 shows at 5 ns OH from the cylinder dissolves in water which makes a negative CV. This affects the free energy profile since position of surface changes and we will track the wrong distance. Also, the OH⁻ ion interacts with the OH⁻ and Ca²⁺ ions dissolved in water.



(a)



(b)

Figure 5.13. (a) distance of OH⁻ from the 00.1 CH surface as a function of simulation time from MTD and (b) coordination number of OH-Ow as a function of time simulated by MTD

5.4.3 Dissolution problem in MTD

To try and make MTD studies of ion adsorption onto CH surfaces several attempts were made to modify the MTD parameters, Namely

1. Locating an upper wall for OH and Ca²⁺ at the surface at 2 Å but the simulation crashes

2. Changing MTD parameter and using lower Gaussian energy but dissolution still occurred, albeit that dissolution is expected as explained above (p. 90), it makes interpretation of FEPs difficult another CV may need to be chosen to better determine this dynamic system.

Also, the option of freezing the surface was investigated. A comparison between the water structure at a dynamic and frozen 00.1 CH surfaces was made, Figure 5.14.

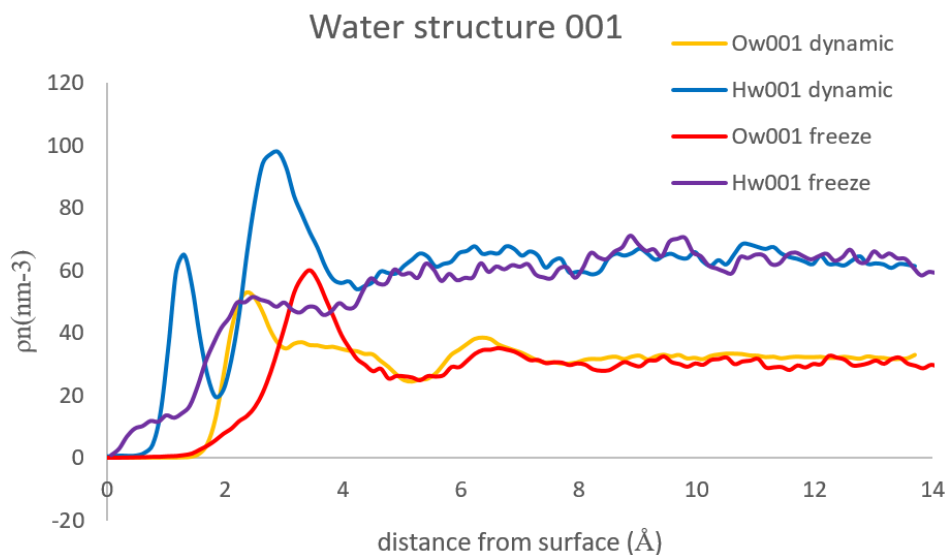


Figure 5.14. SPC/Fw water structure above 00.1 CH surface with two conditions of frozen and dynamic surface

As one can see the structure of water above 00.1 CH surface for both Ow and Hw for the dynamic surface is very different from the frozen surface. Therefore, if we freeze the surface we may get unreliable results for aqueous ions interacting with the surface.

To bring the following parts to a conclusion for the MTD simulations of adsorption of Ca and OH into 00.1 CH surface

- We cannot confidently use MTD for the adsorption of Ca^{2+} and OH^- into the CH surface
- The main reason for this statement is the dissolution of Ca^{2+} and OH^- from surface to water
- The main problem is regarding the dissolution of OH^- into water as this OH^- is the defined surface atom
- Dissolved OH^- changes its position and occasionally interacts with the Ca ion thus affects the FEP

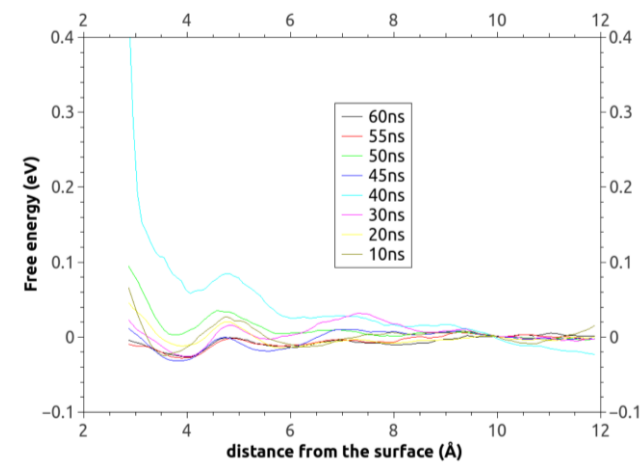
- Possible reasons for dissolution is that in MTD we add energy to the surface with our bias potential and another reason is that dissolution enthalpy of portlandite in water is more negative in our MD simulation when compared to the experimental value. Experimental heat of dissolution of portlandite in water is -0.19 eV and with ERICA FF we modeled it to be -0.56 eV. Please see Chapter 4 (section 4.3.2 and table 4.3) for more information.
- These two factors cause dissolution
- It was concluded to try MD and see if the surface was stable without the bias potentials used in the MTD simulations.
- The free energy profiles however between 52 and 60 ns for both Ca and OH suggest that both Ca^{2+} and OH^- may adsorb via outer sphere type interactions.

5.5 MD simulation of adsorption of Ca^{2+} and OH^- onto 00.1 CH surface

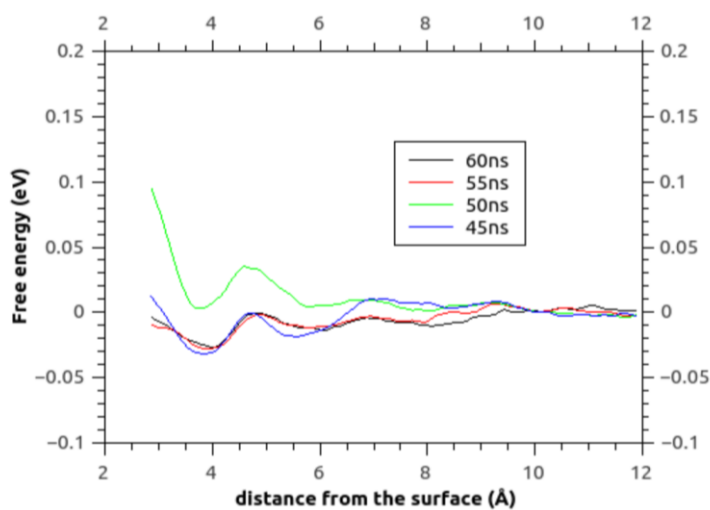
In this section, the results obtained for simple MD simulations of adsorption of Ca^{2+} and OH^- onto the 00.1 CH surface. Our results show that dissolution problem of OH and Ca into the water is solved in MD simulations of the 00.1 CH surface. Figure 5.15.a and 5.15.b shows free energy minima close to 4Å, 6Å and maybe 8Å, similar to those observed in the MTD simulations above. The minimum at 4Å is approximately -0.03 eV. Galmarini et al. (2) observed a free energy minimum at 8Å of -0.05 eV by utilizing the MTD method but did not see a minimum at 4Å. Generally, we can see free energy fluctuation over time and we cannot say with high certainty that it is converged or not. Free energy profiles at 45 and 55 ns and 60 ns are very close to each other however at 50 ns it is getting a bit distant from other times. Please note the minima at 6 Å is -0.004 eV and at 8 Å is -0.003 eV so are approximately 10 times weaker. These are probably fluctuations as these values are very small in comparison to kT (0.0259). Figure 5.15 (c) shows the distance of Ca^{2+} from the surface as a function of time. Several adsorption and desorption events can be seen. The longest residence time was observed between 29 to 32 ns. At least 5 adsorptions were observed for a time more than 300 ps. approximately for $\frac{1}{4}$ of time Ca stays in the minima at 4 Å. Despite the limitations of the MTD simulation the minimum at 4 Å is also clearly seen there (Figure 5.8.a), so is probably not a total artifact.

Figure 5.16 shows the variation of coordination number Ca-OW as a function of time. CN varies between 6.2 and 8.3. Ca loses 1 water molecule –indicating outer-sphere adsorption at $\sim 3.6\text{-}4.4$ Å.

(a)



(b)



(c)

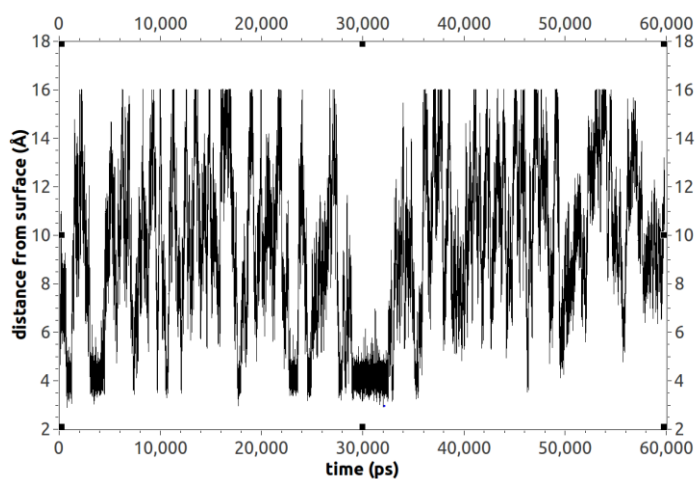


Figure 5.15. Ca adsorption onto 00.1 CH surface simulated by MD (a) free energy profiles at 10 ns intervals (b) free energy profile at the end of simulation (c) distance of Ca from 00.1 CH surface as a function of time

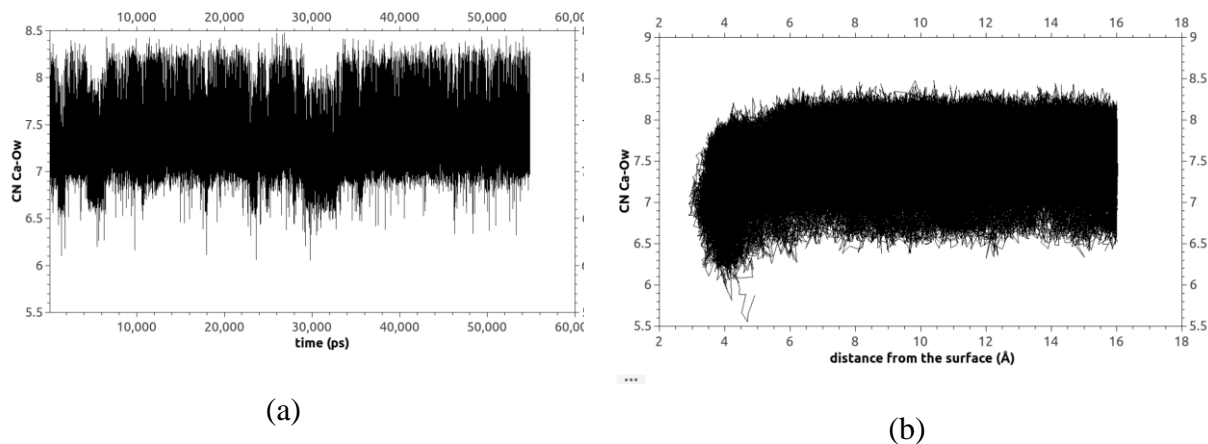


Figure 5.16. (a) CN Ca-Ow as a function of simulation time for adsorption of Ca onto 00.1 CH surface simulated by MD (b) CN Ca-Ow as a function of distance from surface for adsorption of Ca into 00.1 CH surface simulated by MD

The average of CN Ca-Ow is 7.42 without CN at 4 Å. Average of CN Ca-Ow is 6.45 at 3.6-4.4 Å. Minimum CN of Ca-Ow is approximately 6. The distance CN plot clearly shows adsorption at 4 Å. CN versus time shows a relatively prolonged adsorption of Ca around 30 ns.

In figure 5.17 one can see a snapshot of adsorption configuration of Ca at the 00.1 CH surface. Visual inspection shows that Ca adsorbs between a group of OHs. The horizontal distance of adsorbed ion from OHs on the surface are similar, at around 2.1 Å showing that Ca likes to interact with OHs in the top layer as well as the surrounding water. Please note that this is a snapshot chosen in the region where Ca stays at 4 Å (between 29 and 32 ns) but the position of Ca was not monitored and this needs to be confirmed with further analysis. Its vertical position is close to the position where the next layer of Ca would be found in a growing crystal.

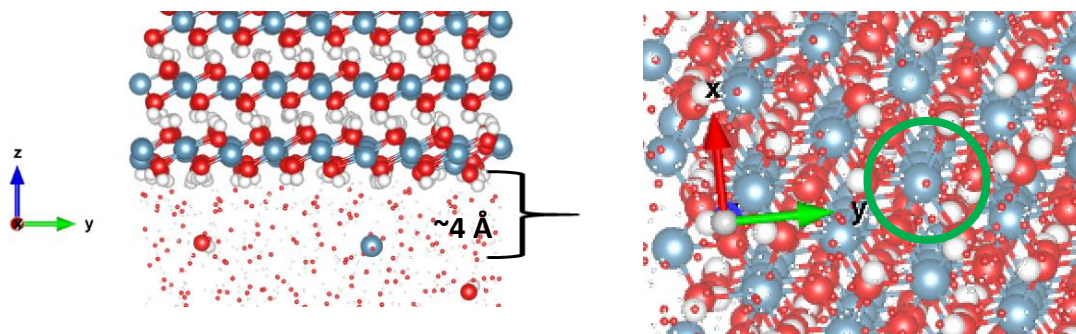


Fig 5.17. Snapshot of adsorption of Ca^{2+} onto 00.1 C surface simulated by MD after at 10 ns and 4 Å (a) side view and (b) top view

Figure 5.18(a) shows the Free energy profile of OH^- adsorption into 00.1 CH surface simulated by molecular dynamics up to 60 ns, no dissolution of the surface was encountered. The simulation has not completely reached convergence but figure 5.18 (b) shows FEPs of a similar shape with some variations in the energy level. Figure 5.18 (c) shows the distance of OH from the surface oxygen. As one can see from this figure several adsorption and desorption events can be identified. Adsorption at 3.8 Å distance from the surface has a minimum in the 60ns FEP of -0.04 eV. At least 8 adsorption phenomena were observed with residence times of more than 300 ps. For 1/3 of the simulation time the OH can be found in the 3.8 Å attractive minimum.

Figure 5.19 shows the adsorption configuration of OH onto the 00.1 CH surface at 10 ns. As one can see from this figure OH adsorbs between a group of 3 OHs on the surface. Please note that it is a snapshot at 10 ns representative of a close approach of OH to the surface but the position of OH was not monitored. Also, it is worth mentioning that OH adsorbs with its oxygen toward the H of the hydroxyl at the surface.

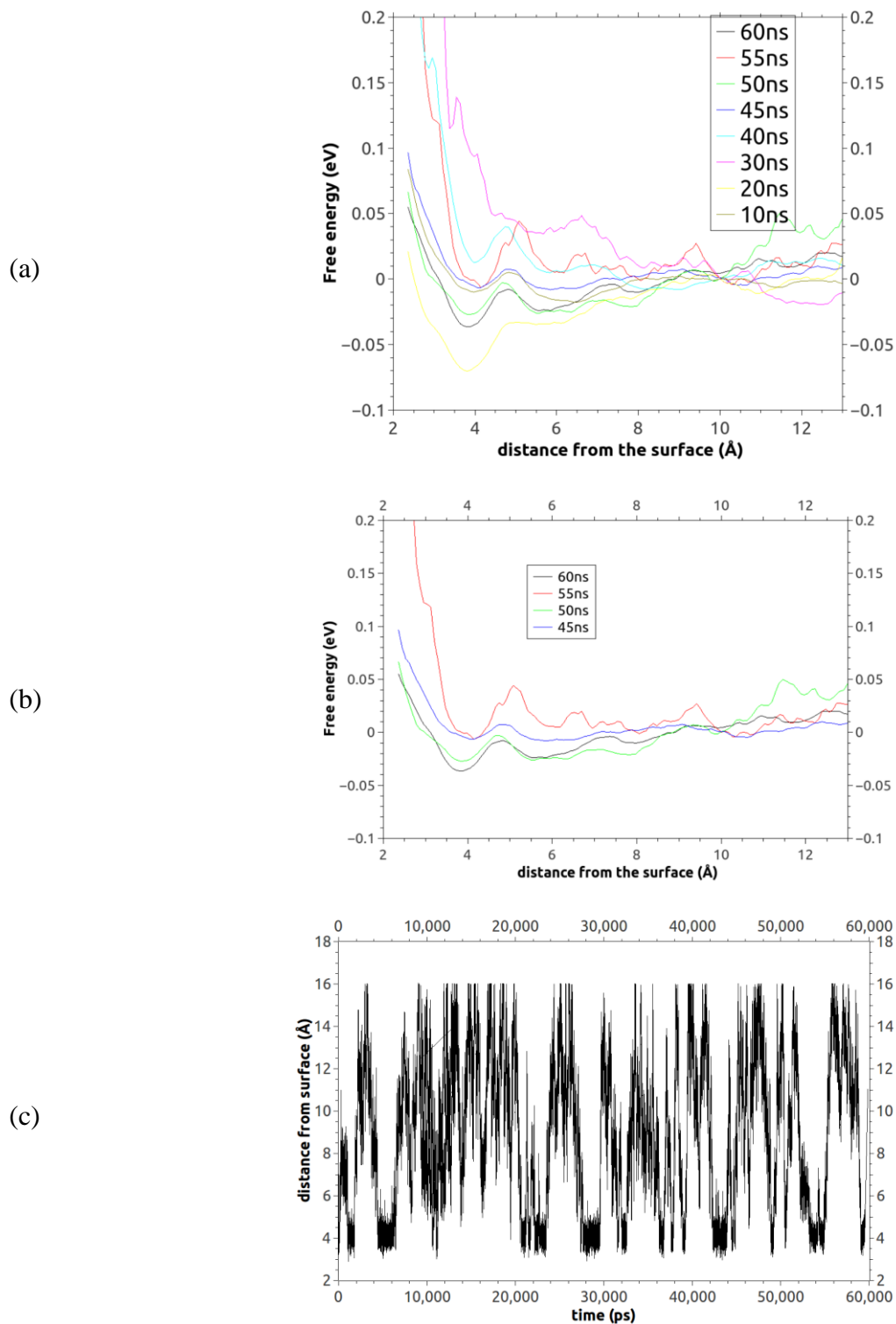


Figure 5.18. OH adsorption onto 00.1 CH surface simulated by MD (a) free energy profile of in 10 ns interval (b) free energy profiles at the end of simulation (c) distance of OH from 00.1 CH surface as a function of time simulated by MD

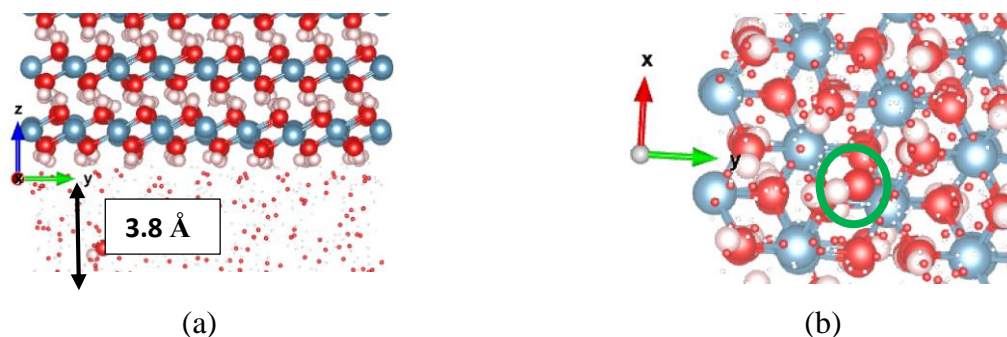


Fig 5.19. Snapshot of adsorption of Ca^{2+} into 00.1 CH surface simulated by MD at 10 ns and 3.8 Å distance from the surface (a) side view (b) top view

Figure 5.20 shows the Coordination number of OH-Ow. CN varies between 4.2 and 7 and OH loses 1.5 water molecules –indicating outer-sphere adsorption at ~ 3.8 Å. The average of CN OH-Ow is 7.2 without CN at 3.8 Å. The average of CN OH-Ow is 4.7 at 3.8 Å. The minimum CN of Ca-Ow is approximately 4.2. Previous work by Galmarini et al (5) on the adsorption of OH onto this 00.1 CH surface did not show such clear adsorption sites in their MTD simulations. This could be due to the low simulation times of just a few ns as well as the different water models. It seems that in these unconstrained MD simulations the OH ion approaches the first water layer and then finds it difficult to get closer to the surface.

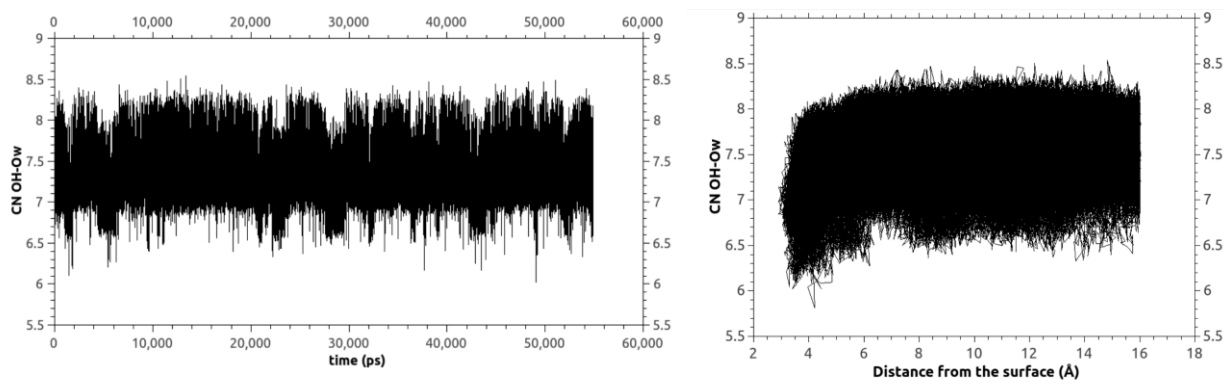


Figure 5.20. (a) CN OH-Ow as a function of time for adsorption of OH onto 00.1 CH surface simulated by MD (b) CN OH-Ow as a function of distance from surface for adsorption of Ca onto 00.1 CH surface simulated by MD

Conclusions for this part of the simulations regarding adsorption of Ca and OH into 00.1 CH surface simulated by MD is as follow:

- For both Ca^{2+} and OH^- weak adsorption energy minima are located after the first layer of water.
- Ca^{2+} adsorption is different from Galmarini et al (5) since we see adsorption at 4 Å but they did not observe that, only at 8 Å. This interaction is slightly more pronounced than in the Galmarini et al. (5) work.
- These minor modifications in the FEP for this work compared to the and Galmarini et al (5) work are probably due to the different water models.

5.6. Summary and Conclusion regarding structure of water above CH surfaces and simulation of Ca and OH into 00.1 CH surface using MTD and MD methods.

In the above sections we went through the simulation of the structure of water above 3 surfaces of portlandite. A comparison with Galmarini et al (5) results which used the TIP4P2005 water model was also made. It was realized that the 00.1 and 10.0 CH surface SPC/Fw water model produce similar results for the structure of water above the surfaces. However, for the 10.1 CH surface, the only difference between SPC/Fw and TIP4P2005 is a small peak of O_w at the same position of OH as in the surface. The MTD simulations along with visual inspection shows that this is due to the dissolution of OH from the 10.1 CH surface into the water. The simulation of the adsorption of Ca^{2+} and OH^- onto 00.1 CH surface by use of metadynamics, was complicated due to this dissolution of Ca^{2+} and OH^- into the water. Although the Ca^{2+} adsorption seemed to reach reasonable convergence we were not able to confidently fully interpret the results. The main reason for the dissolution was thought to be the energy input into the system when adding the potential bias in the MTD simulations. Also, the more negative dissolution enthalpy found with the ERICA FF when compared to experimental values (-0.56 cf -0.19 eV) is expected to contribute therefore to look at these adsorptions with ERICA FF the use of standard MD simulations was attempted. However, please note that this dissolution would be expected in real cement systems considering that in the simulation the concentration of $\text{Ca}(\text{OH})_2$ is 0.5 mM (pH 11.7) which is below the expected equilibrium concentration of 10 mM at pHs around 11.5. Therefore, we expect

dissolution since the system is under saturated and the surface definition or the current CV needs to be reconsidered to better capture the dynamics of this system.

If we compare the MD (and MTD for Ca^{2+}) results obtained in this work and that of Galmarini et al. (5) for Ca^{2+} and OH^- ion adsorption onto 00.1 CH surface they are different. This is partly due to different water model since we used SPC/Fw water model and Galmarini et al. (5) used TIP4P2005 water model. Dissolution of OH^- and Ca^{2+} ions with the SPC/Fw water model did not occur in case of TIP4P2005 and the cement FF used (where in fact a positive enthalpy of dissolution was found for portlandite (5)). The main difference between our work and Galmarini et al. (5) is that they did not observe minima for Ca adsorption at 4\AA . This is again might be due to different interaction of Ca^{2+} ion with the SPC/Fw water model in comparison to TIP4P2005 water model as well as the much lower simulations times of Galmarini et al (5). The OH^- ion interacts and adsorbs quite regularly in our MD simulations close to the first water layer at the surface $\sim 4\text{\AA}$ which was not so clear on the MTD simulations of Galmarini et al (5) again mostly attributed to the different water models.

5.7 Preliminary MTD simulations of adsorption of Ca adsorption onto 00.1 Ca terminated C-S-H surface.

In the previous sections of this chapter we focused on adsorption of ions onto the surface of portlandite. C-S-H is a very important part of cement hydrate which constitutes most of the cement hydrates (>50%). Therefore, it is important to have an insight toward adsorption of ions on the surface of C-S-H. In following we have made some preliminary simulations of adsorption of the Ca ion onto the surface of C-S-H, a calcium terminated 00.1 surface using MTD. A calcium terminated surface was used for these preliminary MTD simulations as, in preliminary MD simulations a silica terminated surface was found to be unstable in the presence of calcium ions and re-arranged such that it approached a Ca terminated surface (8). Also in cementitious systems relatively high concentrations of Ca ions (>20 mM) are often in the pore solution during hydration. This results in a positive surface potential from the adsorption or incorporation of calcium ions at the C-S-H surface (9). The often-assumed negative surface potential for C-S-H which can be seen after thorough washing or at low Ca/Si ratios (10), was not found to be stable

but on the addition of Ca ions in solution, i.e. the strong interactions and rearrangements guided us towards starting with a calcium terminated surface (8). Other groups have used cleaved interlayers of tobermorite to create 00.1 surfaces and adjusted in an ad-hoc fashion to modify Ca/Si ratios (11). We feel the brick model (7) used to create these Ca terminated C-S-H surfaces should give more “realistic” surface arrangements.

5.7.1 Simulation details for adsorption of Ca and OH onto 00.1 C-S-H surface

The 00.1 Ca terminated C-S-H surface was produced by Ziga Casar in our group using the brick model of Kunhi Mohamed et al (7). Figure 5.21 depicts an atomistic diagram illustrating the simulation box used.

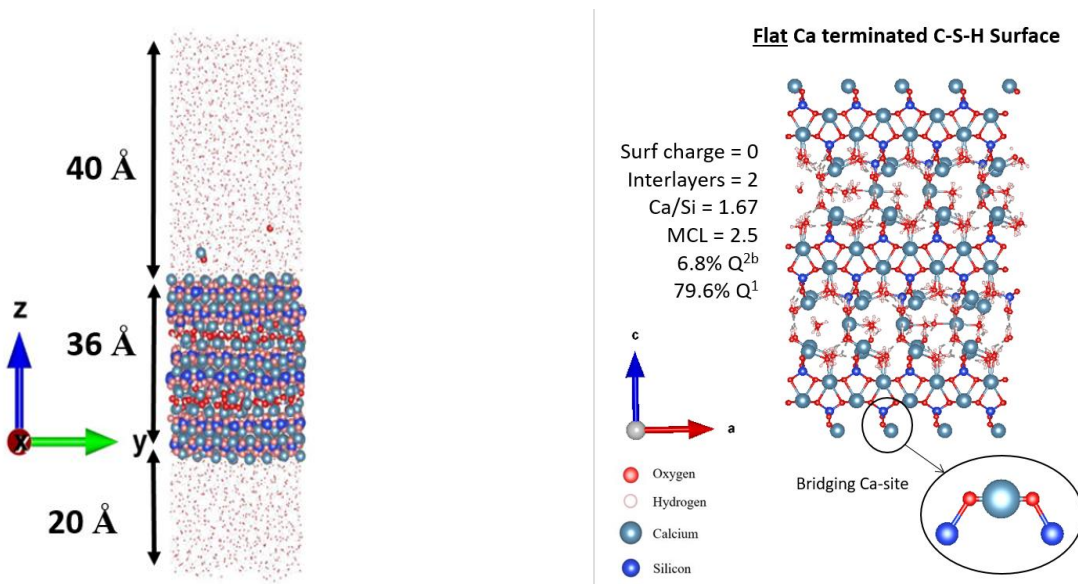


Figure 5.21) a) Diagram of slab and simulation box and b) detail on 00.1 Ca terminated C-S-H surface

Ca in the top layer and Ca in the main layer are separated by 3.2 Å. The dimensions of the box are 22 Å x 36 Å x 170 Å. With a surface charge of zero, the Ca/Si ratio of the slab is 1.67. We employed the center of mass of all Ca in the main layer as the surface for Ca adsorption, with ERICA FF2 as the modeling force field. This was chosen to try and avoid any dissolution or exchange of ions as observed in the previous sections with calcium hydroxide when using the ERICA FF suite. We used a 0.0002 ps time step and did standard MTD with an upper wall of 20

Å and a lower wall of 0 Å (main layer Calcium). We first ran an EM and then an MD simulation for 10.0 ps, followed by a 12 ns MTD simulation. The Gaussian width was set to be 0.2 Å, while the Gaussian height was chosen to be 0.005 eV.

5.7.2 Analysis of results a for adsorption of Ca and OH onto 00.1 C-S-H surface

The FEPs of Ca adsorption onto a 00.1 Ca terminated C-S-H surface for up to 12 ns is shown in Figure 5.22.

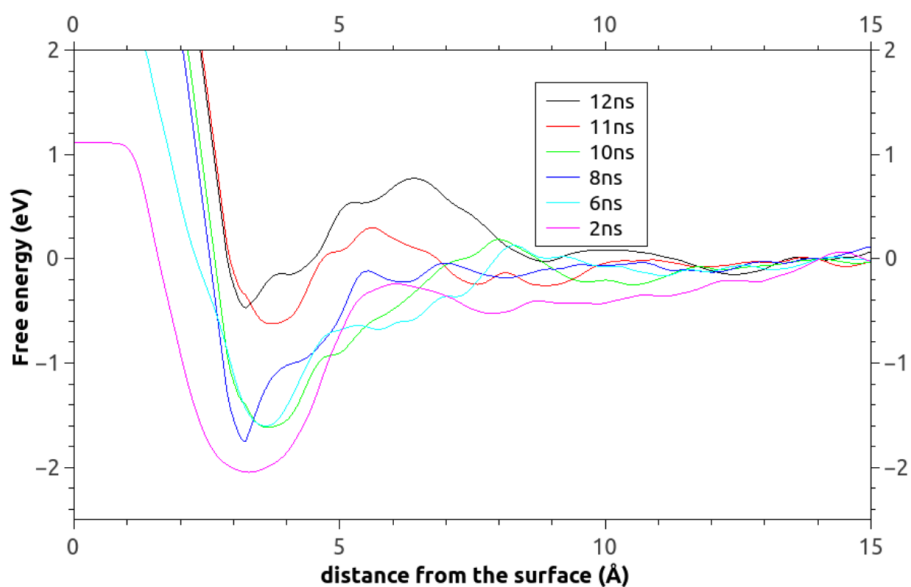
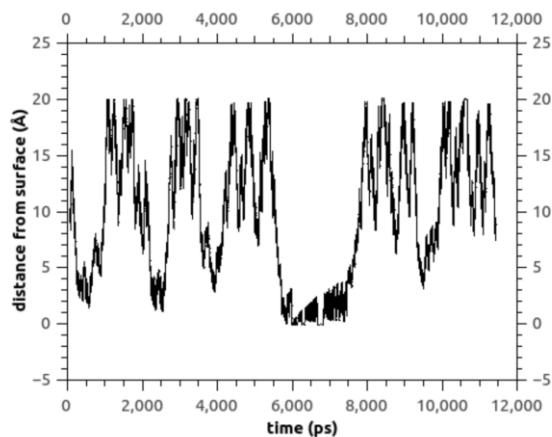


Figure 5.22. Free energy profiles of adsorption of Ca onto 00.1 Ca terminated C-S-H surface

Strong physical adsorption was predicted during the simulation period, as shown in this picture. However, convergence was not observed, and we need to run the simulation for longer, as we detect fluctuations in the FEPs. The 11 and 12 ns profiles are relatively similar. If we look at the 12 ns FEP we see a broad minimum was found at between 3 and 6.5 Å. This broad minimum seems to have 3 components at around 3.25, 4.5 and 6 Å. The 3.25 Å is close to the sites of Ca in the surface layer. Figure 5.23 depicts the distance between Ca and the internal surface (i.e. main layer of Ca), as well as the CN Ca-Ow relationship.

(a)



(b)

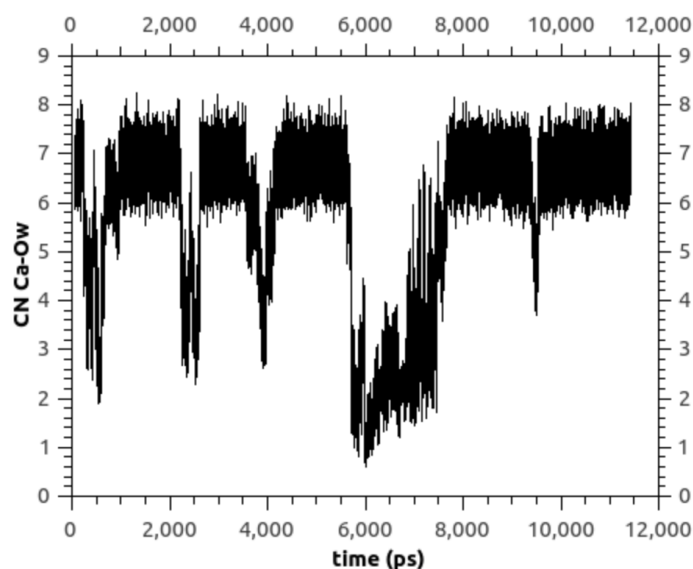


Figure 5.23 a) Distance of Ca ion from internal surface (main layer Ca) b) CN Ca-Ow for MTD simulation of Ca adsorption onto 00.1 calcium terminated C-S-H surface.

Figure 5.23 shows that at least five adsorption events for more than 200 ps. Between 6 and 8 ns, the strongest adsorption was found and it loses 5-6 water molecules. During this 6-8 ns period the Ca is coordinated with 1 Ow and 4 Osi. Our visualization shows that; this is more of an incorporation into the structure than an adsorption. Because the lower wall is 0 Å (i.e. the main layer of Ca), we predict that between 6 and 8 ns Ca ion would gravitate further into the structure if no wall was placed.

We have main two interaction events, one at 0 Å and the other at 3.2 Å, but the minima in the free energy profile are only at 3.2 Å. This could be due to the lower wall location. As figure 5.24

shows from 6-8ns period is more like an incorporation into the structure, i.e. the main layer of the C-S-H Ca layer than an adsorption as it is 3.2 Å below the surface Ca positions.

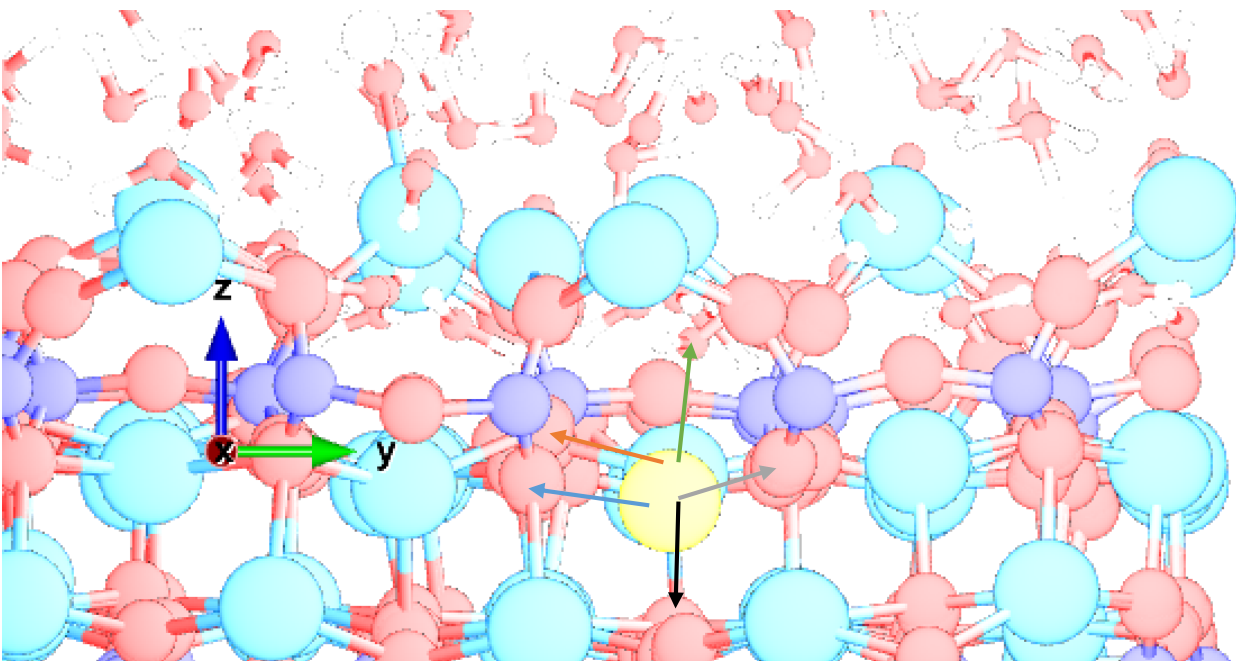


Figure 5.24. side view of Interaction of Ca ion with ca terminated 00.1 C-S-H surface by MTD. The Ca ion shown by yellow color. Color code: Light blue: Ca/ Orange: Osi/ dark blue: Si/ red Oxygen (small) ...time was chosen at 7.2 ns....arrows: Ca-Ow (green length -3.05Å)/Ca-Osi (orange-2.46 Å, blue-2.63 Å,black-2.34 Å, grey-2.24 Å)

Please note that Ca does not replace any Ca in the main layer, it is forming an interstitial defect in the Ca layer. After this “incorporation in the main layer of Ca the ion then comes back out and adsorbs at the 3.2 Å minimum at 8 ns, i.e. at the position of the surface Ca ions. Figure 5.25 depicts this adsorption of Ca ions onto the surface (with the lower wall set to 0 Å).

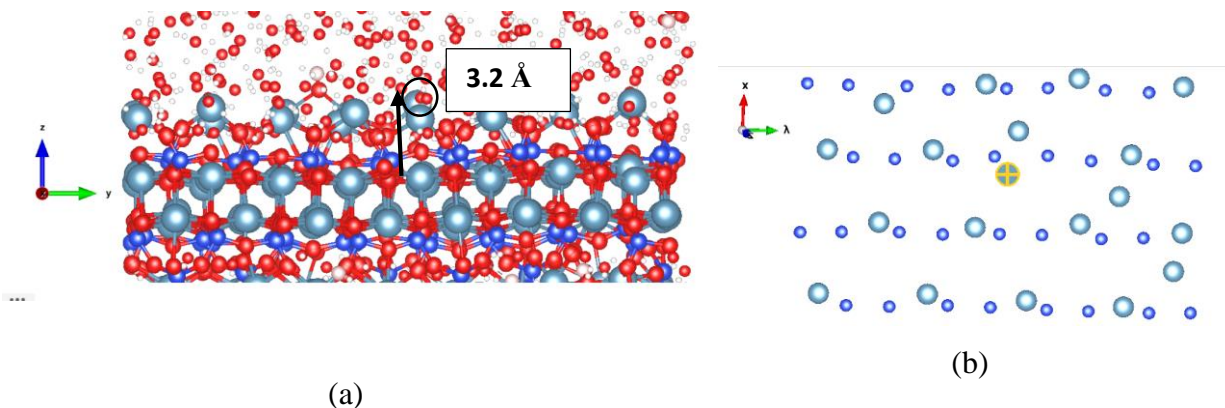


Fig 5.25 a) Ca position (circled) during adsorption if we put lower wall of 0 Å (side view) b) Ca position (circled) during adsorption if we put lower wall of 0 Å (Top view). Color code: Light blue: Ca(Ca ion highlighted)/ Red: Osi/dark blue: Si/ Red: Oxygen/...time was chosen at 8.2 ns

As can be seen in Figure 5.25(b), with a lower wall of 0 Å Ca ion is in place, it will adsorb between a group of Ca and Osi. However, in separate preliminary simulations we discovered that if we do not locate the bottom wall at 0 Å the Ca ion, can pass through the middle layer of calcium, as shown in figure 5.26 (a).

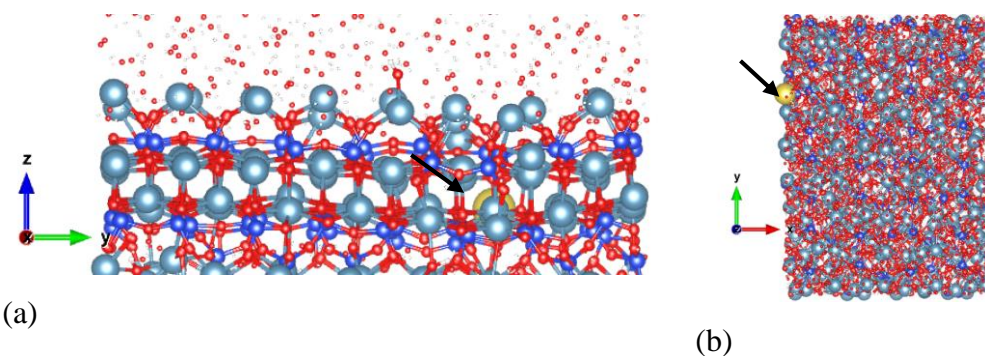


Fig 5.26. Ca position (yellow) during interaction if we do not put lower wall of 0 Å a) side view b) Top view Color code: Light blue: Ca / Red: Osi / dark blue: Si / Red: Oxygen / adsorbing Ca ion: yellow

As one can see from figure 5.26 if we do not locate any wall Ca ion will go to the main layer. Our visual inspection shows that it will happen around 3 ns time of simulation and stays there for at least 1 ns since we ran this simulation for a total of 4 ns.

5.7.3 Conclusion regarding adsorption of Ca ion onto 00.1 Ca terminated C-S-H surface.

We draw following conclusions regarding preliminary MTD simulations of adsorption of Ca onto 00.1 Ca terminated C-S-H surface.

During the 12 ns the surface was stable and no dissolution was observed contrary to our simulations with portlandite. At this Ca/Si ratio (1.67) Ca has high desirability to go to the structure of C-S-H. That can happen by distorting the main layer structure (i.e. Si and Osi). To avoid that we have to define a lower wall at the Ca in the main layer. Also, we detected strong physical adsorption of Ca onto 00.1 Ca terminated C-S-H surface. We have found one broad minimum in the FEP at 12 ns. Further simulation time should be carried out to confirm these first preliminary results.

5.8 Summary and Conclusions

This chapter involved 4 parts. In part 1 we went through a simulation of the structure of water above 3 surfaces of portlandite. A comparison with Galmarini et al (5) results which used the TIP4P2005 water model was also made. It was realized that the 00.1 and 10.0 CH surface SPC/Fw water model produce very similar results for the structure of water above the surfaces. Also, for the 10.1 CH surface it was globally similar, the only difference between SPC/Fw and TIP4P2005 is a small peak of O_w at the same position of OH at the surface. Visual inspection suggests that this is could be a precursor to the dissolution of OH in the 10.1 CH surface into the water as highlighted in the MTD and longer MD simulations. Such dissolution could be expected as for the $Ca(OH)_2$ concentrations in our simulation the CH will be undersaturated. However, our dissolution enthalpy of -0,56 eV would perhaps speed up the dissolution of the experimental -0.19 eV and give us less time to explore the CH surface before dissolution. Another factor would be to modify the surface definition and choice of CV to better monitor these dynamic systems. In part 2 we went through a simulation of adsorption of Ca^{2+} and OH^- into 00.1 CH surface by use of metadynamics. However due to the dissolution of Ca and OH into the water during metadynamic simulation we were not able to fully interpret the results. Therefore, to look at these adsorptions with ERICA FF the use of standard molecular dynamic simulations was attempted. In part 3 we went through simulation performed in part 2 by this time with the MD i.e. no biasing was applied. Dissolution problem which were occurred in MTD was not observed in MD for the 00.1 CH surface. We found

that MD (part 3) and MTD (part 2) gave similar results for depth of minima and location for Ca adsorption (00.1 CH surface). In particular, a weak outer-sphere type adsorption at a distance of 4 Å, just where the highly structured water layer demonstrated in part 1 of the chapter ends. This adsorption site had not previously been seen (e.g. by Galmarini et al (5)) and probably due to the different water models. The dissolution problems found in the MTD simulations indicate that the CH – water (SPC/Fw) interaction need to be further refined to make the ERICA FF suitable for more detailed investigations of the CH surfaces i.e. to get a dissolution enthalpy closer to -0.19 eV (the experimental values should be attempted) as well considering other surface definitions and CVs.

In part 4 we presented results of adsorption of Ca^{2+} ion onto 00.1 Ca terminated C-S-H surface. We found that there is strong physical adsorption of Ca^{2+} onto 00.1 Ca terminated C-S-H surface and both inner and outer sphere adsorption was found i.e. Ca^{2+} adsorbs above the surface, at the surface and can also incorporate into the structure by going towards the main layer. For C-S-H we have carried out a series of preliminary simulations which look promising and the ERICA FF2 is performing well, more simulation time is needed to validate our initial findings. In the future it would be interesting to look at the behavior of other surface terminations, introducing charged surfaces (to mimic different pH conditions for different types of cements) which should be rewarding avenues.

5.9 References

1. Berger R.L., McGregor J.D. Effect of Temperature and Water-Solid Ratio on Growth of $\text{Ca}(\text{OH})_2$ Crystals Formed During Hydration of Ca_3SiO_5 . *J Am Ceram Soc.* 1973, 56, 73–9.
2. Galmarini S, Aimable A, Ruffray N, Bowen P. Changes in portlandite morphology with solvent composition: Atomistic simulations and experiment. *Cem. Concr. Res.* 2011,4,1330–1338.
3. de Leeuw N.L, Parker S.C. Molecular-dynamics simulation of MgO surfaces in liquid water using a shell-model potential for water. *Phys Rev B – Condens. Matter Mater Phys.* 1998,58,13901–10.
4. Plimpton SJ, Thompson AP. Computational aspects of many-body potentials. *MRS Bull.* 2012,3,110-112;

5. Galmarini S, Bowen P. Atomistic simulation of the adsorption of calcium and hydroxyl ions onto portlandite surfaces - Towards crystal growth mechanisms. *Cem Concr Res.* 2016,81,16–23.
6. Kalinichev A.G, Kirkpatrick R., Molecular Dynamics Modeling of Chloride Binding to the Surfaces of Calcium Hydroxide, Hydrated Calcium Aluminate, and Calcium Silicate Phases, *Chem. Mater.* 2002, 8, 3539–3549
7. Kunhi Mohamed A., Parker S.C., Bowen P., Galmarini S., An atomistic building block description of C-S-H -Towards a realistic C-S-H model, *Cem Conc Res* ,2018,107, 221-235,
8. Casar Z. (LMC, EPFL)– personal communication 2021
9. Labbez C., Nonat A., Pochard B., Jönsson B., Experimental and theoretical evidence of overcharging of calcium silicate hydrate, *JCIS* 2007, 309, 303–307
10. Barzgar S., Lothenbach B., Tarik M., Giacomo A. Di, Ludwig C. The effect of sodium hydroxide on Al uptake by calcium silicate hydrates (CASA), *JCIS* 2020,572, 246-256
11. I Androniuk, AG Kalinichev, Molecular dynamics simulation of the interaction of uranium (VI) with the C–S–H phase of cement in the presence of gluconate; *Applied Geochemistry* 2014 ,113, 104496-104498
12. Galmarini S. Atomistic Simulation of Cementitious Systems. EPFL Thesis No. 5754, 2013.

Chapter 6:

Molecular simulations of adsorption of gluconate onto surfaces of portlandite and C-S-H

In this chapter first, the interaction of a gluconate molecule with portlandite surfaces using molecular dynamics (MD) will be described. The use of MD rather than MTD was chosen as the portlandite surfaces were not found to be stable in MTD simulation (Chp. 5.4.3) Then some preliminary results on the adsorption of this organic molecule on a calcium terminated C-S-H surface using MTD will be presented.

6.1 Introduction

Different retarding and accelerating admixtures are employed to influence the setting and hardening behaviors of cement, which is highly prevalent in practical concrete engineering [1]. According to their basic components, retarding admixtures can be divided into inorganic and organic admixtures [2]. Phosphates, borates, fluorine silicates, and chemical compounds based on zinc are examples of inorganic retarding admixtures [3, 4]. Saccharides, ligninsulfonates, hydroxycarboxylic acid, and their salts are examples of organic retarders [5]. One type of typical hydroxycarboxylic acid salt is sodium gluconate (SG) [6]. The strong retarding effect, good adaptability with the superplasticizer system, and low cost of SG make it a popular choice for practical concrete projects [7, 8]. Zhou et al [9] carried out a number of experiments on the effects of SG on cement paste dispersion and strength development. According to Li et al. [10], in the event of addition doses ranging from 0.03 percent to 0.15 percent (of dry cement weight), the compressive strengths of cement mortars diminish to varying degrees. According to Ma et al. [11], the right amount of SG can greatly increase the dispersion performance of cement pastes containing polycarboxylate superplasticizer (PCE). Meanwhile, according to certain research, the influence of SG on the performance and hydration process of cement pastes is dependent on the amount of SG added. According to Tan et al. [12], the dispersion of the PCE-SG system is determined by the prevailing effect, i.e., the contribution to dispersion predominates at SG dosages of less than 0.10 percent. However, at doses greater than 0.10 percent, the competitive adsorption effect takes over, resulting in decreased dispersion ability. When the dosage was less than 0.03 percent, Ma et al. [13, 14] considered SG to encourage the creation of AFt phases

(hydrated $\text{Al}_2\text{O}_3 - \text{Fe}_2\text{O}_3$ – tri phases, where tri is for 3 anions which are normally sulphate or carbonate) at an early hydration time. When the dosage is greater than 0.05 percent, SG, on the other hand, suppresses the creation of AFt. The effects of SG on cement hydration behaviors and retarding mechanisms are not entirely known, and Bishop and Barron [15] mention various possibilities. Zhang et al. [16] proposed that SG be used to postpone AFt production slightly before boosting it once it has started. Perez [17] claims that SG can be completely adsorbed on C_3S surfaces, causing significant hydration inhibition. The hydration of C_3S is slowed by SG, which extends the induction duration. The CH and C-S-H formation are strongly impacted by SG doses, according to Von Daake and Stephan [18], whereas the renewing hydration reaction proceeds faster once the induction period ends. According to Ma et al. and Wu et al. [19, 20], SG delays cement induction while speeding up C_3S hydration during the hydration acceleration interval. To the best of our knowledge, there has not been a great deal of research on gluconate adsorption on the CH and C-S-H surfaces. The single work done by the Androniuk et al [22] was a molecular dynamic simulation of gluconate adsorption onto the surface of C-S-H with Ca/Si ratio of 0.83 to 1.4. They suggested gluconate adsorbs on the C-S-H phase by forming cation bridging inner-sphere and outer-sphere surface complexes. However, no research has been done on gluconate adsorption on portlandite surfaces. Siramanont (21) performed experiment adding D-gluconate during the precipitation of synthetic C-S-H with concentrations between 3 – 12 mM, similar to the dosages used in cement. They realized that the presence of D-gluconate can affect the synthetic C-S-H precipitation both kinetics and particle agglomeration. D-gluconate was shown to adsorb on C-S-H and also complex with Ca^{2+} in solution. They also found that in the presence of D-gluconate a lower Ca/Si ratio than the pure synthetic C-S-H was produced. They claim that this could be due to either complexation of Ca^{2+} in solution or adsorption onto the C-S-H during growth and nucleation effecting stoichiometry.

Although Androniuk et al [22] performed preliminary MD studies of gluconate adsorption on C-S-H surface, their work contains limitations with respect to the C-S-H surface used and the simulations were limited to a couple of nanoseconds. We will go over molecular dynamics simulations of gluconate onto CH surfaces and present preliminary metadynamic simulations for a calcium terminated C-S-H surface in this chapter. We will go over the technical details first, followed by the results and discussion

6.2 Methods for adsorption of gluconate onto CH surfaces (MD)

In this section, we will go over the details of generation of gluconate in vacuum and water, then details of simulation for gluconate adsorption onto the 00.1 CH surface (neutral and positive) and the 10.1 CH surface (neutral and positive).

6.2.1 Details of generation of gluconate molecule for simulations in vacuum and water

We used the Generalized Amber Force Field (GAFF) [23] to model gluconate in vacuum, and we started with EM and then MD for 10 ns to ensure that the molecule was stable. The vacuum box size for gluconate was: $5\text{\AA} \times 7\text{\AA} \times 7\text{\AA}$. We utilized ambertool to build GAFF parameters for gluconate, and then converted parameters from amber to LAMMPS using the amber2lmp code. For our simulation, we employed the NPT ensemble at ambient temperature. We utilized the GAFF force field with the SPC/Fw water model to simulate gluconate in water, and these two models are thankfully compatible. For 10 nanoseconds, we measured the MD of gluconate in water. The dimensions of the box are as follows: $22\text{\AA} \times 25\text{\AA} \times 60\text{\AA}$. The simulation is stable once more for the mixture of water and gluconate.

6.2.2 Details on MD simulations of gluconate, sodium, water and portlandite surfaces

We used the ERICA FF and GAFF models to produce a box containing gluconate, sodium, water and portlandite. Please note that for mixing rules between atom types we used Lorentz-Berthelot mixing rule, the standard in the LAMMPS software. The dimensions of the box are approximately $22\text{\AA} \times 25\text{\AA} \times 120\text{\AA}$. For performing simulation there is slab of portlandite with size of 30\AA following by water with size of 65\AA and then 25\AA vacuum (fig 6.1.b). All of the simulations listed below were made up to around 10 ns:

- Adsorption of gluconate on 00.1 CH surface both positive and neutral
- Adsorption of gluconate on 10.1 CH surface both neutral and positive.
- Investigation of adsorption gluconate on 10.1 neutral CH surface with carboxylic group of the gluconate placed near the surface at distance of 2\AA for 2ns

All simulations in this part started with EM, then 1 ns equilibration, and finally analysis of the production portion.

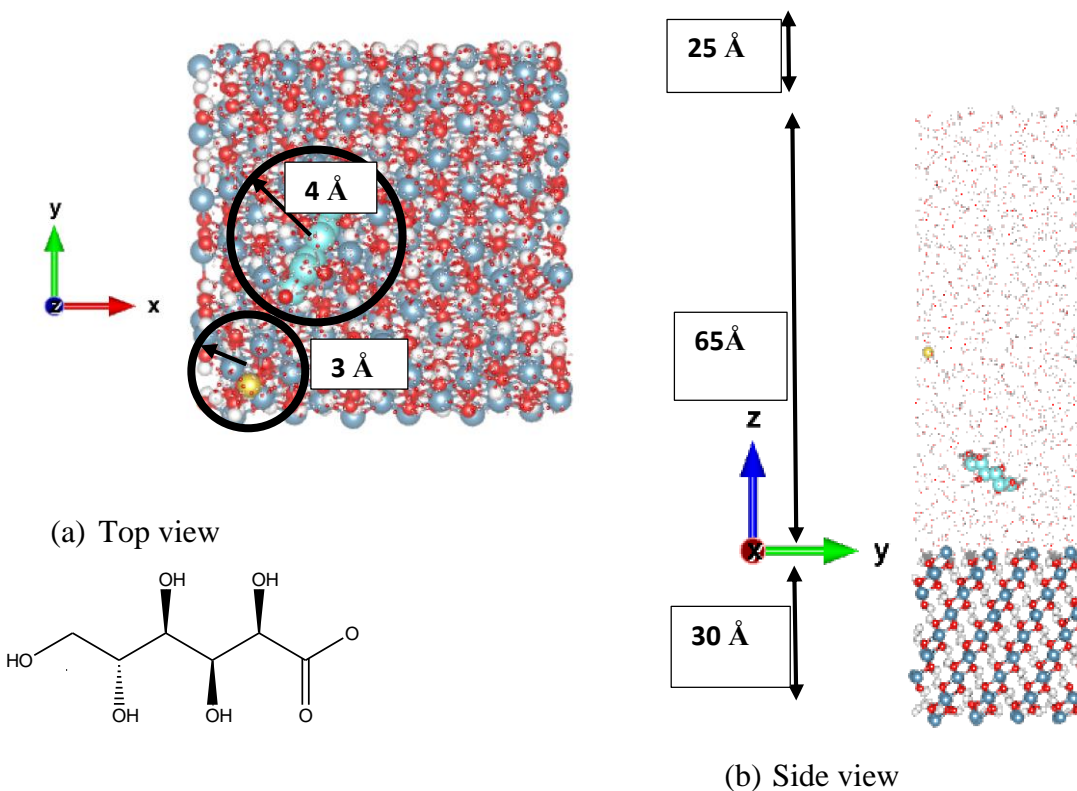


Fig 6.1. A) top view showing constraining cylinders and chemical structure of gluconate molecule b) side view atomistic representation of sodium and gluconate in 10.1 CH water box. Color code: /red- oxygen / light blue: carbon / blue: calcium /White: H, yellow - sodium ion.

We used two constraining cylinders in all simulations in this section (figure 6.1(a)), to constrain movement and complex formation, for Na (radius 3Å) and for gluconate (radius of 4Å from center of mass of gluconate). The Oxygen in middle of the two cylinders was chosen to constrain movement, one for gluconate and the other for sodium. To minimize too much surface wandering, an oxygen was fixed in the slab's center. In order to make the surface positive, we removed one OH from the region of the OH in the cylinder's center and placed the OH in the water, with free movement. One might note that concentration of gluconate in water for both 00.1 and 10.1 CH surfaces is 1mM. The center of mass (COM) of the gluconates molecules and the Center of Mass (COM) of the carboxylate group were tracked during the MD simulations by running the MD with the PLUMED MTD code but without adding any bias potentials.

6.3 Results and discussion

This section discusses the gluconate adsorption data from in this MD study on 00.1 CH, 10.1 CH surfaces, and MTD of adsorption of gluconate on 00.1 Ca-terminated C-S-H surface.

6.3.1 Adsorption of gluconate onto 00.1 CH surface – MD simulations

Figure 6.2 depicts the structure of water above the 00.1 CH surface (from Chp.5.3.1), as well as the distance between the COM of carboxylic group and the COM of gluconate from oxygen from the surface for both neutral and positive surfaces

The minimal distance from the neutral surface is 9Å. The minimal distance from the surface for the positive surface is 7Å. Thus, making the surface positive allows the gluconate to get closer to the surface in these MD simulations. Another remark is that the carboxylic group stays for more time close to surface (for positive surface) for approximately 6 nanoseconds (4-10 nanoseconds) at a distance of around 8Å of the carboxylate COM from the surface. The COM of gluconate remains similarly at around 8Å from the positive surface (Figure 6.2(c)), i.e. in a more or less parallel orientation (Figure 6.3 (b)). For the neutral surface (Figure 6.2 (b)) the orientation varies more throughout the simulation from perpendicular with carboxylate closer to surface (e.g. 4-5 ns), through parallel (1-3 ns Figure 6.3 (a)) to perpendicular with carboxylate further away from the surface (8-9 ns). Overall indicating that gluconate prefers positive surfaces to neutral surfaces an expected stronger repulsive electrostatic interaction between the OH terminated 00.1 CH surface and negative charge of the carboxylic group. Conversely it interacts more strongly with the positive surface owing to an attractive columbic component between the positive surface and the carboxylic group. This 00.1 CH surface has a highly structured water layer up to around 4.5Å (Fig 6.2 (a)), and gluconate stays beyond this layer and cannot penetrate it the timeframe of our MD simulation.

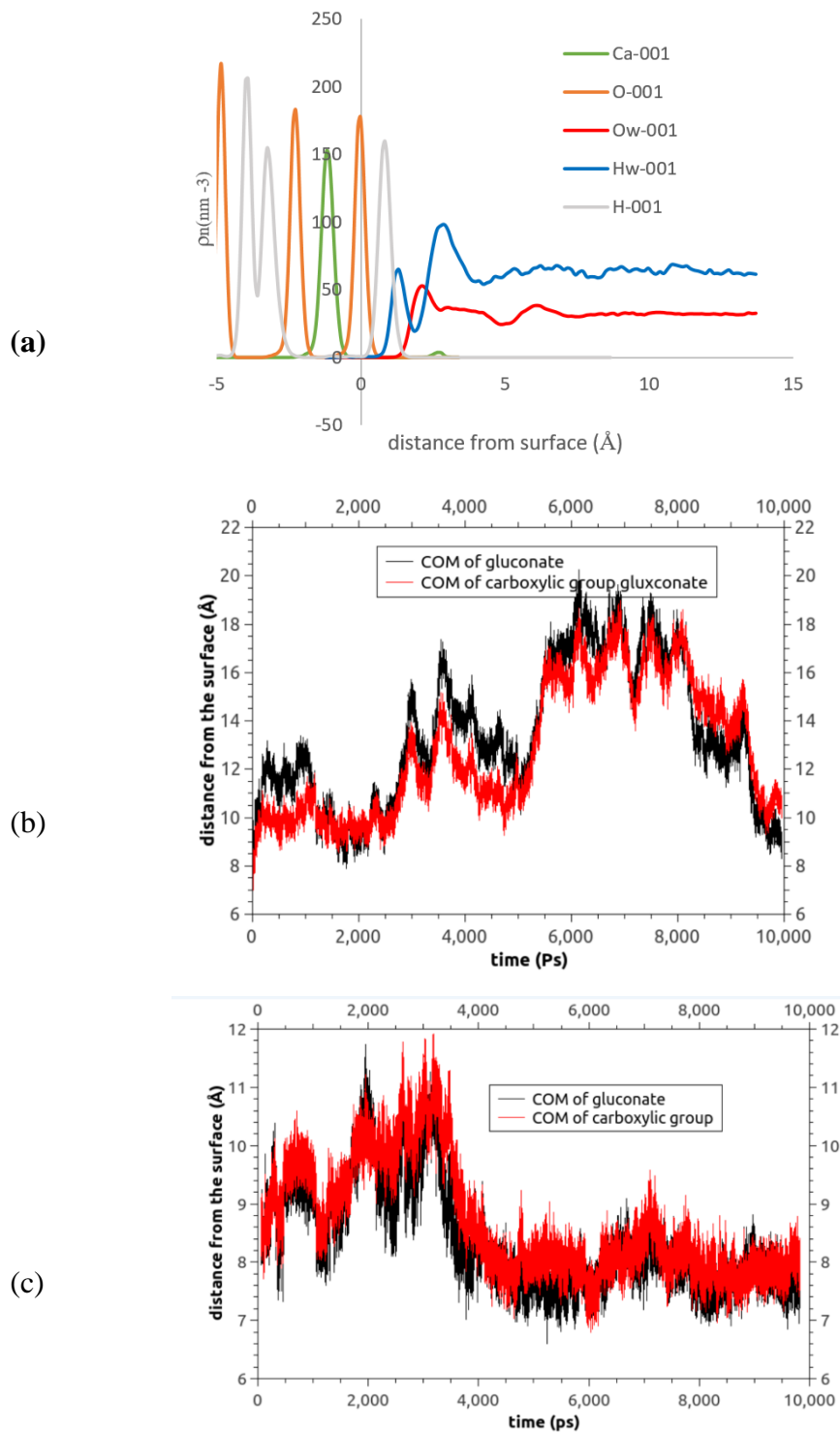


Figure 6.2.a) water structure above 00.1 CH surface b) distance of COMs and carboxylic group and gluconate molecule from 00.1 CH neutral surface – MD simulations c) distance of COMs of carboxylic group from 00.1 CH positive surface – MD simulations.

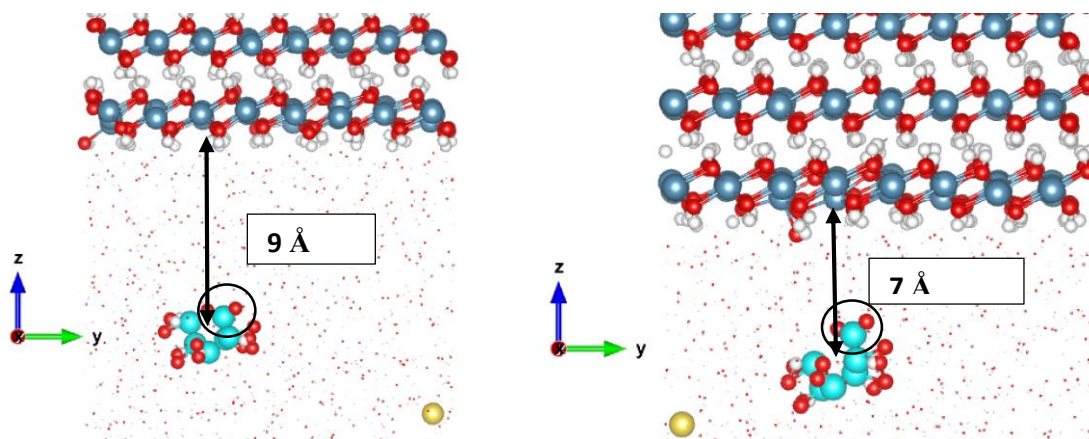


Fig 6.3. a) Representative snapshots of orientation of gluconate molecule from MD simulations at a distance of 9 Å from 00.1 CH neutral surface at 2ns showing parallel orientation. b) Orientation of gluconate molecule at a distance of COM of gluconate of 9 Å from 00.1 CH positive surface at 6ns showing an almost parallel orientation but with the carboxylate group slightly twisted towards the surface. Color code: /red- Oxygen/light blue: carbon/blue: calcium/ White H, yellow: Sodium ion. Please note that carboxylate group is shown by black circle

6.3.2 Adsorption of gluconate onto 10.1 CH surface – MD simulations

10.1CH is a surface that is terminated by Ca. As a result, we may expect an interaction between the Ca on the surface with a negatively charged carboxylic group. Again, in order to avoid ion pair formation, we use two constraining cylinders for gluconate and Na in the MD simulations. Figure 6.4 shows snapshot of initial structure (6.4.a) and after 2ns (6.4.b) before dissolution events occurred after 6ns. The dissolution behavior is shown in figure 6.5 making the analysis of the results challenging after 6 ns. In fig 6.5.the first dissolution event shows a hydroxyl leaving the surface. In figure 6.5.b we show a snapshot at 7 ns with 8 OH ions dissolved and 2 Ca ions dissolved.

Figure 6.6 shows the distance of the two COM – gluconate molecule and carboxylate group as a function of the simulation time. In contrast to 00.1 CH surface there is larger distance between

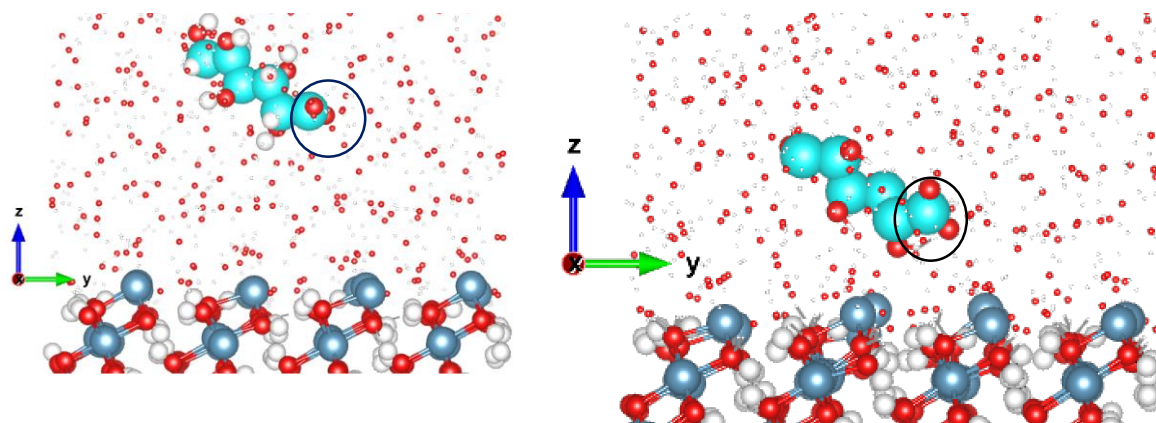


Fig 6.4. Representative snapshots of gluconate 10.1 CH surface from MD simulations at a) initial structure before minimization b) after 2 ns. Color code: /red- Oxygen/light blue: carbon/blue: calcium/ White H, yellow: Sodium ion. Please note that carboxylate group is shown by black circle

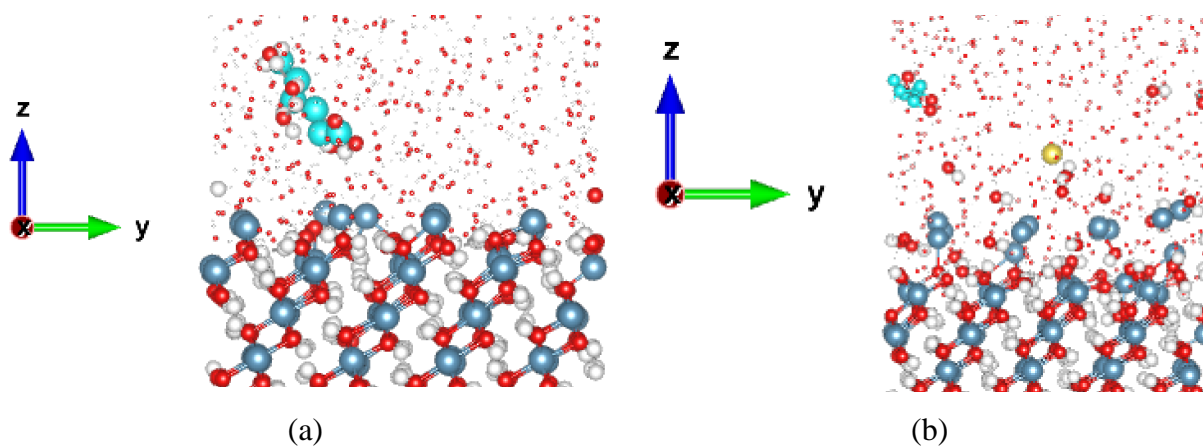


Figure 6.5. Snapshot from MD simulation at neutral 10.1 CH surface in water. (a) after 6 ns as dissolution starts (b) after 7ns – showing several Ca and OH ions from the surface in solution. Color code: /red - O /light blue: C / blue: Ca / White: H, yellow: Na.

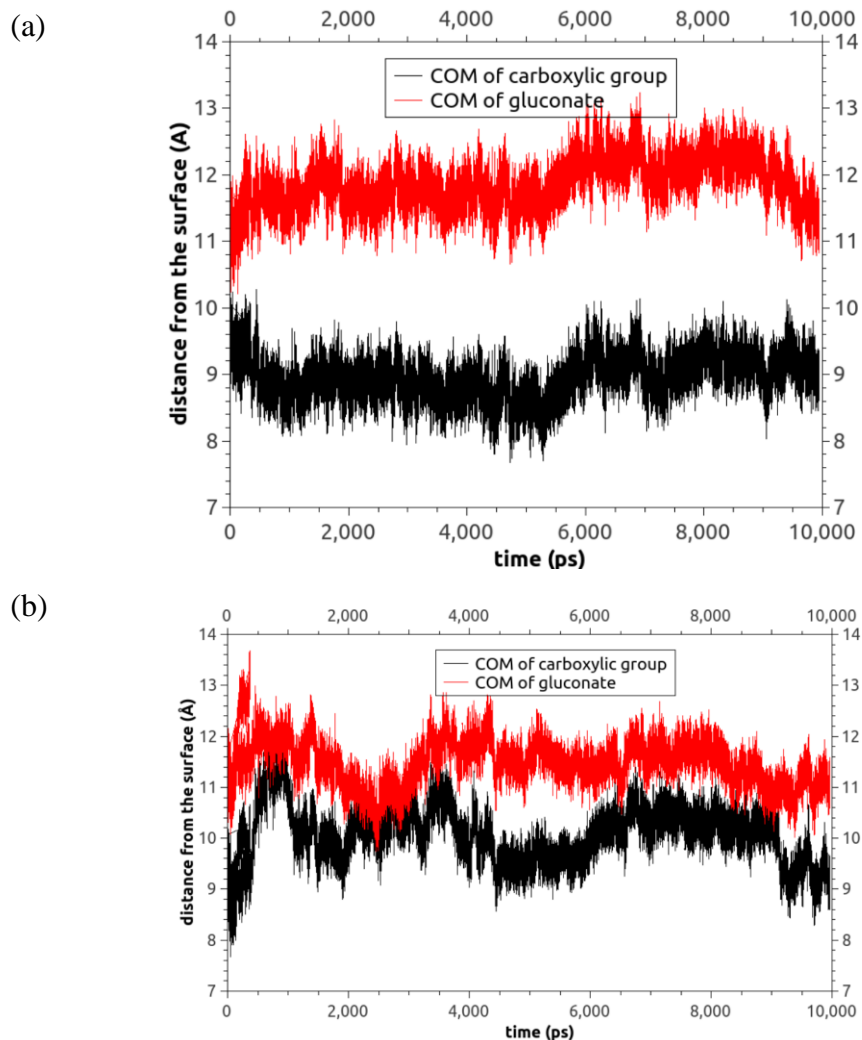


Figure 6.6 a) distance of COM for carboxylic group and gluconate molecule from 10.1 CH neutral surface b) distance of COM of carboxylic group and gluconate molecule from 10.1 CH positive surface – from MD simulations.

COM of gluconate and COM of carboxylic group even before dissolution complicates the interpretation. This can be an indication of vertical interaction with the surface with the carboxylic group always oriented towards the surface. However, we cannot over interpret after 6ns since the surface atom chosen dissolves in the water. This behavior is however more accentuated for neutral surface, again even before 6 ns.

6.3.3 Investigation of gluconate adsorption site on 10.1 neutral CH surface at distance of 2Å

Interpretation of the MD runs in the previous section was hindered because of the dissolution problems after 6 ns. Also, with the limited time in traditional MD interaction of the gluconate with the 00.1 CH surface is not fully sampled in just 12 ns. Consequently, a simulation was set up placing the gluconate molecule at 2Å from the surface, similar to those carried out by Androniuk et al. where they assumed stable interactions after placing molecules at close distances and see if they were stable for 1-2ns at least. The carboxylic group of gluconate stays within close proximity to the neutral 10.1 CH surface for the entire 2 ns production run, with much lower distance fluctuations than in the previous sections' MD runs. This implies that the carboxylic group has a strong interaction and may form an ion pair with Ca at the 10.1 CH surface as illustrated in the snap shot of figure 6.7. The Ca – O_{carboxylate} distance was on average 2.2 Å similar to the observation of Androniuk et al (22) who showed that gluconate makes an ion pair with Ca at the surface of C-S-H. They observed gluconate can create different complexes with Ca²⁺ ions present on the surface (cation bridging complexation).

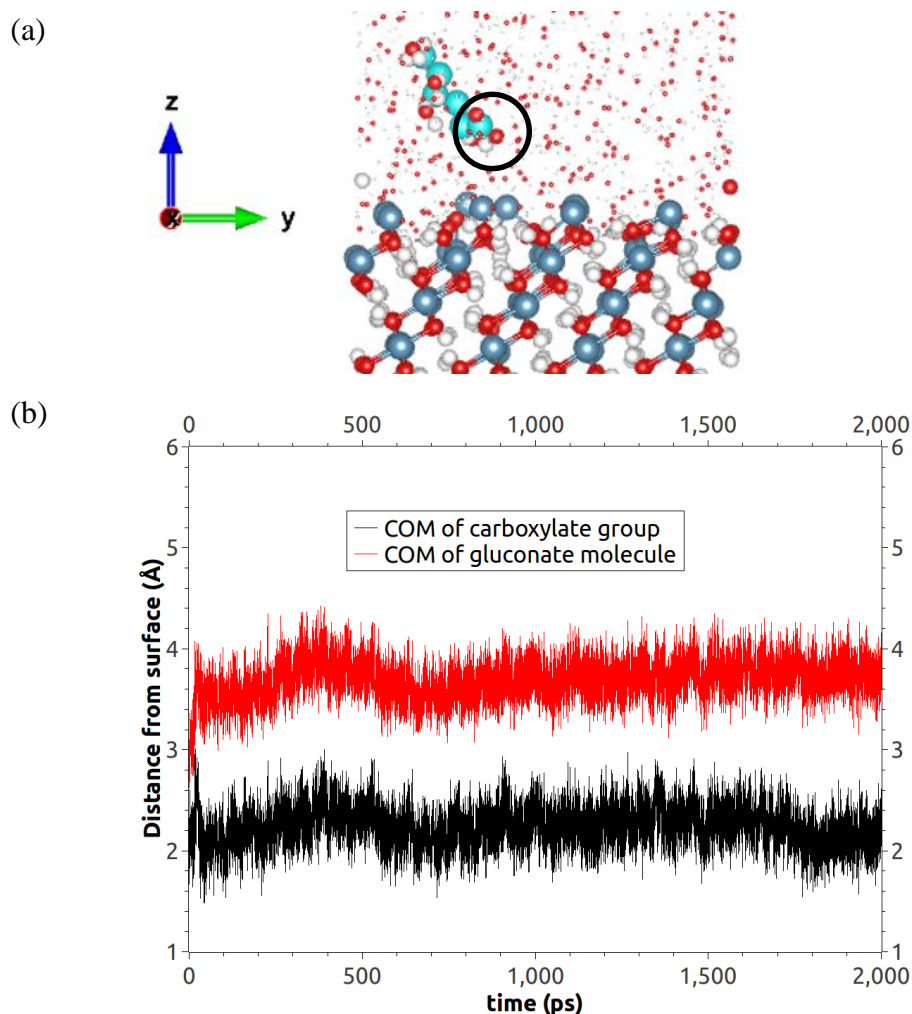


Figure 6.7. (a) snapshot after 1ns of gluconate above 10.1 CH surface after being placed initially at 2Å (b) COM plots of carboxylate and gluconate molecule from the surface. Color code: /red- Oxygen/light blue: carbon/blue: calcium/ White:H, yellow: Sodium ion. Please note that Carboxylate group is shown by black circle.

6.4 Summary and conclusions – gluconate interaction with CH surfaces

We simulated Gluconate interaction onto 00.1 and 10.1 CH surfaces (both positive and neutral) using MD. The following preliminary conclusion can be made, as further simulation time is needed to verify convergence:

- For 00.1 CH surface gluconate get closer to the surface when we make it positive (7 Å with respect to 9Å)

- For 10.1 CH surface we observed dissolution after 6 ns so we cannot over interpret the results, but before dissolution the orientation of the gluconate molecule was perpendicular to the surface with the carboxylate group closest to the surface at around 9 Å
- For 10.1 CH surface if we locate the gluconate at a 2 Å distance from the surface in the initial configuration it is stable for at least 2 ns. This indicates a possible ion pair formation between the carboxylate group of gluconate and Ca at top layer of the 10.1 CH surface.
- Future work could be to extend the MD simulation time for the 00.1 surface as well as placing the gluconate close to the surface (neutral and positive) to see if stable configurations similar to that for the 10.1 CH surface can be found.
- If the dissolution problems of CH surfaces, by modifying the ERICA FF can be solved then further work using MTD could be envisaged to better sample possible adsorption sites on these CH surfaces.

6.4 Simulation of gluconate adsorption onto a 00.1 Ca terminated C-S-H surface by MTD

For this part again 2 collective variables were defined i) as distance of COM of gluconate as well as ii) COM of carboxylic group from the Ca at the top layer on the surface of our C-S-H model. The Ca terminated surface, C-S-H slab, water and vacuum gap were the same as described in chapter 5.5.1. We defined the center of mass of all the Ca atoms at the top surface as the surface. We used NVT ensemble and performed energy minimization followed by 300 ps equilibration and then metadynamics simulations. Please note that for mixing rules between atom types we used Lorentz-Berthelot mixing rule, which is the LAMMPS default. The gaussian height is 0.005 eV and the Gaussian width is 0.2 Å. The reader might note that the concentration of gluconate is 0.5 mM in our simulation. LAMMPS input file for Gluconate Adsorption onto 00.1 Ca terminated C-S-H surface is shown in annex 3.

6.4.1 Simulation of gluconate adsorption on a 00.1 Ca terminated C-S-H surface.

Figure 6.8 depicts the free energy profile of the gluconate carboxylic group adsorption onto the surface. Despite the fact that the simulation has not reached convergence, a first look at the

results suggest strong physical adsorption may be able to take place, as many minima between 3 Å and 9 Å are observed. The FEPs at 11ns and 12 ns are relatively similar, and the COM of carboxylic group has minima around 3.5 Å and 7.5 Å from the surface. Both are relative deep minima compared to the local maxima (well depths around 0.4 eV) albeit positive absolute free energies at this stage of the simulations. Figure 6.9 depicts the distance between the carboxylic group's Center of Mass (COM) and the COM of whole gluconate molecule (Fig. 6.9(a)), as well as the number of coordination pairs between the carboxylic group's COM and water molecules (Fig. 6.9(b)).

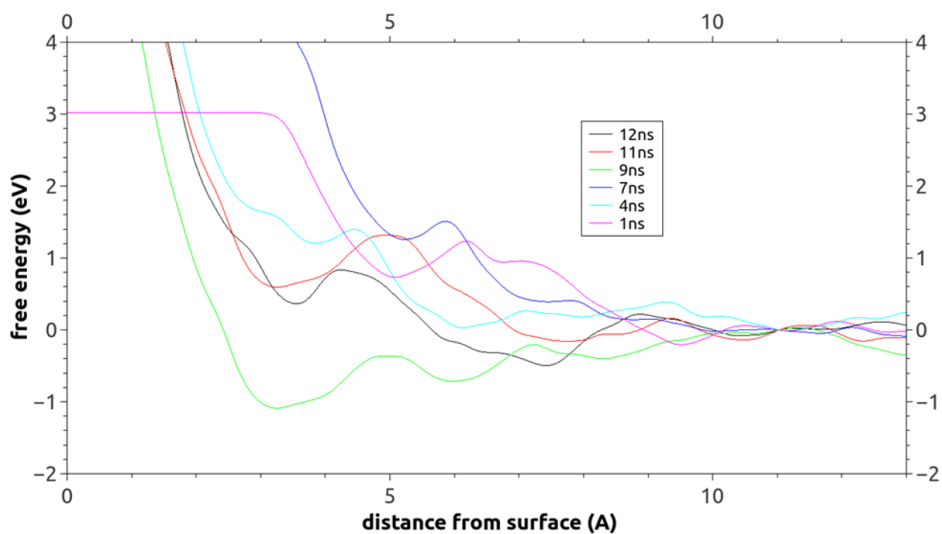


Figure 6.8) Free energy profile of adsorption of carboxylic group of gluconate onto the 00.1 Ca terminated C-S-H surface via MTD.

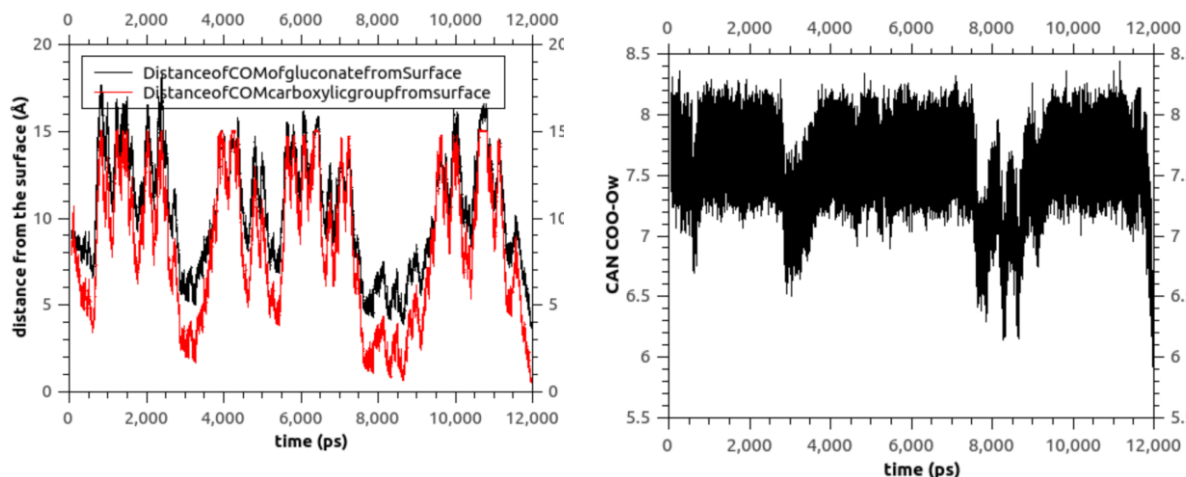


Fig 6.9) a) distance of COM of carboxylic group and gluconate molecule from surface b) Coordination number (CN) of the gluconate carboxylate group and water COO-Ow

As can be seen in figure 6.9 (a), a vertical orientation with the carboxylic group of gluconate towards the surface is predominant. The carboxylate group getting very close to the surface at several points in the simulation. Between 7.5 and 9 ns, the strongest adsorption and longest residence period was found. In figure 6.9 (b) only small changes in water coordination are seen, in particular for the very closest approach of the carboxylate group to the surface. At these positions (times ~ 3 ns and ~ 7.5 -9 ns) since only the carboxylate group is strongly interacting with the surface only the water molecules coordinated to the carboxylate group should be influenced, explaining these small changes.

Figure 6.10 depicts the adsorption configuration at the 3.5 Å and 7.5 Å minima in the FEP for the 11 ns of simulation time (figure 6.7). In figure 6.10 (a), the carboxylic group adsorbs between a group of Ca and oxygen coordinated with silicon (O_{Si}) in a vertical fashion. The distance of COO- COM from Ca is 3.5 Å and from O_{Si} is 4.9 Å, with the Ca- O_{COO} distance being 2.4 Å. For the 7.5 Å snap shot (figure 6.11), it is in a flatter orientation, albeit with the carboxylate COM a little closer to the surface than the gluconate COM.

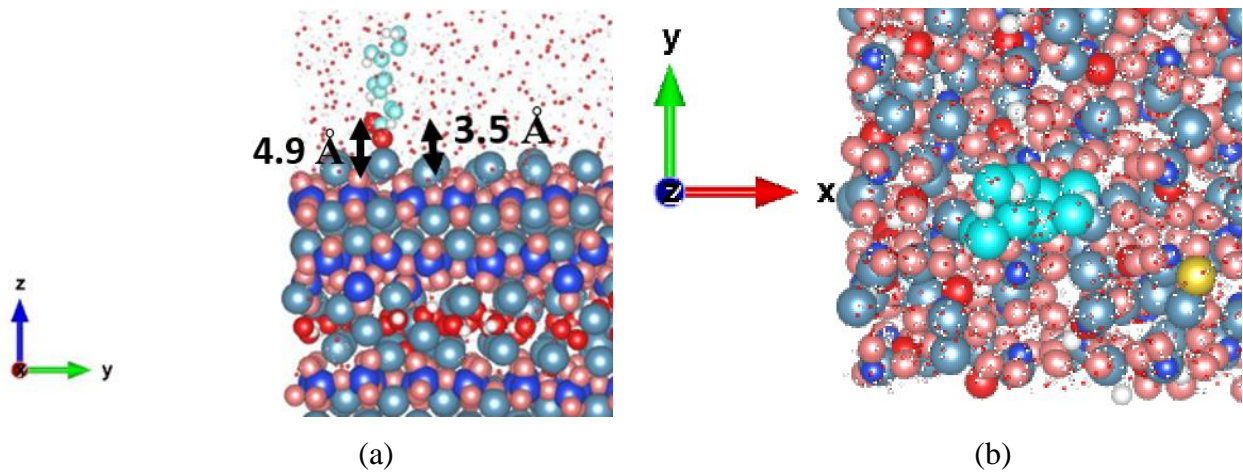


Fig 6.10 a) adsorption of gluconate at 11 ns with distance of 3.5 Å of COM of carboxylic group side view b) top view Color code: Light blue: Ca /orange: Osi/dark blue Si/ red: Oxygen/ very light blue: Carbon

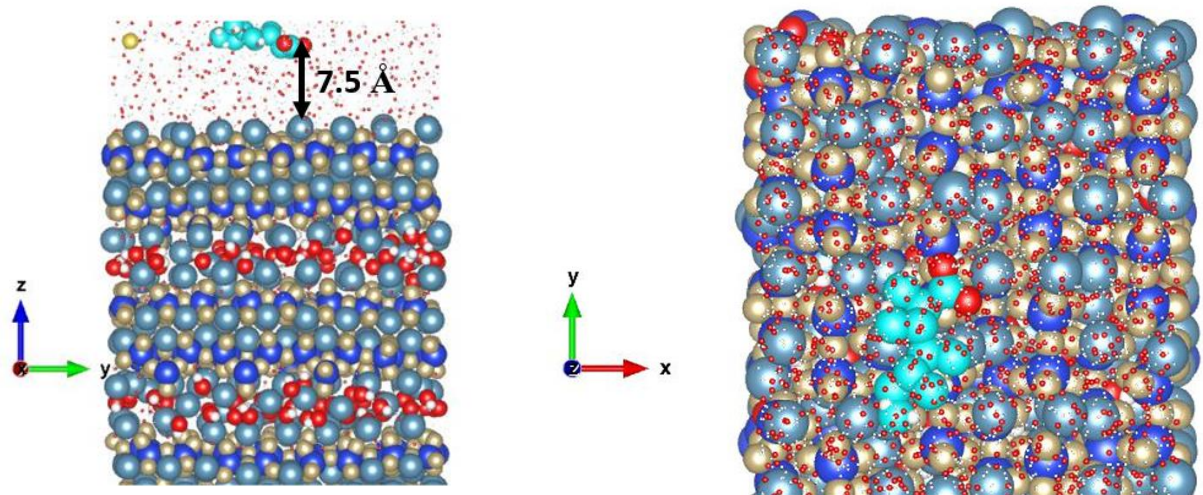


Fig 6.11) adsorption of gluconate at 11 ns with distance of 7.5 Å of COM of carboxylic group a) side view b) top view.

Color code: Light blue:Ca - orange:Osi - dark blue:Si - red:Oxygen - very light blue : Carbon

6.4.2 Summary and conclusions – Gluconate adsorption onto C-S-H

Our result for stability of gluconate near the C-S-H surface is similar to Androniuk et al study (22). Although they only performed MD but we also performed MTD to look at adsorption of gluconate molecule onto 00.1 Ca terminated Surface. This result, if confirmed with longer simulation times, can help to better understand the hydration phenomena of cement hydration in presence of gluconate although in our simulation we used lower concentration of gluconate compared to the study performed by Siramanont (21). They observed that the presence of D-gluconate affects the synthetic C-S-H precipitation, slowing down nucleation and growth kinetics (21). They showed that D-gluconate adsorbs on C-S-H and can also complex with Ca^{2+} in solution. This adsorption is probable from our current preliminary simulations, at least on the C-S-H surface we investigated. This surface should however be very representative of the C-S-H 00.1 surface for these high Ca/Si ratio synthetic C-S-Hs (>1.5). Harris et al (24) have recently shown that at such Ca/Si ratios it likely that the surface has high calcium contents, recently confirmed with zeta potential measurements, where +35 mV (25) are typical of synthetic C-S-H samples studied by Siramanont (21). The foil-like nature of these synthetic C-S-H samples have predominantly 00.1 surfaces, making our results particularly pertinent. Our result shows that interaction of gluconate with the 00.1 Ca terminated C-S-H terminated surface is very strong therefore it could modify the C-S-H growth kinetics in presence of gluconate as seen by Siramanont (21). Such a modification in C-S-H growth would be a complimentary mechanism of the retardation effect of gluconate on cement hydration i.e. in addition to the adsorption of gluconate onto the anhydrous cements' phases such as C_3S slowing down dissolution.

Siramanont (21) also saw very well-ordered agglomeration phenomena at high gluconate dosages (12 mM) and the strong interaction with the 00.1 basal plane of these foil-like synthetic C-S-H particles could also be a reason behind the apparent edge-to-edge agglomeration mechanism proposed by Siramanont (21).

In the future longer simulation runs should be carried out to get convergence and carry out more detailed analysis to confirm our first conclusions on these preliminary investigations on C-S-H surfaces.

6.5 Summary and conclusion – gluconate adsorption onto CH and C-S-H

Our MD simulations in this chapter shows that gluconate does not adsorb rapidly onto 00.1 and 10.1 CH surfaces and did not penetrate the first water layer at the surface. However, making the surface positive does induce the gluconate to stay at a closer distance to the surface for more time. When gluconate is placed close to a surface on the Ca-terminated 10.1 CH surface there is a strong adsorption for at least 2 ns, indicating that MTD could be used for more representative interactions with the CH 00.1 and 10.1 surfaces are to be envisaged. To do this the dissolution of the CH surfaces needs to be remedied by modification of the Ca-OH-H₂O interactions in the ERICA force field. If gluconate also is shown to interact strongly with CH surfaces it could modify CH nucleation and growth kinetics and influence cement hydration kinetics as CH precipitation, as well as C-S-H, is a key factor and could contribute to the retardation effects observed with gluconate in cement hydration.

In the case of simulations of adsorption of gluconate onto a 00.1 Ca terminated C-S-H surface the surface was found to be stable when using ERICA FF. This allowed the use of MTD where we found two minima in our preliminary simulations at close distances to the surface. Therefore, MTD simulation is capable to push gluconate molecule toward the surface. At 3.5 Å distance of COM of carboxylic group to the surface gluconate adsorbs vertically with COO group close to the surface however at 7.5 Å it is adsorbed as a flat molecule in an outer sphere type interaction.

We suggest to run Gluconate adsorption onto Ca terminated C-S-H surface for more time. It can give an insight to better understand how gluconate can affect the growth of C-S-H (with which sites and in which direction) and we propose to look the higher concentration of gluconate (more close to experimental conditions) to compare result of effect of gluconate in morphology of C-S-H.

Also, other C-S-H surface terminations could be investigated where pH and Ca content in the supernatant may change the surface concentration of Ca and thus help to fully understand these effects and the work can be expanded to look at interactions with various other cement additives as well as gluconate

6.7. References

- [1] B. Li, X. Lv, W. Yunquan, and J. Zhang, “Effect of amino trimethylene phosphonic acid on hydration of portland cement,” *Journal of Building Materials*, 19, 417,423, 2016.
- [2] J. Rickert, “Influence of a long-term retarder on the hydration of clinker and cement,” *Cement Concrete Aggregate*, 26, 92–10.1, 2004.
- [3] K. Yang, C. Zhang, Y. Guo, and Z. Llu, “Study on retarding the set of sulpho-aluminate cement,” *Journal of the Chinese Society*, 30, 155–160, 2002,
- [4] X. Kong, Z. Lu, J. Shi, D. Wang, S. Hou, and H. Liu, “Impacts of phosphoric acid and phosphates on hydration kinetics of Portland cement,” *Journal of the Chinese Society*, 40, 1553–1558, 2012.
- [5] A. Peschard, A. Govin, J. Pourchez et al., “Effect of polysaccharides on the hydration of cement suspension,” *Journal of the European Ceramic Society*, 26, 1439–1445, 2006.
- [6] T. Pyatina and T. Sugama, ““High-temperature alkaline stability of cement set retarders and their performance at 70–90°C,” *Advances in Cement Research*, 25, 25–35, 2013.
- [7] G. Li, T. He, and Y. Wu, “Effect of sodium gluconate on the fluidity and flow loss of pastes with β -naphthalenesulfonic acid-based superplasticizer,” *Journal of the Chinese Society*, 38, 768–773, 2010,
- [8] J. Cheung, A. Jeknavorian, L. Roberts, and D. Silva, “Impact of admixtures on the hydration kinetics of Portland cement,” *Cement and Concrete Research*, 41, 1289–1309, 2011.
- [9] F. Zou, H. Tan, Y. Guo, B. Ma, X. He, and Y. Zhou, “Effect of sodium gluconate on dispersion of polycarboxylate superplasticizer with different grafting density in side chain,” *Journal of Industrial and Engineering Chemistry*, 55, 91–10.0, 2017.
- [10] G. Li, Y. Li, C. Shi, Q. Wang, and C. Chen, “Influence of retarder on the fluidity and strength of the sulphate aluminium cement paste containing naphthalene-based superplasticizer,” *Bulletin of the Chinese Ceramic Society*, 33, 3295–3299, 2014.

- [11] B. Ma, G. Li, X. Li., “Study on the effects by compounding the polycarboxylic type superplasticizer with sodium gluconate,” *Journal of Wuhan University of Technology*,3, 52–55, 2011.
- [12] H. Tan, F. Zou, B. Ma, Y. Guo, X. Li, and J. Mei, “Effect of competitive adsorption between sodium gluconate and polycarboxylate superplasticizer on rheology of cement paste,” *Construction and Building Materials*, 144, 338–346, 2017.
- [13] S. Ma, W. Li, S. Zhang, D. Ge, J. Yu, and X. Shen, “Influence of sodium gluconate on the performance and hydration of Portland cement,” *Construction and Building Materials*, 91, 138–144, 2015.
- [14] E. E. Hekal and E. A. Kishar, “Effect of sodium salt of naphthalene-formaldehyde polycondensate on ettringite formation,” *Cement and Concrete Research*, 29, 1535–1540, 1999.
- [15] M. Bishop and A. R. Barron, “Cement hydration inhibition with sucrose, tartaric acid, and lignosulfonate: analytical and spectroscopic study,” *Industrial & Engineering Chemistry Research*,45, 7042–7049, 2006.
- [16] X. Zhang, Y. He, C. Lu, and Z. Huang, “Effects of sodium gluconate on early hydration and mortar performance of Portland cement-calcium aluminate cement-anhydrite binder,” *Construction and Building Materials*,157,1065–1073, 2017.
- [17] J. P. Perez, “-e mechanism of action of sodium gluconate on the fluidity and set of Portland cement,” in *Proceedings of the 12th International Congress on the Chemistry of Cement*, Montreal, Canada, July 2007.
- [18] H. von Daake and D. Stephan, “Impact of retarders by controlled addition on the setting, early hydration and microstructural development of different cements,” *Magazine of Concrete Research*, 68, 10.11–1024, 2016.
- [19] B. Ma, G. Li, X. Li et al., “Study on the effects by compounding the polycarboxylic type superplasticizer with sodium gluconate,” *Journal of Wuhan University of Technology*, 33, 50–53, 2011,

- [20] Y. Wu, T. He, F. Shen et al., “Influences of the compounding of sodium gluconate with superplasticizer on the process of cement hydration,” *Journal of Xi’an University of Architect & Technology (Natural Science Edition)*, 40, 806–809, 2008,
- (21) J. Siramanont “Effect of Ions and Admixtures on the Growth of Synthetic Calcium Silicate Hydrate (C-S-H)”, EPFL thesis No. 9007 (2018)
- (b) J. Siramanont and P. Bowen “Effect of D-Gluconate on Nucleation and Growth of Synthetic Calcium Silicate Hydrate (C-S-H)”, *Proc. 12th Inter. Conf. Superplasticizers and Other Chemical Admixtures in Concrete*, 403- 414, 2018
- [22] L. Androniuk, C. Landesman, A. Kalinichev, Adsorption of gluconate and uranyl on C-S-H phases: Combination of wet chemistry experiments and molecular dynamics simulations, *physics and chemistry of earth*, [99](#), 2017, 194-203
- [23] Wang, J., Wolf, R. M.; Caldwell, J. W. Kollman, P. A.; Case, D. A. “Development and testing of a general AMBER force field”. *Journal of Computational Chemistry*, **2004**, 25, 1157-1174.
- [24] M. Harris, G. Simpson, K. Scrivener, P. Bowen “A method for the reliable and reproducible precipitation of phase pure high Ca/Si ratio (>1.5) synthetic calcium silicate hydrates (C-S-H)” accepted CCR – 2021
- [25] M. Harris, EPFL – personal communication, 202

Chapter 7:

Molecular simulations of adsorption of sulfate onto surfaces of portlandite and C-S-H

7.1 Introduction

Sulfate, in the form of gypsum, basanite (calcium sulfate hemihydrate), or anhydrite, is always present in Portland cement. Sulfate's major function is to regulate the characteristics of early-age cement. The addition of sulfate, on the other hand, affects not only the setting time but also the evolution of the compressive strength of cement mortars and concrete (1). Sulfate reacts with aluminate phases to delay C_3A hydration, hence regulating early age characteristics (2).

Etringite, Aft ($Al_2O_3 - Fe_2O_3 - tri$), and later monosulfoaluminate (AFm) are the results of the reaction between C_3A (and to a lesser extent, C_4AF) and sulfate (3). The amount of sulfate in Portland cement thus controls the balance between the Aft and AFm phases. As a result, the addition of sulfate alters the phase assemblage's composition, the amount of hydrates produced, the remaining porosity, and, as a result, performance (4). Thermodynamic calculations demonstrate that when sulfate content rises, more ettringite and fewer AFm phases occur, resulting in a greater hydrate volume and lower porosity. These theoretical findings are supported by experimental findings, which show that the development of more ettringite is associated with a rise in compressive strength. (5)

However, compressive strength often decreases at 3–4% sulfate content, despite the fact that the volume of the hydrates is expected to rise due to increased ettringite production [6,7,8]. The cause of this occurrence is still unknown.

Sulfate also has significant effect on C-S-H. Quennoz et al. found substantial differences in the time it took for gypsum to deplete in pure C_3A and C_3S/C_3A systems, showing that C-S-H affects sulfate availability in these systems. The S/Ca ratio in C-S-H, as determined by SEM-EDS, is much greater (between 0.04 and 0.1) before the aluminate peak in C_3S/C_3A combinations, according to their findings. After the aluminate peak, the sulfate concentration in C-S-H drops to about one-fourth of its starting value [9]. Berodier and Scrivener found a change in C-S-H morphology owing to sulfate adsorption in OPC combined with quartz [10], Gallucci et al. [11]

reported STEM-EDS measurements that were in good agreement with both of these results. These findings reveal that sulfate interacts with both C₃A and C-S-H during the acceleration period of hydration.

In this chapter, the goal is to look at how sulfate interacts with CH surfaces and present preliminary simulations on adsorption of Sulfate onto the 00.1 Ca terminated C-S-H surface. We'll start by replicating the Ca-SO₄ ion pair production results from Byrne et al. (12) as a validation of the ERICA force field being used. Following that, we will go over the method section and then look at the results for calcium-sulfate ion pair production, molecular dynamic simulation of sulfate adsorption into 00.1 and 10.1 CH surfaces. Then we go through explanation of our approach for simulation of adsorption of sulfate onto 00.1 Ca terminated C-S-H surface, albeit the simulations have not yet been successful in this regard.

7.2 Method

7.2.1 Details of simulation for study of Calcium-sulfate ion pair formation by MTD

Byrne et al. (12) generated two force fields to explore the creation of calcium sulfate ion pairs in their latest research. This was covered in depth in the Method chapter, chapter 2, of the thesis. To model the production of ion pairs and verify that the ERICA force field (FF1) was functioning well, one calcium and one sulfate ion were placed in a box of water containing 470 water molecules. In the NPT ensemble, we did EM first, then MD for 2ns. Then we run MTD for 21 ns to imitate calcium sulfate ion pair production. We utilized a Gaussian width of 0.3 Å and a Gaussian height of 0.005 eV for MTD.

7.2.2 Details of the MD simulation of sulfate adsorption on 00.1 and 10.1 CH surfaces

The adsorption of sulfate into 00.1 and 10.1 CH surfaces was simulated by MD using ERICA FF1. Due to dissolution issues (highlighted in chapter 5), we avoided doing MTD on portlandite surfaces once again. We did EM first, then 1 ns of NPT equilibration. For the 00.1 CH surface, we ran MD for 40 ns, but for the 10.1 CH surface, we first located sulfate in close proximity to the surface (S-Osurface 3.5 Å) and only performed MD for 6 ns, again because of dissolution issues with the 10.1 CH surface highlighted in Chapter 6. As for the previous chapter for mixing

rules between atom types we used Lorentz-Berthelot mixing rule. We used a 25 Å x 26 Å x 70 Å box. Ion pair creation was permitted i.e. we were running unconstrained MD. The MD was run in the PLUMED code without adding a bias to easily output free energy profiles and follow the ion-surface distance co-variable.

7.3 Results and discussion

7.3.1. Analysis of ion pair formation results for Calcium- Sulfate - MTD

We attempted to compare Byrne et al. (12) results for calcium sulfate ion pair formation to see how ERICA FF1 was performing. The outcome of the calculation of calcium sulfate ion pair formation from the work of Byrne et al. (12) is shown in Figure 7.1.

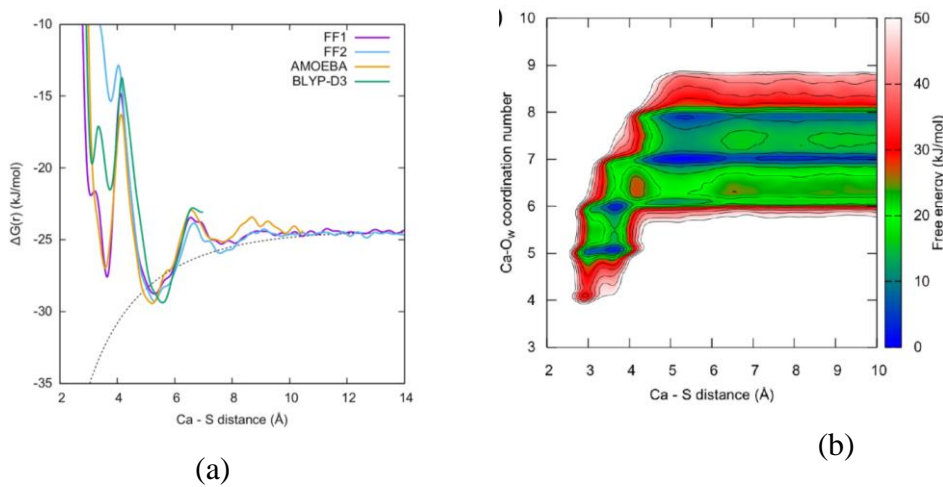


Figure 7.1. a) free energy function of calcium-sulfate ion pair formation simulated with different force fields used by Byrne et al. (from (12)) b) two-dimensional collective variable for Calcium sulfate ion pair formation (from (12))

They compared the results of two force fields developed in their work with the AMOEBA FF and DFT calculations (12). They used two collective variables in their work, one is the coordination number of Ca-O_w and the other one is the Ca-S distance. However, we only used one collective variable to check ERICA FF1, which is the Ca-S distance. The reason for this choice is that it is computationally less expensive and makes the simulation simpler. Fig 7.1.a

shows two minima in the FEP and Fig 7.2 shows the convergence plot and final free energy plot compared with the results obtained by Byrne et al (12).

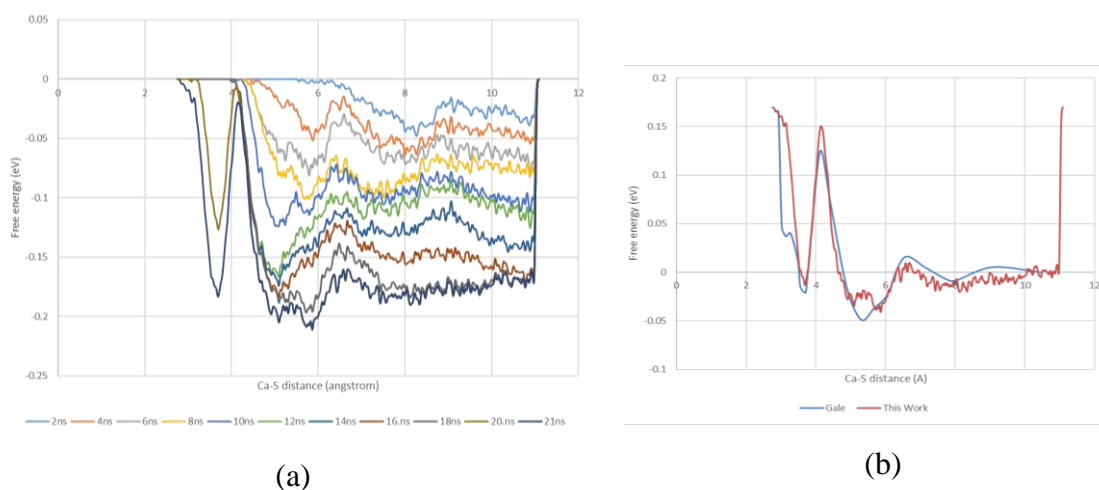


Figure 7.2. a) convergence plot of free energy profile as a function of time for calcium sulfate ion pair formation b) a comparison for free energy profile between this work and Byrne et al work (12)

As one can see from figure 7.2, as time passes, we get close to convergence. The final plot at 21 ns is very similar to the obtained results by Byrne et al (fig 7.2 (b)). We observed two minima, one at 2.8 Å and another one at 4.7 Å. As Byrne et al (12) results in figure 7.1.b show, a significantly lower CN at a closer distance is expected. This means that at 2.8 Å, the solvation of Ca is much less than 4.7 Å, when forming the ion pair. In conclusion, the ERICA FF is functioning correctly for sulfate-calcium- water interactions.

7.3.2 Analysis of results for adsorption of sulfate into 00.1 and 10.1 CH surfaces - MD

Regarding 00.1 CH surface distance from O (OH) surface was monitored by PLUMED code. Figure 7.3 shows the water structure on the 00.1 CH surface, distance of S from O (OH) on the surface and the coordination number of the sulphate ion.

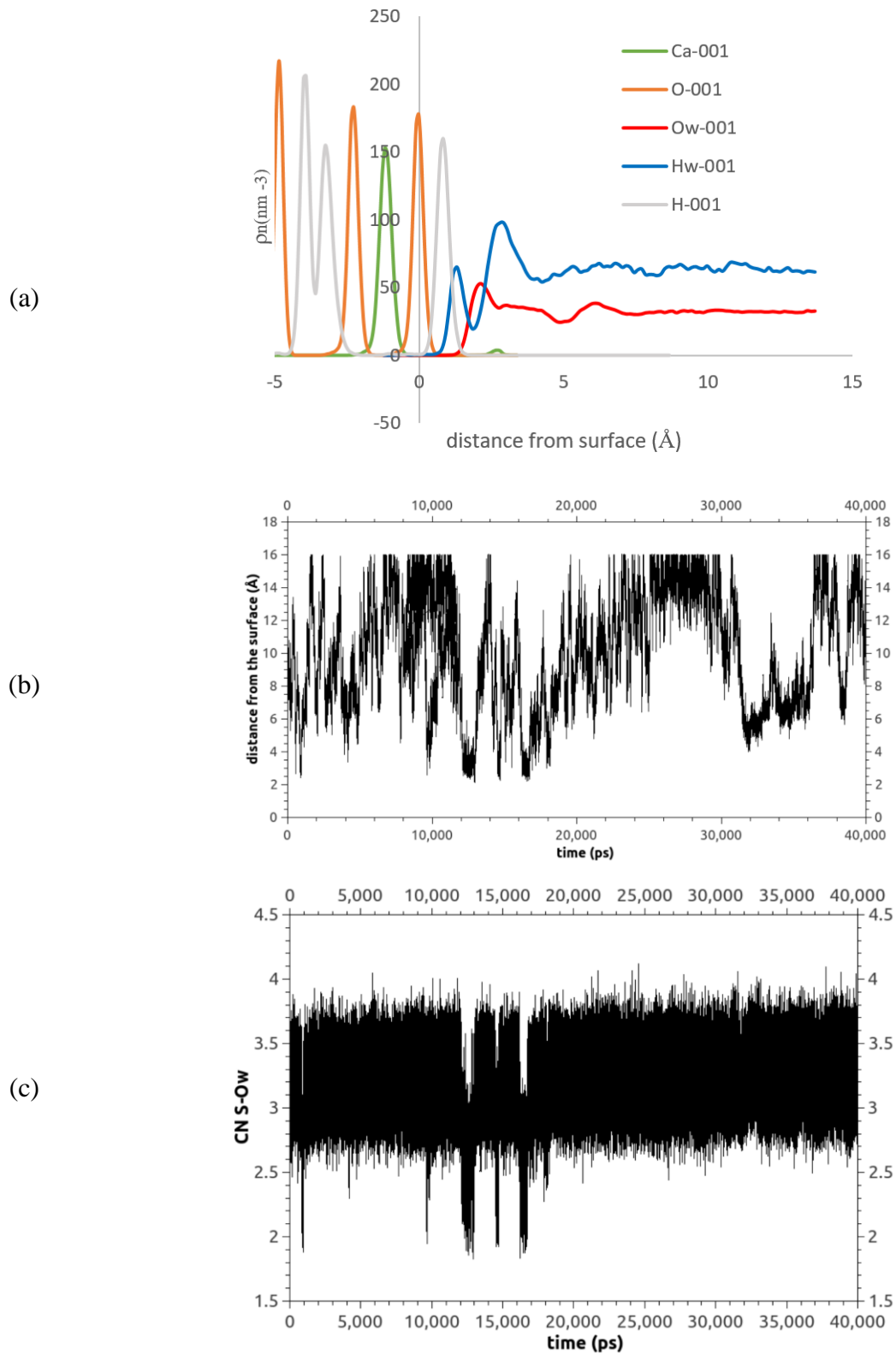


Figure 7.3. a) water structure above 00.1 CH surface b) distance of S from 00.1 CH surface c) CN -S (sulphate ion)-Ow as a function of time

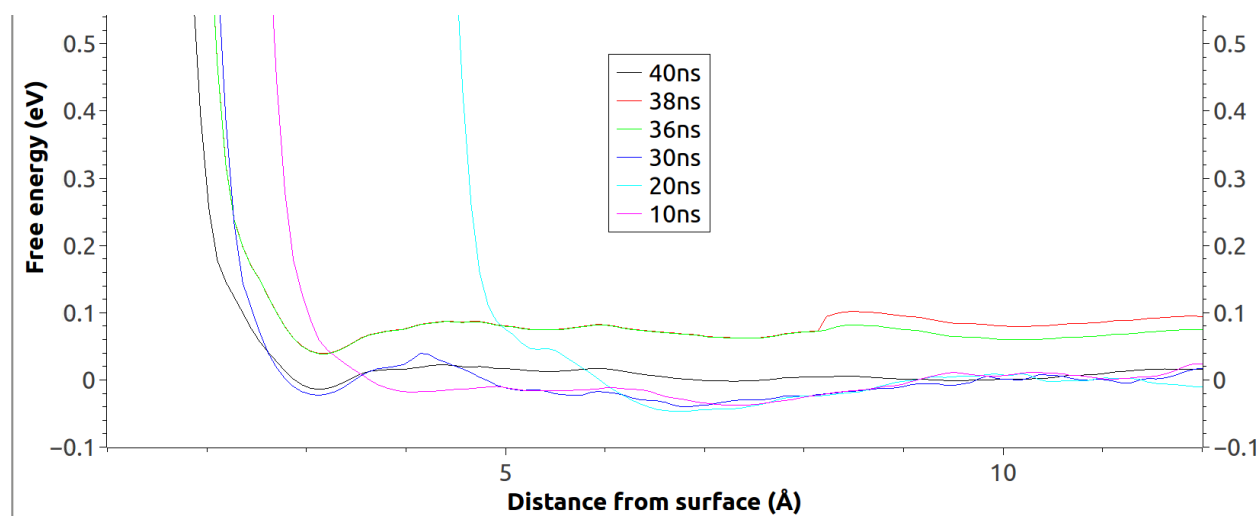
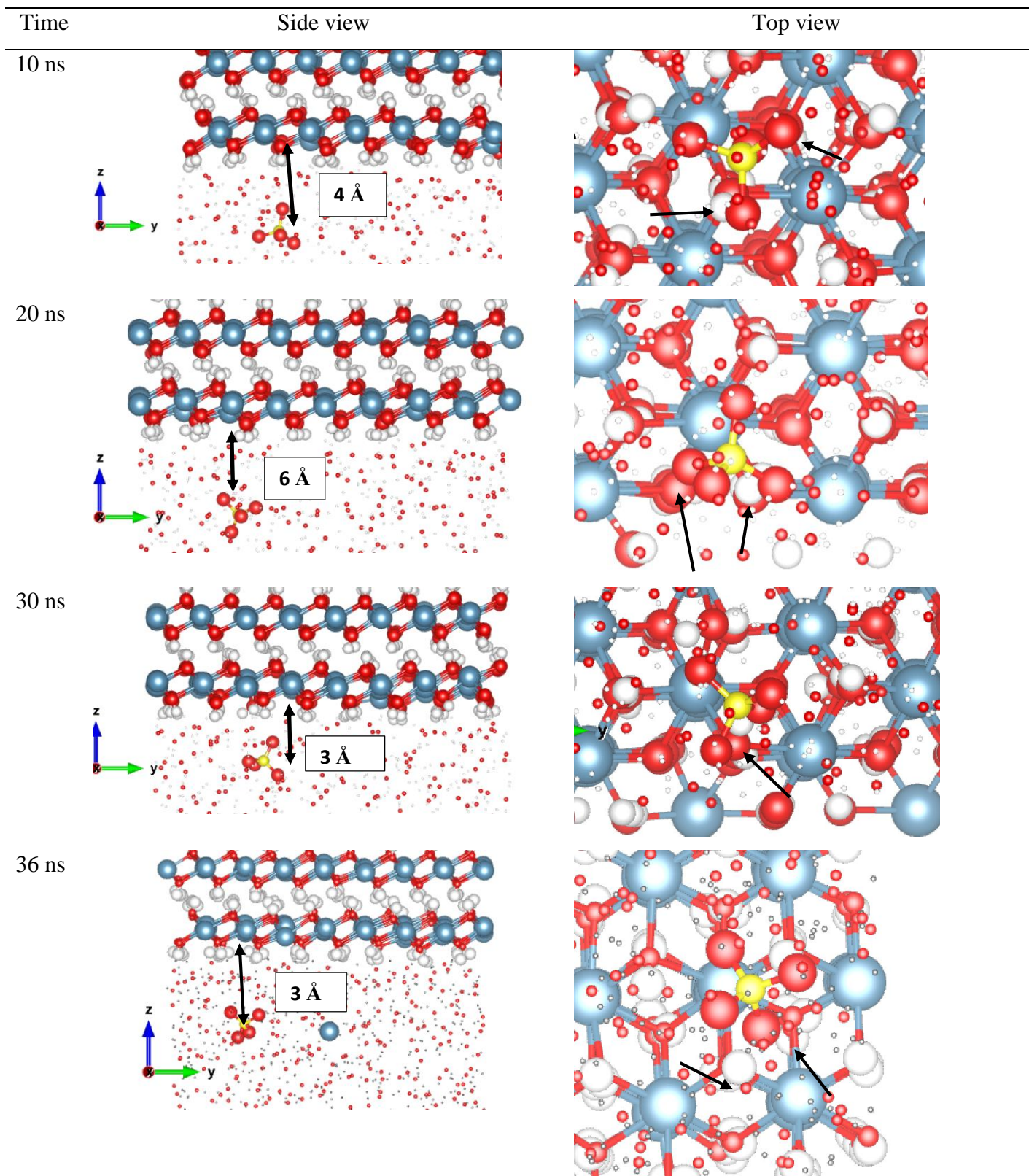


Figure 7.4. Free energy profile of adsorption sulfate into 00.1 CH surface as a function of time from MD (distance is that of the S atom in the sulphate ion).

The minimum distance of S from the surface is 2 Å. As the S-Os distance is 1.46 Å, Os is likely to be closer than 2 Å depending on the orientation but globally indicates inner sphere adsorption albeit relatively weak (attractive well around 0.025 eV with respect to zero energy). In order to make the plot I considered distance of 10 Å as zero energy and then I normalized in that respect. However, at least four adsorption phenomena for more than 300 ps are indicated in figure 7.3 (b) where the S atom is around 3 Å from the surface oxygen. Sulfate passes through the layered structure of water (figure 7.3.a) which extends to around 4 Å. According to the CN plot, we can see two strong adsorptions at 6 and 8 ns which sulfur loses approximately 1 water molecule. The sulphate ion (Os) can thus penetrate the water layer to some degree.

Figure 7.4 shows the free energy profiles up to 40 ns for adsorption of sulfate onto 00.1 CH surface. As one can see from this figure, the position of minima changes during time of simulation which shows different adsorption of sulfate ion, indicating this is a very weak interaction. However, the plots at between 30 to 40 ns are quite similar with respect to the minimum at 3 Å. The reason for different minima in this plot might be due to different angular configurations of the sulfate ion toward the surface, i.e. simple fluctuations because of the very weak interaction. In order to understand this better in Figure 7.5 we show snapshots of adsorption at different times for the weak attractive minima identified in the FEPs.



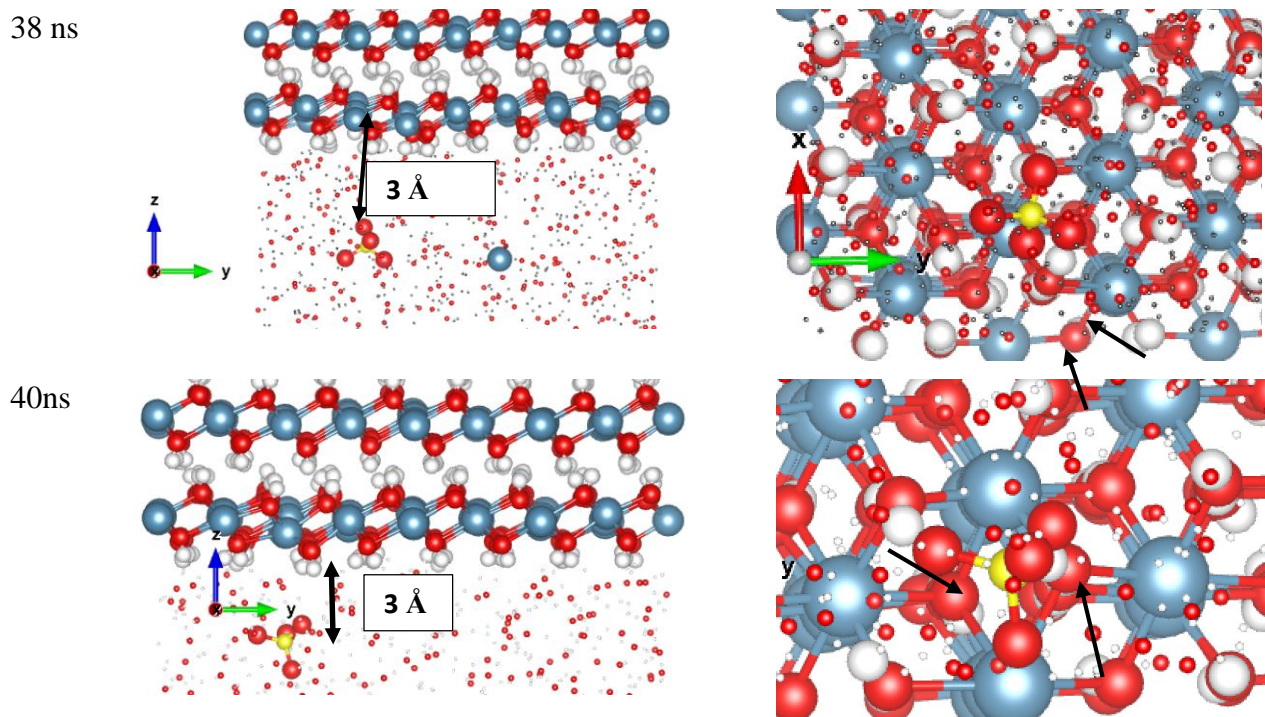
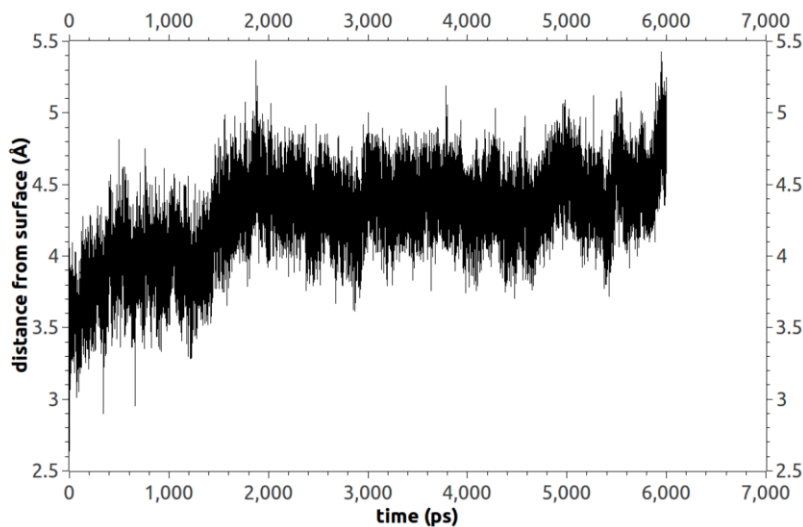


Fig 7.5. Representative snapshots of sulfate in an attractive minimum with respect to the 00.1 CH surface at different times of simulation. Color code: Ca-blue/Oxygen-Red/Sulfur-Yellow/ H: white

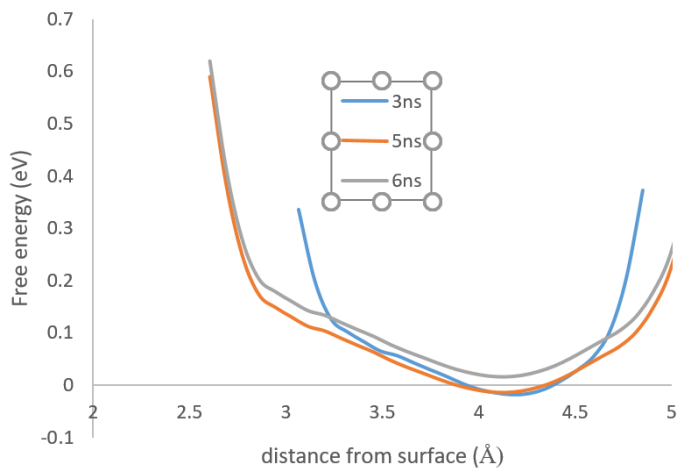
At 10 ns one of oxygen of sulfate is in vertical position to the surface and at this time sulfate is situated between two OH groups. These two OHs are shown with black arrows (Fig.7.5 10 ns top view). At 20ns a planar arrangement of 3 oxygens of the sulfate tetrahedral face is facing the surface. At 30 ns one of the oxygens is again more directly pointing at the surface and 40 ns shows again the planar tetrahedral surface. At 20 ns again, sulfate is situated close to the 2 OHs as shown with arrows (Fig. 7.5 20 ns top view). However, in 30 and 40 ns time of simulation it seems that sulfate is situated above only one OH site. At 36 ns it is toward two OH groups and at 38 ns it is toward 2 OH groups. The distance between Os and Hoh is 2 Å which shows that it is a bit more than 1.8 Å to be defined as a hydrogen bond but nonetheless a clear indication of interaction.

In the case of the 10.1 surface we saw in chapter 6 that it has dissolution problems after around 6 ns. Thus, to gain some information about the possible interaction of the sulfate ion with the 10.1 surface the ion was placed at 3.5 Å and an MD run for 6ns. Visual inspection shows that the sulfate ion is stable for the length of simulation (6 ns) and the distance of S-O(OH) change from

3.5 to 5.3 Å (fig 7.6.a). It is above the Ca site on the 10.1 CH surface and although it drifts away there does seem to be an outer sphere-type interaction (Fig 7.6(b)) via the Ca on the surface.



(a)



(b)

Fig 7.6. (a) Distance of S of sulfate ion from O of 10.1 CH surface OH (b) shows the Free energy profile between 3-6 ns which shows deep broad minima between 3.5 to 4.5 Å from the surface.

In presence of sulfate aqueous solution morphology has been shown to change from an equiaxed faceted crystal (00.1, 10.1 and 110 facets) to a hexagonal (13) platelet where the 00.1 (platelet basal plane) and 10.1 facets (edges) are dominant in the morphology

From our preliminary simulations the sulphate seems to interact a little more strongly with the CH 00.1 surfaces than the 10.1 surface. It is not clear if there is a strong adsorption from our limited MD simulations that could change the relative interfacial energies and thus the morphology (e.g. as for the simulation in chapter 4 on going from vacuum to water (cf S8 Annex 1). However, if the sulphate spends more time close to the 00.1 surface than the 10.1 surface one could hypothesize that the crystal would grow slower in the 00.1 direction thus making it the dominant surface from a kinetic viewpoint. Further simulations using MTD with a modified ERICA FF to solve the dissolution problems would be an interesting next step.

7.3.3 Summary and Conclusions – CH

In this chapter we first validated the ERIFCA FF by comparing with Byrne et al. results for ion pair formation of Ca-SO₄ (12) and get very similar results albeit using only one collective variable was used. Then we performed MD simulation of sulfate adsorption onto 00.1 and 10.1 CH surfaces. For 00.1 CH surface we recognize different interaction strengths due to different configuration of the sulfate ion. We have observed both inner sphere and outer sphere adsorption, albeit very very weak suggesting these are just natural fluctuations. For the 10.1 surface we found out that sulfate ion is stable at around 4 Å distance from the 10.1 CH surface. This might be due interaction between Ca at the surface of 10.1 CH and sulfate ion and will be evaluated further by tracking the coulomb interaction vs time as a next step in the data analysis.

7.3.4 Preliminary attempts to investigate adsorption of sulfate onto C-S-H

In this study we tried to simulate adsorption of sulfate onto a 00.1 Ca terminated C-S-H surface. Box details and simulation details are the same as Chapter 5 (Ca adsorption into 00.1 Ca terminated C-S-H surface), except here we replace the two hydroxyl ions with the sulfate ion. Ca in the top layer and Ca in the main layer are separated by 3.2 Å. The dimensions of the box are 22 Å x 36 Å x 170 Å. With a surface charge of zero, the Ca/Si ratio of the slab is 1.67. We employed the Canter of masses of all Ca at the top layer of the surface as for Ca adsorption, with ERICA FF2 as the modeling force field. We used a 0.0002 ps time step and did standard MTD with an upper wall of 20 Å and a lower wall of 0 Å. The Gaussian width was set to be 0.2 Å, while the Gaussian height was chosen to be 0.005 eV.

Unfortunately, our attempts at simulating sulfate adsorption onto 00.1 Ca terminated C-S-H surface have not yet proven successful (please see Annex 4 we inserted LAMMPS input file for adsorption of sulfate onto 00.1 Ca terminated C-S-H surface). The main reason is that after 120 ps sulfate gets too close to the Ca top layer, it interacts with oxygen of silicon in the layer below the surface Ca at the top layer and the cross interaction in our model (ERICA FF2) did not give satisfactory repulsive interaction of Osi and Os therefore this leads to the crashing the simulation. We tried putting a lower wall between sulfate ion and Ca at the top layer for the distance of 3 Å but still simulation crashes. We feel that a modification of the Os –Osi parameter of in ERICA FF2 is needed, perhaps reconsidering the mixing rule used as standard in LAMMPS for others better suited to such interactionsto solve this problem but was beyond the time limit of the current PhD study.

7.4. References

- [1] R. G. Blezard, in: *The History of Calcareous Cements*, edited by P. C. Hewlett, *Lea's Chemistry of Cement and Concrete*, 4th Edition (Butterworth-Heimann, Oxford, 1998), 1–23.
- [2] A. Bentur, *Cementitious materials – Nine millennia and a new century: Past, present, and future*. American Society of Civil Engineers, 150th Anniversary Paper. *J. Mater. Civ. Eng.*, JAN/FEB 2002, 2–22.
- [3] H. F. W. Taylor, *Cement chemistry*. 2nd Edition. (Thomas Telford, London, 1997).
- [4] E. M. Gartner, J. F. Young, D. A. Damidot, and I. Jawed, *Hydration of Portland cement*, in: J. Bensted, P. Barnes (Eds.), *Structure and Performance of Cements*, 2nd ed. (Spon Press, London – New York, 2002), 57–113.
- [5] I. Odler (ed.), *Special Inorganic Cements* (Spon Press, London – New York, 2000).
- [6] A. K. Chatterjee, in *Special Cements*, edited by J. Bensted, P. Barnes, *Structure and Performance of Cements*, 2nd ed. (Spon Press, London – New York, 2002), 186–236.
- [7] G. Artioli, *Scientific methods and cultural heritage* (Oxford University Press, Oxford, 2010).
- [8] V. S. Ramachandran, V. M. Malhotra, C. Jolicoeur, and N. Spiratos, *Superplasticizers: properties and applications in concrete* (CANMET, Materials Technology Laboratory, Ottawa, 1998).

- [9] A. Quennoz, K.L. Scrivener, Interactions between alite and C3A-gypsum hydrations in model cements, *Cem. Concr. Res.* 44 (2013) 46–54.
- [10] E. Berodier, K. Scrivener, Understanding the filler effect on the nucleation and growth of C-S-H, *J. Am. Ceram. Soc.* 97 (2014) 3764–3773.
- [11] E. Gallucci, P. Mathur, K. Scrivener, Microstructural development of early age hydration shells around cement grains, *Cem. Concr. Res.* 40 (2010) 4–13.
- [12] E.H. Byrne, P. Raiteri, J.D. Gale, Computational Insight into Calcium-Sulfate Ion Pair Formation, *J. Phys. Chem. C.* 121 (2017) 25956–25966
- (13) Galmarini S. Atomistic Simulation of Cementitious Systems. EPFL thesis no.5754, 2013.

Chapter 8: Conclusions

A summary of the work accomplished in this thesis is offered in this final chapter. Afterward I will present an outlook for work that would be pertinent to perform in the future.

8.1 ERICA Force Field suite

We defined and validated a force field, ERICA FF created in three parts (ERICA FF1, 2, and 3) to mimic structural properties, reaction enthalpies, and mechanical properties of diverse cementitious systems in Chapter 4 of this work. The force field has parameters for the species Ca, OH, sulfate, water, Si, Al, Na, K and Cl. The results are generally in good accord with experimental data, indicating that these force fields can be utilized to simulate cementitious systems with reasonable accuracy. In terms of structural quality, 19 cementitious materials were simulated with relative errors in distances of less than 5.2 percent in all cases. We calculated an error estimate for the force field with an 80 percent confidence interval based on 17 simulated reaction enthalpies. Calculations of hydration enthalpies of ions in water were used to further validate the ERICA FF. We also simulated the mechanical properties of five cementitious materials, all of which are quite close to experimental values. These findings show that the ERICA FF model may be used to reasonably accurately simulate cementitious materials. Limitations with the ERICA force field were highlighted in chapters 5, 6 and 7 mainly concerned with dissolution of calcium hydroxide (CH) surfaces in either MTD (CH 00.1 and 10.1) or even MD (mainly the 10.1 CH surface) and the interaction of sulphate with the C-S-H surface. Improvements are needed to make the ERICA suite more compatible with these systems.

8.2 Interaction ions and small molecules with CH surfaces

In chapter 5 we went over simulations of the structure of water above three surfaces of portlandite in part one. The results of Galmarini et al. (1) who employed the TIP4P2005 water model, were also compared. It was found for the 00.1 and 10.0 CH surfaces the SPC/Fw water model produced very similar results for the structure of water above the surfaces. The sole variation between SPC/Fw and TIP4P2005 for the 10.1 CH surface is a minor peak of O_w at the same position of OH as in the surface. This is related to the dissolving of OH in the 10.1 CH surface into the water, according to visual observation from the metadynamics (MTD) in part 2

of the chapter. Here MTD was used to simulate the adsorption of Ca and OH onto the 00.1 CH surface. However, we were unable to completely interpret the results due to the dissolution of Ca and OH into the water during the simulation. Such dissolution would be expected in real systems considering that in the simulation concentration of $\text{Ca}(\text{OH})_2$ is 0.5 mM which gives a pH of 11.7. In a real system of pH is around 11.4 the equilibrium concentration of Ca^{2+} is close to 10 mM. Therefore, we expect dissolution since the system is under saturated. As a result, standard molecular dynamic simulations were used to investigate these adsorptions with ERICA FF. In part 3, we looked over the simulations that we had done in part 2 with the MD. The dissolution problem that occurred in MTD did not exist in MD. In the MD study we found that for both Ca and OH weak adsorption energy minima are located after the first layer of water. Ca adsorption is different from Galmarini et al (1) since they did not see adsorption at 4 Å and only observed minima at 8 Å. This interaction is slightly more pronounced than in the Galmarini et al. (1) work. These minor modifications in the FEP for this work compared to the and Galmarini et al (1) work are probably due to the different water models.

We performed simulation on adsorption of gluconate onto 00.1 and 10.1 CH surfaces (positive and negative) Gluconate did not adsorb onto the 00.1 and 10.1 CH surfaces according to our simulation in Chapter 6 (at least for the time that we ran simulation around 10ns). This is primarily due to the fact that we used MD. Making the surface slightly positive, on the other hand, allows the gluconate to stay closer to the surface for longer. For 10.1 CH surface there was significant dissolution after 6 ns even in MD. Consequently, the gluconate was located at a 2 Å distance from the surface in the initial configuration it was stable for at least 2 ns, i.e. the length of the simulation that was run. This indicates a possible ion pair formation between the carboxylate group of gluconate and Ca at top later of the 10.1 CH surface.

In Chapter 7, we first replicate Byrne et al (2) results for the creation of Ca-SO_4 ion pairs and obtain the similar results using only one collective variable. Following that, we ran MD simulations of sulfate adsorption on 00.1 and 10.1 CH surfaces. Due to the variable orientation of the sulfate ion with respect to the 00.1 CH surface, we observed different adsorption interactions with the two surfaces investigated, both inner sphere and outer sphere. We discovered that sulfate ion is stable at close distances (around 5 Å) from the 10.1 CH surface, which could be related to the formation of an ion pair between Ca on the 10.1 CH surface and sulfate ion. From

our preliminary simulations the sulphate seems to interact a little more strongly with the 00.1 surfaces than the 10.1 surface. From our limited MD simulations, it is not clear if there is a strong enough interaction to change the relative interfacial energies and thus the morphology but it does seem a strong possibility. Also, if the sulphate spends more time close to the 00.1 surface than the 10.1 surface a kinetic effect on the relative growth rates could also influence the change in morphology seen experimentally with (hexagonal platelet) and without (equiaxed faceted particles) the presence of sulphate.

8.3 Interaction of ions and small molecules with Ca terminated 00.1 C-S-H surface.

One of the main initial goals of the thesis was to develop a force field that was suitable to study the incorporation of elements into calcium silicate hydrate (C-S-H) and the creation of representative C-S-H surfaces. Chapter 4 showed that ERICA FF (FF2) gave very good results for the best mineral model, namely, 14 Å tobermorite. This was then tested on the defective tobermorite model developed by Mohamed et al using their brick model (3) by a colleague at EPFL. Indeed, the ERICA force field was successful in producing a stable C-S-H bulk structure (4). With this success the colleagues introduced C-S-H surfaces using the brick model. In this thesis we took a Ca terminated 00.1 C-S-H surface and tested it for Ca interactions using MTD.

Regarding adsorption of Ca adsorption, we discovered that there is significant physical adsorption of Ca onto the 00.1 Ca terminated C-S-H surface. As there is plenty of space in the surface structure for an ion of the size of Ca, consequently it can accept calcium for short times even at the depth of the main Ca layer. It does not bond so it can move back out but does remain at the surface Ca layer position for significant time, illustrating a strong interaction with the C-S-H surface. This is expected from the positive surface potentials measured for cementitious systems but here we show that we can start trying to quantify these interactions using MTD.

When simulating gluconate adsorption, we identified two possible local minima at 11 and 12 ns in close proximity to a 00.1 Ca terminated C-S-H surface using MTD. This demonstrated that the MTD simulation can push the gluconate molecule nearer the surface. At a distance of 3.5 Å from the carboxylic group's COM, gluconate will adsorb vertically the COO group toward the surface, but at a distance of 7.5 Å, it is adsorbed as a flat molecule. So, in this work, substantial physical

gluconate adsorption is possibly to be expected. This result, when confirmed, could help to better understand the hydration phenomena of cement hydration in presence of gluconate although in our simulation we used lower concentration of gluconate in compare to study performed by Siramanont (5) which closely resembled its dose in real cement systems. Our result shows that interaction of gluconate with the Ca terminated C-S-H surface is very strong therefore it could modify the C-S-H growth kinetics in presence of gluconate as seen by Siramanont (5). Such a modification in C-S-H growth would be an additional mechanism to the retardation effect of gluconate on cement hydration, i.e. complimentary to the adsorption of gluconate onto the anhydrous cement phases thereby slowing down dissolution.

These simulations show that the ERICA force field (ERICA FF2) was successful in its use for simulations of C-S-H surfaces and the interaction with the Ca ion and the gluconate molecule.

8.4 Outlook and Future Work

The interaction of Ca^{2+} , OH^- , and SO_4^{-2} on the surface of portlandite and C-S-H was the subject of this thesis. We recommend that more ions, such as aluminum, magnesium, and zinc, be investigated on the surface of cement hydrates. Because these ions can have a significant impact on C-S-H growth, the influence of additional organic molecules on the surface of portlandite and C-S-H should also be considered.

We also believe that ERICA FF could be improved to make it more generic and accurate, particularly in the case of reaction enthalpies. This can be accomplished by altering a few parameters and using machine learning to improve accuracy. We strongly advise making changes to ERICA FF version 1 in order to alleviate the problem of OH and Ca (from portlandite) dissolving in water (in the case of the 00.1 and 10.1 surfaces when using metadynamics and even for the 10.1 surface in MD simulations), albeit dissolution should be expected because of our over negative dissolution enthalpy these perhaps occur quicker than necessary. Alternatively, other surface definitions and co-variables could be investigated to study the dynamics of these important interfaces.

In the future, we recommend further investigating the morphology of portlandite in the presence of sulfate. This can be accomplished through the use of metadynamics and the determination of

the surface energy of various portlandite surfaces, once the force field or definition of surface or a more judicious choice of metadynamics covariables has been improved as discussed above.

More work can be done by conducting simulations of Calcium, sulfate and gluconate adsorption onto the surface of C-S-H for longer periods of time, which will bring the simulations closer to convergence and provide a better understanding of C-S-H growth. Other surface terminations and surface orientations could be envisaged as the ERICA FF2 showed successful simulations thus far but minor improvements for the sulfate interaction (possibly by modify the interface mixing potential rules) are needed.

The force field developed and the application to the various ions and molecules show that great promise using such atomistic tools to better understand cementitious materials interfaces is possible and thus future work will be able contribute to helping create more efficient eco-friendly cements.

8.5 References

1. Galmarini S, Bowen P. Atomistic simulation of the adsorption of calcium and hydroxyl ions onto portlandite surfaces - Towards crystal growth mechanisms. *Cem Concr Res.* 2016, 81, 16–23.
2. E. H. Byrne, P. Raiteri, J. Gale, Computational insight to calcium sulfate ion pair formation., *J. Phys. Chem. C.* 2017,46, 25956– 25966
3. A. Kunhi Mohamed, S. C Parker, P. Bowen, S. Galmarini, An atomistic building block description of C-S-H -Towards a realistic C-S-H model, *Cem. Conc. Res.* ,2018,107, 221-235,
4. Z. Casar (LMC, EPFL)– personal communication 2021
5. J. Siramanont and P. Bowen “Effect of D-Gluconate on Nucleation and Growth of Synthetic Calcium Silicate Hydrate (C-S-H)”, *Proc.12th Inter. Conf. Superplasticizers and Other Chemical Admixtures in Concrete*, 2018, 403- 414,

Annexes

Annex 1 - Supplementary Information for paper of chapter 4 submitted to the journal of Cement and Concrete Research

S1. Total energy calculations

To calculate the total energy in molecular mechanics, we have to evaluate the appropriate energy term for every atom-atom interaction in the system. Generally, the total energy is expected to have contributions from the Coulombic (electrostatic) interactions, the short-range interactions (often referred to as the Van der Waals (VdW) term), the bonded interactions and angle interactions. The equations used and charges assigned to the different atoms are given in equations E1-E8 and Table S1.

$$E_{Total} = E_{VdW} + E_{Coul} + E_{Bond} + E_{Angle} \quad (E1)$$

In the SPC/Fw water model [1], the bonded term includes bond stretch and angle bend energy and is represented by the harmonic term. For all bonded pairs, Coulombic and VdW terms are considered except for O_{Si_Core}-O_{Si_Shell} that only Coulombic and bond terms were considered (We refer to the LAMMPS documentation [2] on the implementation of the adiabatic core-shell model). In our model, there are four types of bonds: O_{OH}-H_{OH} in hydroxyl is represented by Morse bond potential, O_w-H_w bond in water is represented by harmonic term, as are the O_{Si_Core}-O_{Si_Shell} bond and the sulfate bonds between S-O_s.

For Morse (E2) and harmonic bonds (E3) we used the below equations:

$$E_{Morse} = D [1 - \exp(-\alpha(r - r_0))]^2 \quad (E2)$$

$$E_{Harm} = K (r - r_0)^2 \quad (E3)$$

Where D and K are bond coefficients r_0 is the equilibrium bond length, and α is stiffness parameter.

For the angles we used the harmonic angle description (E4):

$$E_{HA} = K (\theta - \theta_0)^2$$

(E4)

For VdW we have used three sets of potentials: 12-6 Lennard-Jones (E5), N-M Potential (E6), and Buckingham potential (E7):

$$E_{L-J} = 4\varepsilon \left[\left(\frac{\sigma}{r} \right)^{12} - \left(\frac{\sigma}{r} \right)^6 \right] \quad (\text{E5})$$

$$E_{N-M} = \frac{E_0}{(n-m)} \left[m \left(\frac{r_0}{r} \right)^n - n \left(\frac{r_0}{r} \right)^m \right] \quad (\text{E6})$$

$$E_{Buck} = A e^{-\frac{r}{\rho}} - \frac{C}{r^6} \quad (\text{E7})$$

The last contribution is a Coulombic or electrostatic potential which is shown in equation 8:

$$E = \frac{C Q_i Q_j}{r} \quad (\text{E8})$$

Where the numerical value of charges Q_i and Q_j (multiplied by the electronic charge e), are as given in table S1. Please note that $C = (4\pi\varepsilon_0)^{-1}$ is the Coulombic constant and ε_0 is the vacuum permittivity.

Table S1. Charges of atom species in different force fields discussed in the main text.

	Cement FF1	Cement FF2	Erica FF	Byrne	SPC/Fw	CLAYFF	Dang
Ref	[3]	[4]		[5]	[1]	[6]	[7]
Ca	+ 2.00	+ 2.00	+ 2.00	+ 2.00	-	+ 1.36	-
O_{OH}	- 1.40	- 1.40	- 1.40	-	-	- 0.95	-
H_{OH}	+ 0.40	+ 0.40	+ 0.40	-	-	+ 0.425	-
O_w	- 1.1128*	-1.1128*	- 0.82	- 0.82	- 0.82	- 0.82	-
H_w	+ 0.5564	0.5564	+ 0.41	+ 0.41	+ 0.41	+ 0.41	-

Si	+ 4.00	+ 4.00	+ 4.00	-	-	-	-
O_{si_Shell}	-	- 2.85	- 2.85	-	-	-	-
O_{Si_Core}	- 2.00	+ 0.85	- 2.00	-	-	-	-
Os	-	-	- 0.84	- 0.84	-	-	-
Al	-	+ 3.00	+ 3.00	-	-	+ 1.575	-
S	-	-	+ 1.36	+ 1.36	-	-	-
Na	-	-	+ 1.00	-	-	+ 1.00	+ 1.00
Cl	-	-	- 1.00	-	-	- 1.00	- 1.00
K	-	-	+ 1.00	-	-	+ 1.00	+ 1.00

* On the site of the TIP4P water model [8]

S2. ERICA FF1 parameters

Van der Waal interactions

Oxygens: O_S – Sulfur Oxygen, O_w – Water Oxygen, O_{OH} – Hydroxyl Oxygen

Hydrogens: H_w – Water Hydrogen, H_{OH} – Hydroxyl Hydrogen

a) Buckingham Potential – Equation E7

Atom 1	Atom 2	Force Field	A [eV]	ρ [Å]	C [eV Å ⁶]	Ref
Ca	O _S	Byrne et al.	1815.7	0.2834	0.0	[5]
Ca	O _{OH}	Cement FF3	2251.05	0.297	0.0	[4]
O _w	O _S	Byrne et al.	12534.5	0.246	0.0	[5]
O _w	H _{OH}	Erica FF	21562.5	0.1065	0.0	
O _{OH}	O _{OH}	Cement FF3	22764.0	0.149	6.97	[4]

O _s	O _s	Byrne et al.	103585.02	0.2	0.0	[5]
----------------	----------------	--------------	-----------	-----	-----	-----

b) N-M Potential – Equation 6

Atom 1	Atom 2	Force Field	E ₀ [eV]	r ₀ [Å]	n [-]	m [-]	cutoff [Å]	Ref
O _{OH}	H _{OH}	Cement FF3	0.0073	2.71	8.5	9	6	[4]

c) L-J Potential – Equation 5

Atom 1	Atom 2	Force Field	ε [eV]	σ [Å]	Ref
O _w	O _w	SPC/Fw	0.0067	3.16	[1]
O _w	O _{OH}	Erica FF	0.00747	3.18	
O _s	O _{OH}	Erica FF	0.00747	3.18	
O _w	Ca	Byrne et al.	0.00095	3.35	[5]

Bonds

Atom 1	Atom 2	Force Field	Bond type	Equation	Parameters	Ref
O _w	H _w	SPC/Fw	Harmonic	E2	K = 22.96 eV r ₀ = 1.012 Å	[1]
O _s	S	Byrne et al.	Morse	E3	D = 5.0 eV α = 1.2 Å ⁻¹	[5]

$$r_0 = 1.505 \text{ \AA}$$

Angles

a) Harmonic angle, equation E4

Centre Atom	Atom 1	Atom 2	Force Field	E [eV]	Θ_0 [deg]	Ref
O _w	H _w	H _w	SPC/Fw	1.64567	113.24	[1]
S	O _s	O _s	Byrne et al.	7.50	109.47	[5]

S3. ERICA FF2 parameters

Van der Waal interactions

Oxygens: O_{Si} – Silicon Oxygen (Shell), O_w – Water Oxygen, O_{OH} – Hydroxyl Oxygen

Hydrogens: H_w – Water Hydrogen, H_{OH} – Hydroxyl Hydrogen

a) Buckingham Potential – Equation E7

Atom 1	Atom 2	Force Field	A [eV]	ρ [Å]	C [eV Å ⁶]	Ref
Ca	O _{Si}	Cement FF2	2152.36	0.309	0.09944	[4]
Ca	O _w	Cement FF2	1286.60	0.297	0.00	[4]
Ca	O _{OH}	Cement FF2	2251.05	0.297	0.00	[4]

Si	O _{Si}	Cement FF2	1283.91	0.321	10.66	[4]
Si	O _w	Cement FF2	1283.56	0.321	10.66	[4]
Si	O _{OH}	Cement FF2	983.56	0.321	10.66	[4]
O _{Si}	O _{Si}	Cement FF2	22764.30	0.149	27.88	[9]
O _{Si}	O _w	Cement FF2	22764.30	0.149	28.92	[9]
O _{Si}	O _{OH}	Cement FF2	22764.00	0.149	13.94	[4]
O _{Si}	H _w	Cement FF2	512.00	0.250	0.00	[4]
O _{OH}	O _{OH}	Cement FF2	22764.30	0.149	6.97	[4]
Al	O _{Si}	Cement FF2	1474.40	0.301	0.00	[4]
Al	O _{OH}	Cement FF2	1032.00	0.301	0.00	[4]
Al	O _w	Cement FF2	590.04	0.301	0.00	[4]

For the original interaction we refer to the paper [4] ...

b) N-M Potential, equation E6

Atom 1	Atom 2	Force Field	E ₀ [eV]	r ₀ [Å]	n [-]	m [-]	Ref
O _{Si}	H _{OH}	Cement FF2	0.0073	2.71	9	6	[4]
O _w	O _{OH}	Cement FF2	0.0013	4.63	9	6	[4]
O _w	H _{OH}	Erica FF	0.0550	2.00	9	6	
O _{OH}	H _{OH}	Cement FF2	0.0073	2.71	9	6	[4]

c) L-J Potential, equation E5

Atom 1	Atom 2	Force Field	ε [eV]	σ [Å]	Ref
O _w	O _w	SPC/Fw	0.0067	3.16	[1]

Bonds

Atom 1	Atom 2	Force Field	Bond type	Equation	Parameters	Ref
O _w	H _w	SPC/Fw	Harmonic	E2	K = 22.96 eV r ₀ = 1.012 Å	[1]
O _{Si_Core}	O _{Si_Shell}	Cement FF2	Harmonic	E2	K = 37.5 eV r ₀ = 0 Å	[4]
O _{OH}	H _{OH}	Cement FF2	Morse	E3	D = 7.0525 eV α = 3.1749 Å ⁻¹ r ₀ = 0.94285 Å	[4]

Angles

b) Harmonic Angle, equation E4

Centre Atom	Atom 1	Atom 2	Force Field	E [eV]	θ ₀ [deg]	Ref
O _w	H _w	H _w	SPC/Fw	1.64567	113.24	[1]
Si	O _{OH}	O _{OH}				
Si	O _{OH}	O _{Si}	Cement FF3	7.7482	109.47	[4]
Si	O _{Si}	O _{Si}				
O _{OH}	H _{OH}	Si	Cement FF3	7.7482	141.50	[4]

S4. ERICA FF3 parameters

Erica FF3 includes the parameters from Erica FF2.

Van der Waal interactions

Oxygens: O_{Si} – Silicon Oxygen (Shell), O_S – Sulphur Oxygen, O_w – Water Oxygen, O_{OH} – Hydroxyl Oxygen

Hydrogens: H_w – Water Hydrogen, H_{OH} – Hydroxyl Hydrogen

a) Buckingham Potential – Equation E7

Atom 1	Atom 2	Force Field	A [eV]	ρ [Å]	C [eV Å ⁶]	Ref
Na	O _{Si}	Tilocca et al.	56465.34	0.194	0	[9]
K	O _{Si}	Tilocca et al.	56465.34	0.194	0	[9]

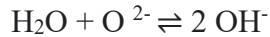
b) L-J Potential, equation E5

Atom 1	Atom 2	Force Field	ϵ [eV]	σ [Å]	Ref
Na	Ca	CLAYFF	0.0052	3.41	[6]
Na	O _w	Predota et al.	0.0058	2.85	[7]
Na	O _{OH}	Erica FF	0.0054	2.8745	
Na	Cl	Predota et al.	0.0044	3.41	[7]
Cl	Ca	Erica FF	0.0043	3.80	[7]
Cl	O _w	Predota et al.	0.0058	3.25	[7]
Cl	O _{OH}	Erica FF	0.0054	3.7835	
Cl	K	Erica FF.	0.0044	3.52	
K	Ca	CLAYFF	0.0052	3.41	[6]
K	O _w	Predota et al.	0.0058	3.81	[7]
K	O _{OH}	Erica FF	0.0054	3.249	
O _s	Na	CLAYFF	0.006071	3.12	[6]
O _s	Cl	CLAYFF	0.0052	4.25	[6]

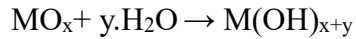
O _s	K	CLAYFF	0.006071	3.12	[6]
----------------	---	--------	----------	------	-----

S5: Water correction term

The water dissociation enthalpy can be calculated according to this reaction



As shown by de Leeuw et al. [10], this can be roughly estimated by calculating the heats of formation of the following reaction type:



Where M is Ca, Al, and Si.

We have used the five reactions shown in the table below to estimate such a correction for our cementitious systems. Where we have the simulated enthalpy of reaction without correction (H_{sim}), the experimental value (H_{exp}), the correction needed for that reaction (H_{corr}) and in the final column the absolute value for the correction for one water molecule (H_{abs}). For the energetic validation of the force field, for the reactions containing water splitting we used a correction term of 10.41 eV, with standard deviation of 0.85 eV. (see main text Table 3, for source of experimental value).

Reaction	H _{sim} (eV)	H _{exp} (eV)	H _{diff} (eV)	H _{corr} (eV)
1- Ca(OH) ₂ → CaO + H ₂ O	-9.47	0.66	10.13	10.13
2- Si(OH) ₄ → SiO ₂ + 2 H ₂ O	-24.97	-6.27	18.70	9.35
3- AlOOH + H ₂ O → Al(OH) ₃ .	10.97	-0.11	-11.08	11.08
4- Al ₂ O ₃ +3H ₂ O → 2Al(OH) ₃	33.54	-0.46	-34.00	11.33
5- 3CaO+2Al(OH) ₃ +3H ₂ O → Ca ₃ Al ₂ (OH) ₁₂	27.93	-5.00	-32.93	10.97
6- 3CaO+2Al(OH) ₃ → Ca ₃ Al ₂ O ₆ +3H ₂ O	-29.99	-0.67	29.32	9.77
Water splitting correction (average)				10.41 (0.85) *

*The standard deviation for the average correction value.

S6 Error estimation for reaction enthalpies.

The error on calculated reaction enthalpies comes from the errors on the calculated energies on the individual structures estimated. With this in mind, we are using the empirical estimation of the force field error developed by Galmarini et al. [3]. The exact calculation of the empirical estimation of the force field error, ϵ_{est}^{FF} (E11) for a reaction enthalpy ΔH (E10) used here can be found in equations S8-10 where S_i are the stoichiometry coefficients, R_i the reactants, P_i the products and H_i the enthalpies.

$$S1^R R1 + S2^R R2 + \dots \geq S1^P P1 + S2^P P2 + \dots \quad (E9)$$

$$\Delta H = \sum S_j^P H_j^P - \sum S_j^R H_j^R \quad (E10)$$

$$\epsilon_{est}^{FF} = 0.065 * \Delta H + 0.00082 * (\sum S_j^P * | + \sum S_j^R * |H_j^R|) \quad (E11)$$

In the case of aqueous species, the energy of the aqueous species is estimated based on the energy difference between two boxes of water with the same number of water molecules but with and without the aqueous species. As long as the number of water molecules is large enough,

the size of the water box should not have any influence on neither the calculated energy of the aqueous species nor on the error on the calculated energy. Thus, for these structures, only 75 water molecules for each aqueous species were considered to calculate the H_j 's in E11.

S7. Details of simulations for structural validation

No	Name	Box size (unit cells)	Ensemble	Equilibration time (ps)	Production time (ps)
1	Gypsum (Ca.SO ₄ .2H ₂ O)	3x1x3	NPT	260	800
2	Anhydrate (CaSO ₄)	3x3x3	NPT	250	900
3	Lime (CaO)	3x3x3	NPT	200	800
4	Portlandite (Ca(OH) ₂)	6x6x6	NPT	200	800
5	14 Å tobermorite (Ca ₅ Si ₆ O ₁₆ (OH) ₂ .26H ₂ O)	4x4x1	NPT	220	850
6	Corundum (Al ₂ O ₃)	3x3x1	NPT	180	700
7	Alite ((Ca ₃ SiO ₅))	2x3x2	NPT	200	800
8	Gibbsite (Al(OH) ₃)	2x3x2	NPT	130	950
9	Millosevichite (Al ₂ (SO ₄) ₃)	3x3x1	NPT	210	840
10	Böhmite (AlO(OH))	3x1x4	NPT	180	800
11	Tricalcium aluminate (Ca ₃ Al ₂ O ₆)	3x3x3	NPT	200	880
12	Hydrogarnet (Ca ₃ Al ₂ O ₁₂ H ₁₂)	3x3x3	NPT	250	10.00
13	Ettringite (Ca ₆ Al ₂ (SO ₄) ₃ (OH) ₁₂ .26H ₂ O)	2x2x1	NPT	220	750
14	Quartz (SiO ₂)	3x3x3	NPT	140	800
15	Sodium Chloride (NaCl)	4x4x4	NPT	220	790
16	Potassium Chloride (KCl)	4x4x4	NPT	200	800
17	Sodium Hydroxide (NaOH)	4x1x4	NPT	300	1200
18	Potassium hydroxide (KOH)	4x4x3	NPT	300	1200
19	Calcium chloride (CaCl ₂)	2x2x3	NPT	300	10.00

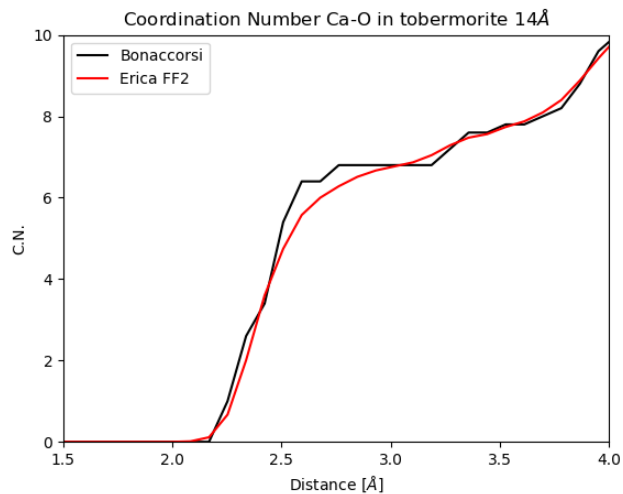
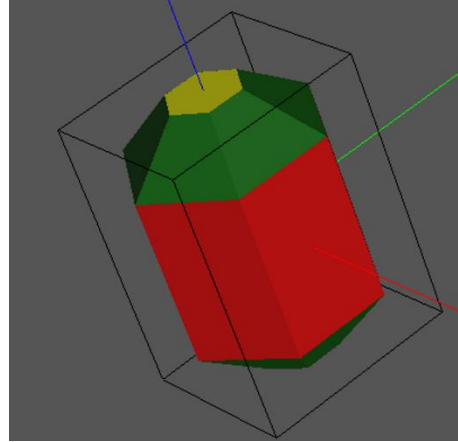
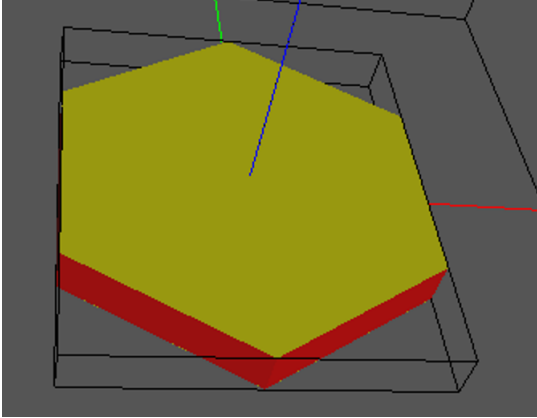


Figure S1. Coordination number versus Ca-O distance for Bonaccorsi's 14Å tobermorite [11] and the resulting structure from the ERICA FF shown in Figure 6 (d) in the main text.

S8. Surface energy calculations and morphology predictions

The Time step used is 0.7 fs. A cutoff of 8.5 Å was used between short-range interaction and long-range interaction like the work of Galmarini et al. [3]. Like previous parts the total time will be given in equilibration time plus production time. We have used periodic boundary conditions in our simulations. For bulk portlandite, bulk water and portlandite-water box, the NPT ensemble was used. The final simulations were carried out for 200+800 ps where the first 200 ps were used for equilibration of the system and the following 800 ps were used for all calculations.

For the morphology prediction we used Wulffman software [12]. This software uses surface energy per each surface to calculate the final equilibrium morphology. Below figure S2 shows the predicted Wulffman shape of portlandite in water and vacuum.



Predicted morphology of portlandite in vacuum. Color code: yellow: 00.1, red: 10.0
 Predicted morphology of portlandite in water. Color code: yellow: 00.1, red: 10.0 green: 10.1
 green: 10.1

Figure S2. Predicted Wulffman equilibrium morphologies from ERICA FF1 for portlandite in vacuum and water.

S9. Elastic Constants

Comparison of calculated elastic tensor coefficients for tricalcium silicate from different force fields

	Erica FF2	IFF [13]	CLAYFF [13]
C_{11} [GPa]	228.91	219.6	118.6
C_{22} [GPa]	228.45	216.0	34.81
C_{33} [GPa]	206.98	189.6	95.4
C_{12} [GPa]	89.61	77.54	34.81
C_{13} [GPa]	60.14	52.79	35.98
C_{23} [GPa]	58.61	52.72	27.95
C_{44} [GPa]	57.65	37.0	33.01

C ₅₅ [GPa]	63.79	43.4	38.22
C ₆₆ [GPa]	66.58	67.65	32.16
C ₁₄ [GPa]	4.43	-	-
C ₁₅ [GPa]	8.95	4.0	17.69
C ₁₆ [GPa]	0.87	-	-
C ₂₄ [GPa]	-1.32	-	-
C ₂₅ [GPa]	24.0	-21.7	1.39
C ₂₆ [GPa]	2.09	-	-
C ₃₄ [GPa]	-0.56	-	-
C ₃₅ [GPa]	1.73	-34.04	6.65
C ₃₆ [GPa]	-4.81	-	-
C ₄₅ [GPa]	-1.91	-	-
C ₄₆ [GPa]	-13.14	-6.39	3.28
C ₅₆ [GPa]	-0.64	-	-
Bulk Modulus [GPa]	120.12	104.7	53.9
Shear Modulus 1 [GPa]	62.67	54.3	33.5
Shear Modulus 2 [GPa]	75.99	54.3	33.5
Poisson Ratio [-]	0.239	0.279	0.243
Young's Modulus [GPa]	188-155	139	83.2

Calculated elastic tensor coefficients for tobermorite 14Å with Erica FF2

C ₁₁ [GPa]	C ₂₂ [GPa]	C ₃₃ [GPa]	C ₁₂ [GPa]	C ₁₃ [GPa]	C ₂₃ [GPa]	C ₄₄ [GPa]
-----------------------	-----------------------	-----------------------	-----------------------	-----------------------	-----------------------	-----------------------

99.44	130.70	60.61	46.38	13.97	19.01	26.15
<hr/>						
C_{55} [GPa]	C_{66} [GPa]	C_{14} [GPa]	C_{15} [GPa]	C_{16} [GPa]	C_{24} [GPa]	C_{25} [GPa]
6.46	39.43	-3.29	0.36	-3.81	-4.23	1.44
<hr/>						

References

- [1] Y. Wu, H.L. Tepper, G.A. Voth, Flexible simple point-charge water model with improved liquid-state properties, *J. Chem. Phys.* 124 (2006). <https://doi.org/10.1063/1.2136877>.
- [2] S. Plimpton, Fast Parallel Algorithms for Short-Range Molecular Dynamics, *J. Comput. Phys.* 117 (1997) 1–42. <https://doi.org/10.1006/jcph.1995.1039>.
- [3] S. Galmarini, A. Aimable, N. Ruffray, P. Bowen, Changes in portlandite morphology with solvent composition: Atomistic simulations and experiment, *Cem. Concr. Res.* 41 (2011) 1330–1338. <https://doi.org/10.1016/j.cemconres.2011.04.009>.
- [4] A.K. Mohamed, P. Moutzouri, P. Berruyer, B.J. Walder, J. Siramanont, M. Harris, M. Negroni, S.C. Galmarini, S.C. Parker, K.L. Scrivener, L. Emsley, P. Bowen, The Atomic-Level Structure of Cementitious Calcium Aluminate Silicate Hydrate, *J. Am. Chem. Soc.* (2020). <https://doi.org/10.1021/jacs.0c02988>.
- [5] E.H. Byrne, P. Raiteri, J.D. Gale, Computational Insight into Calcium-Sulfate Ion Pair Formation, *J. Phys. Chem. C.* 121 (2017) 25956–25966. <https://doi.org/10.1021/acs.jpcc.7b09820>.
- [6] R.T. Cygan, J.J. Liang, A.G. Kalinichev, Molecular models of hydroxide, oxyhydroxide, and clay phases and the development of a general force field, *J. Phys. Chem. B.* 108 (2004) 1255–1266. <https://doi.org/10.1021/jp0363287>.
- [7] M. Předota, A. V. Bandura, P.T. Cummings, J.D. Kubicki, D.J. Wesolowski, A.A. Chialvo, M.L. Machesky, Electric double layer at the rutile (110) surface. 1. Structure of surfaces and interfacial water from molecular dynamics by use of ab initio potentials, *J. Phys. Chem. B.* 108 (2004) 12049–12059. <https://doi.org/10.1021/jp037197c>.

- [8] J.L.F. Abascal, C. Vega, A general purpose model for the condensed phases of water: TIP4P/2005, *J. Chem. Phys.* 123 (2005). <https://doi.org/10.1063/1.2121687>.
- [9] A. Tilocca, N.H. De Leeuw, A.N. Cormack, Shell-model molecular dynamics calculations of modified silicate glasses, *Phys. Rev. B.* 73 (2006) 104209. <https://doi.org/10.1103/PhysRevB.73.104209>.
- [10] N. H. de Leeuw, G. W. Watson and S.C. Parker, Atomistic Simulation of the Effect of Dissociative Adsorption of Water on the Surface Structure and Stability of Calcium and Magnesium Oxide, *J. Phys. Chem.* 47 (1995) 17219–17225.
- [11] E. Bonaccorsi, S. Merlino, A.R. Kampf, The crystal structure of tobermorite 14 Å (plombierite), a C-S-H phase, *J. Am. Ceram. Soc.* 88 (2005) 505–512. <https://doi.org/10.1111/j.1551-2916.2005.00.116.x>.
- [12] A.R. Roosen, R.P. McCormack, W.C. Carter, Wulffman: A tool for the calculation and display of crystal shapes, *Comput. Mater. Sci.* 11 (1998) 16–26. [https://doi.org/10.1016/S0927-0256\(97\)00.167-5](https://doi.org/10.1016/S0927-0256(97)00.167-5).
- [13] G. Clavier, N. Desbiens, E. Bourasseau, V. Lachet, N. Brusselle-Dupend, B. Rousseau, Computation of elastic constants of solids using molecular simulation: comparison of constant volume and constant pressure ensemble methods, *Mol. Simul.* 43 (2017) 1413–1422. <https://doi.org/10.1080/08927022.2017.1313418>.

Annex 2. PLUMED code for adsorption of Ca^{2+} onto 00.1 Ca CH surface

RESTART

UNITS LENGTH=A TIME=ps ENERGY=eV

g1: COM ATOMS=769-816

g2: COM ATOMS=2371

g3: COM ATOMS=961-2370

g4: COM ATOMS=781

g5: COM ATOMS=2372-2373

g6: COM ATOMS=1

g7: COM ATOMS=1-48

g8: COM ATOMS=2374-2375

g9: COM ATOMS=60

g10: COM ATOMS=40

g11: COM ATOMS=817-864

g12: COM ATOMS=337-384

g13: COM ATOMS=481-528

g14: COM ATOMS=721-768

g15: COM ATOMS=289

cen1: CENTER ATOMS=g5

cen2: CENTER ATOMS=g8

surf: CENTER ATOMS=g6

d: DISTANCE ATOMS=g2,surf COMPONENTS

d2: DISTANCE ATOMS=g6,g2 COMPONENTS

d3: DISTANCE ATOMS=g7,g1 COMPONENTS

d4: DISTANCE ATOMS=cen1,g9 COMPONENTS

d5: DISTANCE ATOMS=cen2,g10 COMPONENTS

d6: DISTANCE ATOMS=g11,g1 COMPONENTS

d7: DISTANCE ATOMS=g7,g12 COMPONENTS

d8: DISTANCE ATOMS=g13,g14 COMPONENTS

c: COORDINATION GROUPA=2371 GROUPB=961-1430 R_0=3

UPPER_WALLS ARG=d.z,d6.z,d7.z,d8.z AT=16,14.90,16,17.5 KAPPA=150.0,150,150,150
EXP=2,2,2,2 EPS=1,1,1,1 OFFSET=0,0,0,0 LABEL=uwall

radius1: COMBINE ARG=d2.x,d2.y POWERS=2,2 PERIODIC=NO

radius2: COMBINE ARG=radius1 POWERS=0.5 PERIODIC=NO

radius3: COMBINE ARG=d4.x,d4.y, POWERS=2,2 PERIODIC=NO

radius4: COMBINE ARG=radius3 POWERS=0.5 PERIODIC=NO

radius5: COMBINE ARG=d5.x,d5.y, POWERS=2,2 PERIODIC=NO

radius6: COMBINE ARG=radius5 POWERS=0.5 PERIODIC=NO

radius_uwall: UPPER_WALLS ARG=radius2,radius4,radius6 AT=3.5,3.5,3.5
KAPPA=10.00,0,10.00,10.00

hA1: HISTOGRAM ARG=d.z GRID_MIN=1.0 GRID_MAX=18.0 GRID_BIN=200
BANDWIDTH=0.05

ff: CONVERT_TO_FES GRID=hA1 TEMP=300

DUMPGRID GRID=ff FILE=fes.dat STRIDE=75

PRINT ARG=d.z,c,radius2 STRIDE=75 FILE=COLVAR

Annex 3. Lammmps input file for Gluconate Adsorption onto 00.1 Ca terminated C-S-H surface

```
# ----- Initialize Simulation -----  
  
clear  
  
units          metal  
  
dimension      3  
  
atom_style     full  
  
boundary p p p  
  
box tilt large  
  
restart        10.0000 tmp.restart  
  
read_restart   tmp.restart.59800000  
  
fix csinfo all property/atom i_CSID  
  
#read_data Tobermorite_CSInfo.data fix csinfo NULL CS-Info  
  
#read_data Ca-Surface-new-glu.lmp fix csinfo NULL CS-Info  
  
group ca type 1  
  
group Si type 2  
  
group Osicore type 3  
  
group Osishell type 4  
  
group Ow type 5  
  
group Ooh type 6  
  
group Hw type 7  
  
group Hoh type 8  
  
set group ca charge 2
```



```

set group Si charge 4

set group Osicore charge 0.85

set group Osishell charge -2.85

set group Ow charge -0.82

set group Ooh charge -1.4

set group Hw charge 0.41

set group Hoh charge 0.4

group cores type 3

group shells type 4

group noWater type 1 2 3 4

# ----- Define Interatomic Potential -----

#pair_style hybrid/overlay lj/cut/coul/long 8.5 buck/coul/long 8.5 coul/long 8.5
nb3b/harmonic nm/cut/coul/long 8.5

pair_style hybrid/overlay lj/cut/coul/long 8.5 buck/coul/long 8.5 coul/long 8.5
nm/cut/coul/long 8.5 buck/coul/long/cs 8.5

#pair_coeff * * nb3b/harmonic caSiOsicoreOsishellOwOohHwHoh.nb3b.harmonic ca Si
Osicore Ow Ooh Hw Hoh

pair_coeff 1 1 coul/long

pair_coeff 1 2 coul/long

pair_coeff 1 3 coul/long

pair_coeff 1 4 buck/coul/long 2152.3566 0.309227 0.099440

pair_coeff 1 5 buck/coul/long 1286.6000 0.2970 0.0000

```

pair_coeff	1	6	buck/coul/long	2251.0500	0.2970	0.0000
pair_coeff	1	7	coul/long			
pair_coeff	1	8	coul/long			
pair_coeff	1	9	coul/long			
pair_coeff	1	10	buck/coul/long	1819.6000	0.2833	0.0000
pair_coeff	2	2	coul/long			
pair_coeff	2	3	coul/long			
pair_coeff	2	4	buck/coul/long	1283	0.3205	10.66
pair_coeff	2	5	buck/coul/long	1283.556	0.3202	10.6616
pair_coeff	2	6	buck/coul/long	983.5	0.3255	10.66
pair_coeff	2	7	coul/long			
pair_coeff	2	8	coul/long			
pair_coeff	2	9	coul/long			
pair_coeff	2	10	buck/coul/long	582	0.3202	10.6616
pair_coeff	3	3	buck/coul/long	0	1	0
pair_coeff	3	4	buck/coul/long/cs	0	1	0
pair_coeff	3	5	buck/coul/long	0	1	0
pair_coeff	3	6	buck/coul/long	0	1	0
pair_coeff	3	7	buck/coul/long	0	1	0
pair_coeff	3	8	buck/coul/long	0	1	0
pair_coeff	3	9	buck/coul/long	0	1	0
pair_coeff	3	10	buck/coul/long	0	1	0
pair_coeff	4	4	buck/coul/long	22764.3	0.149	27.88

pair_coeff	4	5	buck/coul/long	22764.3	0.149	28.92
pair_coeff	4	6	buck/coul/long	22764.3	0.149	13.94
pair_coeff	4	7	buck/coul/long	512	0.2500	0.0000
pair_coeff	4	8	nm/cut/coul/long	0.0073	2.71	8.5 9 6
pair_coeff	4	9	coul/long			
pair_coeff	4	10	buck/coul/long	22764.3	0.149	28.92
pair_coeff	5	5	lj/cut/coul/long	0.0067	3.16	
pair_coeff	5	6	nm/cut/coul/long	0.00.13000	4.63	8.5 9 6
pair_coeff	5	7	coul/long			
pair_coeff	5	8	nm/cut/coul/long	0.055 2	8.5 9 6	
pair_coeff	5	9	coul/long			
pair_coeff	5	10	buck/coul/long	12534	0.246	0
pair_coeff	6	6	buck/coul/long	22764	0.149	6.97
pair_coeff	6	7	coul/long			
pair_coeff	6	8	nm/cut/coul/long	0.0073	2.71	8.5 9 6
pair_coeff	6	9	coul/long			
pair_coeff	6	10	nm/cut/coul/long	0.00.13000	4.63	8.5 9 6
pair_coeff	7	7	coul/long			
pair_coeff	7	8	coul/long			
pair_coeff	7	9	coul/long			
pair_coeff	7	10	coul/long			
pair_coeff	8	8	coul/long			
pair_coeff	8	9	coul/long			

pair_coeff	8	10	nm/cut/coul/long	0.055	2	8.5	9	6
pair_coeff	9	9	coul/long					
pair_coeff	9	10	coul/long					
pair_coeff	10	10	lj/cut/coul/long	103585	0.2			
pair_coeff	1	9	lj/cut/coul/long	0	0			
pair_coeff	1	10	lj/cut/coul/long	0	0			
pair_coeff	1	11	lj/cut/coul/long	0	0			
pair_coeff	1	12	lj/cut/coul/long	0	0			
pair_coeff	1	13	lj/cut/coul/long	0	0			
pair_coeff	1	14	buck/coul/long	1286.6000	0.2970	0.0000		
pair_coeff	1	15	lj/cut/coul/long	0	0			
pair_coeff	2	9	lj/cut/coul/long	0	0			
pair_coeff	2	10	lj/cut/coul/long	0	0			
pair_coeff	2	11	lj/cut/coul/long	0	0			
pair_coeff	2	12	lj/cut/coul/long	0	0			
pair_coeff	2	13	lj/cut/coul/long	0	0			
pair_coeff	2	14	lj/cut/coul/long	0	0			
pair_coeff	2	15	lj/cut/coul/long	0	0			
pair_coeff	3	9	lj/cut/coul/long	0	0			
pair_coeff	3	10	lj/cut/coul/long	0	0			
pair_coeff	3	11	lj/cut/coul/long	0	0			
pair_coeff	3	12	lj/cut/coul/long	0	0			
pair_coeff	3	13	lj/cut/coul/long	0	0			

pair_coeff	3	14	lj/cut/coul/long	0	0
pair_coeff	3	15	lj/cut/coul/long	0	0
pair_coeff	4	9	lj/cut/coul/long	0	0
pair_coeff	4	10	lj/cut/coul/long	0	0
pair_coeff	4	11	lj/cut/coul/long	0	0
pair_coeff	4	12	lj/cut/coul/long	0	0
pair_coeff	4	13	lj/cut/coul/long	0	0
pair_coeff	4	14	buck/coul/long	22764.3	0.149 28.92
pair_coeff	4	15	lj/cut/coul/long	0	0
pair_coeff	5	9	lj/cut/coul/long	0.113550000.1	3.4332366937
pair_coeff	5	10	lj/cut/coul/long	0.0162	3.1356765213
pair_coeff	5	11	lj/cut/coul/long	0.06305	3.5998347542
pair_coeff	5	12	lj/cut/coul/long	0.00835	1.9
pair_coeff	5	13	lj/cut/coul/long	0.051350000.1	3.599834754
pair_coeff	5	14	lj/cut/coul/long	0.1133499999	3.3799609508
pair_coeff	5	15	lj/cut/coul/long	0.0111708355	3.215
pair_coeff	6	9	lj/cut/coul/long	0.179700000.1	2.0332366937
pair_coeff	6	10	lj/cut/coul/long	0.08235	1.7356765213
pair_coeff	6	11	lj/cut/coul/long	0.1292	2.1998347542
pair_coeff	6	12	lj/cut/coul/long	0.0745	0.5
pair_coeff	6	13	lj/cut/coul/long	0.117500000.1	2.199834754
pair_coeff	6	14	lj/cut/coul/long	0.1794999999	1.9799609508

pair_coeff	6	15	lj/cut/coul/long	0.0773208355	1.815
pair_coeff	7	9	lj/cut/coul/long	0.129400000.1	3.8332366937
pair_coeff	7	10	lj/cut/coul/long	0.03205	3.5356765213
pair_coeff	7	11	lj/cut/coul/long	0.0789	3.9998347542
pair_coeff	7	12	lj/cut/coul/long	0.0242	2.3
pair_coeff	7	13	lj/cut/coul/long	0.067200000.1	3.999834754
pair_coeff	7	14	lj/cut/coul/long	0.1291999999	3.7799609508
pair_coeff	7	15	lj/cut/coul/long	0.0270208355	3.61
pair_coeff	8	9	lj/cut/coul/long	0.108568388	3.1162366937
pair_coeff	8	10	lj/cut/coul/long	0.0112183879	2.8186765213
pair_coeff	8	11	lj/cut/coul/long	0.0580683878	3.2828347542
pair_coeff	8	12	lj/cut/coul/long	0.0033683879	1.583
pair_coeff	8	13	lj/cut/coul/long	0.0463683879	3.282834754
pair_coeff	8	14	lj/cut/coul/long	0.1083683878	3.0629609508
pair_coeff	8	15	lj/cut/coul/long	0.0061892234	2.898
pair_coeff	9	9	lj/cut/coul/long	0	0
pair_coeff	9	10	lj/cut/coul/long	0	0
pair_coeff	9	11	lj/cut/coul/long	0	0
pair_coeff	9	12	lj/cut/coul/long	0	0
pair_coeff	9	13	lj/cut/coul/long	0	0
pair_coeff	9	14	lj/cut/coul/long	0	0
pair_coeff	9	15	lj/cut/coul/long	0	0
pair_coeff	10	10	lj/cut/coul/long	0	0

pair_coeff	10	11	lj/cut/coul/long	0	0
pair_coeff	10	12	lj/cut/coul/long	0	0
pair_coeff	10	13	lj/cut/coul/long	0	0
pair_coeff	10	14	lj/cut/coul/long	0	0
pair_coeff	10	15	lj/cut/coul/long	0	0
pair_coeff	9	9	lj/cut/coul/long	0.2104000002	3.0664733875
pair_coeff	9	10	lj/cut/coul/long	0.1130500002	2.7689132151
pair_coeff	9	11	lj/cut/coul/long	0.159900000.1	3.233071448
pair_coeff	9	12	lj/cut/coul/long	0.105200000.1	1.5332366937
pair_coeff	9	13	lj/cut/coul/long	0.1482000002	3.2330714477
pair_coeff	9	14	lj/cut/coul/long	0.2102	3.0131976446
pair_coeff	9	15	lj/cut/coul/long	0.1080208356	2.8482366937
pair_coeff	10	10	lj/cut/coul/long	0.015700000.1	2.4713530426
pair_coeff	10	11	lj/cut/coul/long	0.06255	2.9355112755
pair_coeff	10	12	lj/cut/coul/long	0.00785	1.2356765213
pair_coeff	10	13	lj/cut/coul/long	0.050850000.1	2.9355112753
pair_coeff	10	14	lj/cut/coul/long	0.11285	2.7156374721
pair_coeff	10	15	lj/cut/coul/long	0.0106708355	2.5506765213
pair_coeff	11	11	lj/cut/coul/long	0.1093999999	3.3996695085
pair_coeff	11	12	lj/cut/coul/long	0.0547	1.6998347542
pair_coeff	11	13	lj/cut/coul/long	0.0977	3.3996695082
pair_coeff	11	14	lj/cut/coul/long	0.1596999999	3.179795705
pair_coeff	11	15	lj/cut/coul/long	0.0575208355	3.0148347542

pair_coeff	12	12	lj/cut/coul/long	0	0
pair_coeff	12	13	lj/cut/coul/long	0	0
pair_coeff	12	14	lj/cut/coul/long	0	0
pair_coeff	12	15	lj/cut/coul/long	0	0
pair_coeff	13	13	lj/cut/coul/long	0.086000000.1	3.3996695079
pair_coeff	13	14	lj/cut/coul/long	0.148	3.1797957048
pair_coeff	13	15	lj/cut/coul/long	0.0458208356	3.014834754
pair_coeff	14	14	lj/cut/coul/long	0.2099999998	2.9599219016
pair_coeff	14	15	lj/cut/coul/long	0.1078208354	2.7949609508
pair_coeff	15	15	lj/cut/coul/long	0.005641671	2.63

bond_style hybrid harmonic morse

bond_coeff 1 harmonic 22.96 1.0120

bond_coeff 2 morse 7.0525 3.1749 0.942

bond_coeff 3 harmonic 37.5 0

bond_coeff 4 harmonic 316.7 1.4233

bond_coeff 5 harmonic 371.4 0.973

bond_coeff 6 harmonic 330.6 1.0969

bond_coeff 7 harmonic 300.9 1.5375

bond_coeff 8 harmonic 313 1.5241

bond_coeff 9 harmonic 637.7 1.2183

angle_style harmonic

angle_coeff 1 1.64567 113.24

angle_coeff 2 7.74815 109.47000
 angle_coeff 3 7.74815 109.47000
 angle_coeff 4 7.74815 109.47000
 angle_coeff 5 7.74815 109.47000
 angle_coeff 6 50.9 10.2600473693
 angle_coeff 7 67.5 110.1900473966
 angle_coeff 8 39.2 108.4600465979
 angle_coeff 9 46.4 109.5600470693
 angle_coeff 10 47.4 107.2600460836
 angle_coeff 11 62.9 111.510.0476186
 angle_coeff 12 63.3 111.0400474745
 angle_coeff 13 67.4 123.2000528005
 angle_coeff 14 68.3 108.7900467966
 angle_coeff 15 47 108.2200466096
 angle_coeff 16 77.9 130.2500561085

dihedral_style harmonic

dihedral_coeff 1 0.01075 1 1
 dihedral_coeff 2 0 1 3
 dihedral_coeff 3 0.050525 1 2
 dihedral_coeff 4 0.006192 1 3
 dihedral_coeff 5 0.0066888889 1 3
 dihedral_coeff 6 0.0071666667 1 3

```
dihedral_coeff 7      0.00688      1      3
dihedral_coeff 8      0.0086 -1      1
dihedral_coeff 9      0.01075     -1      2
dihedral_coeff 10     0.00774      1      3
dihedral_coeff 11     0      -1      2
dihedral_coeff 12     0.0344 1      1
dihedral_coeff 13     0      1      2
dihedral_coeff 14     0.00344     -1      3
dihedral_coeff 15     0.0473 -1      2
```

```
#kspace_style ewald 0.0000.1
```

```
kspace_style ppm 1e-6
```

```
kspace_modify order 7
```

```
# ----- Run Minimization,Equilibration and MD -----
```

```
# ----- Run Minimization,Equilibration and MD -----
```

```
# ----- Run Minimization,Equilibration and MD -----
```

```
reset_timestep 0
```

```
neighbor 2.0 bin
```

```
comm_modify vel yes
```

```
minimize 1e-6 1e-8 10.000 10.0000
```

```
thermo 10.0
```

```
compute CStemp all temp/cs cores shells
```

```
compute thermo_press_lmp all pressure thermo_temp # press for correct kinetic scalar
```

```

thermo_style custom step etotal pe ke temp press &

      epair evdwl ecoul elong ebond fnorm fmax vol enthalpy c_thermo_press_imp cellalpha
cellbeta cellgamma cella cellb cellc

# output via chunk method

compute prop all property/atom i_CSID

compute cs_chunk all chunk/atom c_prop

compute csPE all pe/atom bond

compute csKE all ke/atom

fix PEoutput all ave/chunk 10.000 1 10.000 cs_chunk c_csPE file csPotential.txt

compute cstherm all temp/chunk cs_chunk temp internal com yes cdof 3.0

fix ave_chunk all ave/time 10.000 1 10.000 c_cstherm file chunk.dump mode vector

fix ke_chunk all ave/chunk 10.000 1 10.000 cs_chunk c_csKE file csKinetic.txt

# 2 fmsec timestep

thermo_modify temp CStemp press thermo_press_imp

timestep 0.0002

write_restart restart.Si

velocity all create 300 134 dist gaussian mom yes rot no bias yes temp CStemp

velocity all scale 300 temp CStemp

# thermostating using the core/shell decoupling

fix thermoberendsen all temp/berendsen 300 300 0.4

fix nve all nve

fix_modify thermoberendsen temp CStemp

neigh_modify delay 0 every 1 check yes

```

```

run 50000

unfix thermoberendsen

unfix nve

fix npt_xy all npt temp 300.0 300.0 0.02 x 0.0 0.0 0.2 y 0.0 0.0 0.2 couple none flip no

fix_modify npt_xy temp CStemp press thermo_press_lmp

neigh_modify delay 0 every 1 check yes

run 10.0000

unfix npt_xy

fix nvt all nvt temp 300 300 0.02

fix_modify nvt temp CStemp

neigh_modify delay 0 every 1 check yes

run 200000

unfix nvt

# ----- Dynamic Run -----

fix nvt all nvt temp 300 300 0.01

fix_modify nvt temp CStemp

fix 15 all plumed plumedfile plumed.dat outfile p.log

dump coord1 all custom 10.000 file.dump id type x y z vx vy vz

compute myRDF all rdf 10.0 1 3 2 3 5 7 1 2 3 3 3 6 7 7 5 5 3 4 1 5 1 6 2 5 2 6

fix 1 all ave/time 10.0000 1 10.0000 c_myRDF[*] file file.rdf mode vector

neigh_modify delay 0 every 1 check yes

run 10.00000000

write_restart tmp.restart

```

Annex 4. Lammmps input file for sulfate Adsorption onto 00.1 Ca terminated C-S-H surface

```
# ----- Initialize Simulation -----  
  
clear  
  
units          metal  
  
dimension      3  
  
atom_style     full  
  
boundary p p p  
  
box tilt large  
  
restart        10.0000 tmp.restart  
  
#read_restart  tmp.restart.20500000  
  
#read_restart restart.2 remap  
  
fix csinfo all property/atom i_CSID  
  
#read_data Tobermorite_CSInfo.data fix csinfo NULL CS-Info  
  
read_data Ca-Surface-new.lmp fix csinfo NULL CS-Info  
  
group ca type 1  
  
group Si type 2  
  
group Osicore type 3  
  
group Osishell type 4  
  
group Ow type 5  
  
group Ooh type 6  
  
group Hw type 7  
  
group Hoh type 8  
  
181
```

group os type 10

group s type 9

set group ca charge 2

set group Si charge 4

set group Osicore charge 0.85

set group Osishell charge -2.85

set group Ow charge -0.82

set group Ooh charge -1.4

set group Hw charge 0.41

set group Hoh charge 0.4

group cores type 3

group shells type 4

group noWater type 1 2 3 4

----- Define Interatomic Potential -----

#pair_style hybrid/overlay lj/cut/coul/long 8.5 buck/coul/long 8.5 coul/long 8.5
nb3b/harmonic nm/cut/coul/long 8.5

pair_style hybrid/overlay lj/cut/coul/long 8.5 buck/coul/long 8.5 coul/long 8.5
nm/cut/coul/long 8.5 buck/coul/long/cs 8.5

#pair_coeff * * nb3b/harmonic caSiOsicoreOsishellOwOohHwHoh.nb3b.harmonic ca Si
Osicore Ow Ooh Hw Hoh

pair_coeff 1 1 coul/long

pair_coeff 1 2 coul/long

pair_coeff	1	3	coul/long			
pair_coeff	1	4	buck/coul/long	2152.3566	0.309227	0.099440
pair_coeff	1	5	buck/coul/long	1286.6000	0.2970	0.0000
pair_coeff	1	6	buck/coul/long	2251.0500	0.2970	0.0000
pair_coeff	1	7	coul/long			
pair_coeff	1	8	coul/long			
pair_coeff	1	9	coul/long			
pair_coeff	1	10	buck/coul/long	1819	0.2833	0
pair_coeff	2	2	coul/long			
pair_coeff	2	3	coul/long			
pair_coeff	2	4	buck/coul/long	1283	0.3205	10.66
pair_coeff	2	5	buck/coul/long	1283.556	0.3202	10.6616
pair_coeff	2	6	buck/coul/long	983.5	0.3255	10.66
pair_coeff	2	7	coul/long			
pair_coeff	2	8	coul/long			
pair_coeff	2	9	coul/long			
pair_coeff	2	10	buck/coul/long	1283.556	0.3202	10.6616
pair_coeff	3	3	buck/coul/long	0	1	0
pair_coeff	3	4	buck/coul/long/cs	0	1	0
pair_coeff	3	5	buck/coul/long	0	1	0
pair_coeff	3	6	buck/coul/long	0	1	0
pair_coeff	3	7	buck/coul/long	0	1	0
pair_coeff	3	8	buck/coul/long	0	1	0

pair_coeff 3 9 coul/long
 pair_coeff 3 10 coul/long
 pair_coeff 4 4 buck/coul/long 22764.3 0.149 27.88
 pair_coeff 4 5 buck/coul/long 22764.3 0.149 28.92
 pair_coeff 4 6 buck/coul/long 22764.3 0.149 13.94
 pair_coeff 4 7 buck/coul/long 512 0.2500 0.0000
 pair_coeff 4 8 nm/cut/coul/long 0.0073 2.71 8.5 9 6
 pair_coeff 4 9 coul/long
 pair_coeff 4 10 buck/coul/long 22764 0.149 28.92
 pair_coeff 5 5 lj/cut/coul/long 0.0067 3.16
 pair_coeff 5 6 nm/cut/coul/long 0.0013000 4.63 8.5 9 6
 pair_coeff 5 7 coul/long
 pair_coeff 5 8 nm/cut/coul/long 0.055 2 8.5 9 6
 pair_coeff 5 9 coul/long
 pair_coeff 5 10 buck/coul/long 12534.455133 0.246 0
 pair_coeff 6 6 buck/coul/long 22764 0.149 6.97
 pair_coeff 6 7 coul/long
 pair_coeff 6 8 nm/cut/coul/long 0.0073 2.71 8.5 9 6
 pair_coeff 6 9 coul/long
 pair_coeff 6 10 nm/cut/coul/long 0.0013000 4.63 8.5 9 6
 pair_coeff 7 7 coul/long
 pair_coeff 7 8 coul/long
 pair_coeff 7 9 coul/long

pair_coeff 7 10 coul/long
pair_coeff 8 8 coul/long
pair_coeff 8 9 coul/long
pair_coeff 8 10 coul/long
pair_coeff 9 9 coul/long
pair_coeff 9 10 coul/long
pair_coeff 10 10 buck/coul/long 103585.02 0.200 0
bond_style hybrid harmonic morse
bond_coeff 3 harmonic 37.5 0
bond_coeff 1 harmonic 22.96 1.0120
#bond_coeff 2 harmonic 37.5 0
bond_coeff 2 morse 7.0525 3.1749 0.942
bond_coeff 4 morse 5 1.2 1.505#gale
angle_style harmonic
angle_coeff 1 1.64567 113.24
angle_coeff 2 7.74815 109.47000
angle_coeff 3 7.74815 109.47000
angle_coeff 4 7.74815 109.47000
angle_coeff 5 7.74815 109.47000
angle_coeff 6 7.5 109.47 #gale
#kspace_style ewald 0.0000.1
kspace_style ppm 1e-6
kspace_modify order 7

```

# ----- Run Minimization,Equilibration and MD -----

reset_timestep 0

neighbor 2.0 bin

comm_modify vel yes

minimize 1e-6 1e-8 10.000 10.0000

thermo 10.0

compute CStemp all temp/cs cores shells

compute thermo_press_lmp all pressure thermo_temp # press for correct kinetic scalar

thermo_style custom step etotal pe ke temp press &

        epair evdwl ecoul elong ebond fnorm fmax vol enthalpy c_thermo_press_lmp cellalpha
cellbeta cellgamma cella cellb cellc

# output via chunk method

compute prop all property/atom i_CSID

compute cs_chunk all chunk/atom c_prop

compute csPE all pe/atom bond

compute csKE all ke/atom

fix PEoutput all ave/chunk 10.000 1 10.000 cs_chunk c_csPE file csPotential.txt

compute cstherm all temp/chunk cs_chunk temp internal com yes cdof 3.0

fix ave_chunk all ave/time 10.000 1 10.000 c_cstherm file chunk.dump mode vector

fix ke_chunk all ave/chunk 10.000 1 10.000 cs_chunk c_csKE file csKinetic.txt

# 2 fmsec timestep

thermo_modify temp CStemp press thermo_press_lmp

```

```
timestep 0.0002

write_restart restart.Si

velocity all create 300 134 dist gaussian mom yes rot no bias yes temp CStemp

velocity all scale 300 temp CStemp

# thermostating using the core/shell decoupling

fix thermoberendsen all temp/berendsen 300 300 0.4

fix nve all nve

fix_modify thermoberendsen temp CStemp

neigh_modify delay 0 every 1 check yes

run 50000

unfix thermoberendsen

unfix nve

fix npt_xy all npt temp 300.0 300.0 0.02 x 0.0 0.0 0.2 y 0.0 0.0 0.2 couple none flip no

fix_modify npt_xy temp CStemp press thermo_press_lmp

neigh_modify delay 0 every 1 check yes

run 10.0000

unfix npt_xy

fix nvt all nvt temp 300 300 0.02

fix_modify nvt temp CStemp

neigh_modify delay 0 every 1 check yes

run 200000

unfix nvt

# ----- Dynamic Run -----
```

```
fix nvt all nvt temp 300 300 0.02

fix_modify nvt temp CStemp

fix 15 all plumed plumedfile plumed.dat outfile p.log

dump coord1 all custom 10.000 file.dump id type x y z vx vy vz

compute myRDF all rdf 10.0 1 3 2 3 5 7 1 2 3 3 3 6 7 7 5 5 3 4 1 5 1 6 2 5 2 6

fix 1 all ave/time 10.0000 1 10.0000 c_myRDF[*] file file.rdf mode vector




neigh_modify delay 0 every 1 check yes

run 10.00000000

write_restart tmp.restart
```

Masood Valavi

PhD in Chemical and Material
Engineering

 (+41)766405592
 Masudvalavi607@gmail.com
 Lausanne -Switzerland



PROFILE

Expert in Molecular Modeling, Computational Chemistry, Thermodynamics, programming, Process modeling by software such as ASPEN, Chemical engineering and also familiar with Machine learning and Data analysis

EXPERIENCE

Internship at CHRYSO
July 2020-present

Expert Simulation Engineer

- Working on molecular simulation of adsorption of inorganic molecules onto surface of cementitious materials by use of molecular and metadynamic simulation
- Programming and analysis of data of adsorption phenomena

PhD researcher at EPFL
Feb. 2018-present

Expert Simulation Engineer

- Molecular modeling and atomistic simulation of cementitious systems using Molecular dynamic and Metadynamic software
- Coding and programming and working with several software such as OVITO, VMD, and etc

EDUCATION

PhD -EPFL-Switzerland
Feb.2018-present

Expert in Simulation and Modeling -Precious Marie Curie Funding

- Molecular modeling and atomistic simulation: Performing several simulations in order to simulate cementitious systems
- Developing Force Field for Cementitious systems
- Thermodynamic modeling: Prediction of heat of reaction and other thermodynamic properties

MSc -University of Limerick-Ireland

Expert in Simulation and Modeling

Feb.2014-2016
189

- Thermodynamic modeling of Crystallization process and process modeling of crystallization process specially focused on pharmaceutical compounds
- Develop thermodynamic models in order to predict solubility of APIs (Pharmaceutical compounds)
- Data analysis of solubility of pharmaceutical compound in water and

PROJECTS

- **Molecular Modeling and Developing Force Field:** In this project I developed a new model (Force Field) in order to simulate cementitious systems and applied developed force field to simulate properties of cementitious systems by employing molecular dynamic
- **Molecular modeling of adsorption of gluconate and ions into surface of cementitious systems**
- In this project I simulated adsorption of gluconate and ions into surfaces of cementitious systems by means of molecular dynamic and metadynamic.
- **Process modeling of gas refinery using Aspen and Promax software:** In this project I simulated a refinery in Iran using Aspen and Promax software. Result of my simulation was used in order to increase the overall efficiency of a refinery
- **Thermodynamic modeling of several systems:** I modified existing thermodynamic models and applied the developed model to simulate Gas Hydrate, polymers, Electrolyte, amino acids and other systems
- **Data analysis on existing thermodynamic data:** In this project I performed huge data analysis on thermodynamic data of solubility of pharmaceutical compounds in water and other solvents
- **Thermodynamic modeling of solubility of pharmaceutical compounds in solvents:** In this project I modified a thermodynamic model and applied that in order to simulate solubility of pharmaceutical compound in water and other solvents

SCRIPTING

MATLAB, Python, LAMMPS, AMBER, PLUMED, METADISE, PROMAX, ASPEN

LANGUAGE

English (Fluent), German (intermediate), Persian(native)

REFERENCES

Professor Paul Bowen-EPFL email: paul.bowen@epfl.ch

Dr. Sandra Galamrini-EMPA email: Sandra.galmarini@empa.ch

Dr Aslam Kunhi Mohamed-ETH email: Akuh@ethz.ch

[For list of Publications please refer to the next page](#)

Publications: [Masood Valavi - Google Scholar](#)

13 published papers in well-known journals, **11** first Author-Currently holding **H-index=8**

Published

1-Solid and solution state thermodynamics of polymorphs of butamben (butyl 4-aminobenzoate) in pure organic solvents, M Svård, L Zeng, **M Valavi**, GR Krishna, ÅC Rasmuson, Journal of pharmaceutical sciences 108 (7), 2377-2382, 3, 2019

2-Prediction of solubility of active pharmaceutical ingredients by semi-predictive Flory Huggins/Hansen model, **M Valavi**, M Ukrainczyk, MR Dehghani, Journal of Molecular Liquids 246, 166-172, 7, 2017

3-Crystallisation thermodynamics, **M Valavi**, University of Limerick thesis, 2017

4-Improving Estimates of the Crystallization Driving Force: Investigation into the Dependence on Temperature and Composition of Activity Coefficients in Solution, **M Valavi**, M Svård, ÅC Rasmuson, Crystal Growth & Design 16 (12), 6951-6960, 10, 2016

5-Prediction of the solubility of medium-sized pharmaceutical compounds using a temperature-dependent NRTL-SAC model, **M Valavi**, M Svård, ÅC Rasmuson, Industrial & Engineering Chemistry Research 55 (42), 11150-11155, 18, 2016

6-Thermodynamic stability analysis of tolbutamide polymorphs and solubility in organic solvents, M Svård, **M Valavi**, D Khamar, M Kuhs, ÅC Rasmuson, Journal of pharmaceutical sciences 105 (6), 1901-1906, 18, 2018

7-Improving estimates of the crystallization driving force: investigation into the dependence on temperature and composition of activity coefficients in solution, M Svård, **M Valavi**, ÅC Rasmuson, American Chemical Society 2016

8-Correlation and prediction of solubility and activity coefficients, **M Valavi**, CGOM, 2016

9-Capability of PHSC equation of state for thermodynamic modeling of aqueous amino acid and peptide solutions, **M Valavi**, MR Dehghani, R Shahriari, Journal of Molecular Liquids 199, 21-28, 7, 2014

10-Calculation of the Density and Activity of Water in Aqueous Systems for Separation of Biomolecules, **M Valavi**, S Shirazian, AF Pour, M Ziary, Journal of Solution Chemistry 42 (7), 1423-1437, 7, 2013

11-Application of modified PHSC model in prediction of phase behavior of single and mixed electrolyte solutions, **M Valavi**, MR Dehghani, R Shahriari, Fluid Phase Equilibria 344, 92-100, 15, 2013

12-Calculation of liquid-liquid equilibrium in polymer electrolyte solutions using PHSC-electrolyte equation of state, **M Valavi**, MR Dehghani, F Feyzi, Fluid Phase Equilibria 341, 96-104, 11, 2013

13-Application of PHSC equation of state in prediction of gas hydrate formation condition, **M Valavi**, MR Dehghani, Fluid phase equilibria 333, 27-37, 18, 2012

Submitted or in preparation

14-Developing ERICA FF for simulation of Cementitious systems, **M. Valavi**, S. Galmarini, Z. Casar, A. Kunhi Mohamed, P. Bowen. Submitted to CCR journal

15-Simulation of adsorption of Ca and OH into 001 surface of CH **M. Valavi**, S. Galmarini, A. Kunhi Mohamed, P. Bowen. in preparation

16-Study on adsorption of Sulfate on the surface of portlandite and C-S-H by means of molecular dynamic and metadynamic simulation **M. Valavi**, S. Galmarini, A. Kunhi Mohamed, P. Bowen. in preparation

17-Investigation on the adsorption of gluconate on the surface of cementitious system **M. Valavi**, S. Galmarini, A. Kunhi Mohamed, P. Bowen. in preparation